Automated Symbolic Upscaling: Model Generation for Extended Applicability Regimes, Part 1

Kyle Pietrzyk[1], Ilenia Battiato[1]

[1]Department of Energy Resources Engineering, Stanford University, 367 Panama St., Stanford, CA 94305

Key Points:

- A strategy for expanding the applicability of classical homogenization theory by generalizing the assumed closure form is presented.
- The strategy is detailed and numerically validated in two reactive mass transport problems experiencing moderately reactive physics.
- Nontrivial homogenized models with effective parameters that couple reactive, diffusive, and advective transport are derived.

Corresponding author: Ilenia Battiato, ibattiat@stanford.edu

Abstract

In porous media theory, upscaling techniques are fundamental to deriving rigorous Darcy-scale models for flow and reactive transport in subsurface systems. Due to limitations in classical upscaling methods, a number of *ad hoc* techniques have been proposed to address physical regimes of higher reactivity, such as moderately reactive regimes where diffusive and reactive mass transport are of the same order of magnitude. In Part 1 of this two part series, we present a strategy for expanding the applicability of classical homogenization theory by generalizing the assumed closure form. We detail the implementation of this strategy on two reactive mass transport problems with moderately reactive physics. The strategy produces nontrivial homogenized models with effective parameters that couple reactive, diffusive, and advective transport. Numerical validation is provided for each problem to justify the implemented strategy.

1 Introduction

Due to the vast spectra of spatiotemporal variations in subsurface processes and geological media, multiscale modeling has remained a cornerstone for analyzing flow and reactive transport beneath the surface (Scheibe et al., 2015; Molins & Knabner, 2019; Mehmani, Anderson, et al., 2021). The technical approaches set forth by this paradigm focus on translating the physical dynamics at finer scales (e.g., the pore-scale) to much larger scales where nontrivial behaviors tend to occur. By providing accurate and computationally efficient predictions of such large-scale behaviors, these analysis methods enhance the understandings of phenomena observed in geological engineering and hydrology, such as acidification reactions in carbonate rocks and biogeochemical reactions (Tang et al., 2015; Yan et al., 2017; Molins et al., 2019; Becker et al., 2022; Mehmani, Castelletto, & Tchelepi, 2021; Wang & Battiato, 2020). While many classical approaches to multiscale modeling continue to be employed (Schiller & Wang, 2018; Battiato et al., 2019), new data-driven strategies are also being developed to reap the benefits of state-of-the-art technologies (Lubbers et al., 2020; Wang & Battiato, 2021).

Within multiscale modeling, considerable efforts have focused on evolving and generalizing *upscaling* techniques, such as the method of volume averaging (MVA) (Whitaker, 1999), homogenization theory (Hornung, 1997), and thermodynamically constrained averaging theory (TCAT) (Gray & Miller, 2014), among others. These techniques provide rigorous approaches to systematically generate macroscopic partial differential equations (PDEs) from first principle equations at the microscale (Battiato et al., 2019). To formulate macroscopic PDEs, supplemental terms and effective coefficients are derived to accurately account for multiscale behaviors (Pietrzyk et al., 2021). In addition to the accuracy and computational efficiency provided by these models, *applicability conditions* (also referred to as *scaling laws* in MVA (Golfier et al., 2009; Wood, 2009) and *permissibility conditions* in TCAT (C. Miller et al., 2018)) can also be obtained during the upscaling procedures (Battiato & Tartakovsky, 2011; Boso & Battiato, 2013), which provide physical constraints under which estimates of the accrued modeling error are known *a priori*. A number of upscaling theories go beyond the derivation of classical Darcy-scale equations for reactive transport and multiphase flow (e.g., modeling nonhysteretic capillary pressure behavior (C. T. Miller et al., 2019)). Some of these include deterministic and stochastic nonlocal modeling techniques (Gelhar & Axness, 1983), such as dual and multicontinuum modeling (Cushman & Ginn, 1993; Neuman, 1993; Haggerty et al., 2000), continuous time random walk modeling (Berkowitz et al., 2006), moment methods (Neuman, 1993), and projector operator methods (Cushman & Ginn, 1993). Even advanced methods for physics-based multiscale modeling with various degrees of coupling have used upscaling techniques as their primary machinery for model development (Battiato et al., 2011; Yousefzadeh & Battiato, 2017; Ahmed et al., 2022).

With continued interest in upscaling and related modeling methods, attention has centered around extending the applicability of such techniques to physical regimes in which the accuracy of effective-medium models has been questioned (Battiato et al., 2009; Arunachalam et al., 2015; Pietrzyk et al., 2021). In particular, significant progress has been made toward extending the applicability of upscaling techniques to highly advective and reactive regimes. In the context of homogenization theory (Hornung, 1997), problem-specific techniques that deviate from the standard theory have been developed to analyze various transport regimes. Early investigations into systems with strong advection involved expanding temporal derivatives in an effort to consider dynamics across multiple time scales (Rubinstein & Mauri, 1986; Mei, 1992; Salles et al., 1993; Auriault & Adler, 1995). Other methods handled strong advection by adding *drift* to the pore-scale equations, which involved transforming the large-scale coordinates to a moving coordinate frame (Garnier, 1997; Donato & Piatnitski, 2005; Marušić-Paloka & Piatnitski, 2005). A similar idea of variable transformation was also used to model strong reactive behavior (Mauri, 1991; "Diffusion in Ran-

dom Media", 1995) along with other various mathematical methods (Lewandowska et al., 2002). These variable transformation methods have since become the standard for homogenizing strongly advective-reactive systems (Allaire & Raphael, 2007; Allaire, Mikelić, & Piatnitski, 2010; Allaire, Brizzi, et al., 2010) and more recent homogenization strategies seem to benefit from their influence (Municchi & Icardi, 2020; Le et al., 2022).

As efforts to further generalize and sophisticate upscaling theories persevere, the syntactical, mathematical, and procedural complexities employed continue to grow. These come in addition to the complexities inherent to realistic geological reactive systems, which can involve multiple coupled physical processes and reaction networks that easily include tens of species or more. The combined complexity is enough to deter scientists and practitioners away from upscaling techniques and drive them towards alternative, less rigorous modeling techniques. However, known applicability conditions and error limits bring value to upscaled models and make them relevant solutions to questions regarding model validity in subsurface flow and reactive transport problems (e.g., CO_2 sequestration, H_2 subsurface storage, etc.). In light of this, it is beneficial to create methods for handling the complexities associated with upscaling techniques, and ultimately democratize upscaling for efficient use in subsurface flow and reactive transport applications.

In this two part series, we propose a general analytical strategy for extending the applicability of homogenized models with respect to classical homogenization theory (Part 1), and implement the strategy into an automated upscaling framework for rapid use in a wide range of complex systems (Part 2). The strategy involves generalizing the assumed forms of ordered solutions by constructing them as linear combinations of closure terms. This leads to the definition of multiple closure problems for a single ordered solution, whereas in classical homogenization theory, only one closure problem is defined and the assumed form of the first order solution consists of only one closure term. We then implement the analytical strategy into Symbolica, a symbolic computational code for fully automating rigorous analytical upscaling procedures on problems with realistic complexities. By streamlining the notoriously lengthy and syntactically complex derivations of upscaling, Symbolica enables users with limited mathematical expertise to rapidly generate and deploy upscaled models for analysis in complex practical systems. As a result, communal access to upscaling techniques is provided in a similar manner to how computational physics softwares provide access to numerical methods.

Aside from speed, democratization, and the ability to apply upscaling theories in complex practical systems, Symbolica is also capable of quickly, and rigorously, traversing dimensionless parameter spaces for valid upscaled models. Originally pointed out in previous works (Auriault & Adler, 1995; Battiato & Tartakovsky, 2011; Boso & Battiato, 2013), the value of this ability has been reemphasized in recent works that consider homogenization techniques for handling highly advective and reactive systems. These works highlight that varying the magnitudes of the dimensionless parameters in a system can lead to different macroscopic models:

> "Namely even starting from the same microscale problem, for different sizes of the characteristic numbers, the homogenization results in different upscaled (macroscale) model depending on the considered regime. Different here means that these can be different types of equations, which cannot be converted to each other by simple fitting of the coefficients." (Iliev et al., 2020)

> "Dimensionless parameters are hence obtained explicitly as ratios of characteristic quantities. Considering these dimensionless parameters, at different orders of magnitude, leads to different macroscopic behaviours in the case of homogenisable situations." (Bloch & Auriault, 2019)

As described, the macroscopic model of a system cannot be trivially assumed for general dimensionless parameter magnitudes; the upscaling procedure must be re-executed for each set of dimensionless parameter magnitudes considered. With Symbolica, the workload associated with upscaling for each combination of dimensionless parameter magnitudes is removed, as the code automatically upscales across the dimensionless parameter space in a short amount of time (Pietrzyk et al., 2021).

In Part 1, we present the general analytical strategy for extending applicability by annotating its implementation in two example reactive mass transport problems and numerically validate the homogenized results. Nontrivial homogenized models and effective parameters are found and discussed in detail. The proposed approach has a number of advantages. Firstly, it directly generalizes and extends the applicability of classically homogenized, reactive mass transport models into moderately reactive regimes,

where diffusive and reactive terms are of the same order. Secondly, the presented strategy is compatible with, and can further generalize, theories for homogenizing highly advective and reactive systems, as well as theories for analyzing inhomogeneous boundary conditions (Municchi & Icardi, 2020). Thirdly, the strategy can be easily implemented into automated upscaling frameworks in an algorithmic fashion for automated closure form and closure problem definition. This capability is explored in Part 2 of this series, where we validate the implementation of the strategy in Symbolica by analyzing two additional reactive mass transport problems. Overall, we find this implementation invaluable, as it enables Symbolica to automatically homogenize complex systems with multiple, moderately strong reactions and produce nontrivial homogenized models.

The manuscript is organized as follows. In Section 2, a general problem of reactive transport in porous media is formulated for multiple solutes and reaction interfaces. The governing equations and boundary conditions are introduced in Subsection 2.1 with a general scaling, a unit-cell formulation, and expansions of the temporal derivative and dependent variables presented in Subsections 2.2, 2.3, and 2.4, respectively. Then, from the previously presented general reactive transport problem, we derive the equations and boundary conditions for the first considered transport problem: a single species undergoing a linear, heterogeneous reaction (Section 3). While the detailed implementation of the proposed homogenization strategy can be found in Appendix A, the main homogenized results are presented in Subsection 3.1 and numerical validation is provided in Subsection 3.2. A second transport problem consisting of two solutes undergoing linearly coupled, heterogeneous reactions is then considered in Section 4, where the equations and boundary conditions are derived from the general reactive transport problem. Again, the detailed implementation can be found in Appendix B while the main homogenized results and numerical validation are provided in Subsections 4.1 and 4.2, respectively. Finally, concluding remarks for Part 1 of this two part series can be found in Section 5.

2 Problem Formulation

Similar to the setup in our previous work (Pietrzyk et al., 2021), we consider a porous medium $\hat{\Omega}_\epsilon \subset \mathbb{R}^b$, where $b \in \{1,2,3\}$, consisting of a pore-space $\hat{\mathcal{B}}_\epsilon$ and an impermeable solid matrix $\hat{\mathcal{G}}_\epsilon$. A smooth interface $\hat{\Gamma}_\epsilon$ is assumed to exist between the two domains. We also assume the physical gradients within this medium are adequately described using two length scales: a larger scale $\hat{\mathcal{L}}$ and a smaller scale $\hat{\ell}$. A length scale ratio

$$\epsilon \equiv \frac{\hat{\ell}}{\hat{\mathcal{L}}} \tag{1}$$

can then be defined, where $\hat{\mathcal{L}} \gg \hat{\ell}$ implies $\epsilon \ll 1$. Unless otherwise stated, hatted variables are assumed to have physical dimension, while variables without hats are assumed to be dimensionless.

2.1 Governing Equations and Boundary Conditions

We assume an incompressible liquid fully saturates the pore-space. The Stokes equation, the incompressible continuity equation, and a no-slip boundary condition govern the velocity and pressure fields of the liquid, such that

$$\hat{\mu}\hat{\nabla}^2\hat{\mathbf{u}}_\epsilon - \hat{\nabla}\hat{p}_\epsilon = \mathbf{0} \quad \text{in } \hat{\mathcal{B}}_\epsilon, \tag{2a}$$

$$\hat{\nabla}\cdot\hat{\mathbf{u}}_\epsilon = 0 \quad \text{in } \hat{\mathcal{B}}_\epsilon, \tag{2b}$$

subject to

$$\hat{\mathbf{u}}_\epsilon = \mathbf{0} \quad \text{on } \hat{\Gamma}_\epsilon, \tag{2c}$$

where $\hat{\mathbf{u}}_\epsilon \equiv \hat{\mathbf{u}}_\epsilon(\hat{\mathbf{x}})$ is the fluid velocity at spatial coordinate $\hat{\mathbf{x}} \in \hat{\mathcal{B}}_\epsilon$, $\hat{\mu}$ is the dynamic viscosity, and $\hat{p}_\epsilon \equiv \hat{p}_\epsilon(\hat{\mathbf{x}})$ is the pressure. Theoretically, we only consider these equations far from the boundaries of $\hat{\Omega}_\epsilon$, such that non-local effects due to macroscale boundary conditions on $\hat{\Omega}_\epsilon$ are negligible.

In addition to the fluid flow, we consider the transport of N species subject to advection, diffusion, and both homogeneous and heterogeneous reactions. For each species i, where $i \in \{1, 2, \cdots, N\}$, we consider bimolecular homogeneous reactions of the type $A+B \leftrightarrow C+D$ in the liquid phase and heterogeneous reactions of the type $M_{(l)} \leftrightarrow M_{(s)}$ at the liquid-solid interface. We note that generalizations to reactions beyond those described here are straightforward. To accommodate multiple heterogeneous reactions occurring on different sections of the interface $\hat{\Gamma}_\epsilon$, we divide the liquid-solid interface into N_Γ parts, such that

$$\hat{\Gamma}_\epsilon = \bigcup_{j=1}^{N_\Gamma} \hat{\Gamma}_\epsilon^{(j)}, \tag{3}$$

where $\hat{\Gamma}_\epsilon^{(j)}$ is the interface j, a subsection of the total interface $\hat{\Gamma}_\epsilon$. This allows multiple heterogeneous reactions to be defined across the various interface subsections $\hat{\Gamma}_\epsilon^{(j)}$ for a single solute. Then, the transport of each reactive species in the pore-space is governed by a system of advective-diffusive-reactive (ADR) equations of the form

$$\frac{\partial \hat{c}_\epsilon^{(i)}}{\partial \hat{t}} + \hat{\nabla} \cdot \left(\hat{\mathbf{u}}_\epsilon \hat{c}_\epsilon^{(i)} - \hat{D}^{(i)} \hat{\nabla} \hat{c}_\epsilon^{(i)} \right) = \hat{R}_\epsilon^{(i)} \quad \text{in } \hat{\mathcal{B}}_\epsilon, \tag{4a}$$

$$\hat{R}_\epsilon^{(i)} = \sum_{k=1}^{N} (-1)^{p_L^{(i,k)}} \hat{\mathcal{K}}_L^{(i,k)} \hat{c}_\epsilon^{(k)} + \sum_{k=1}^{N} \sum_{l=k}^{N} (-1)^{p_{NL}^{(i,k,l)}} \hat{\mathcal{K}}_{NL}^{(i,k,l)} \hat{c}_\epsilon^{(k)} \hat{c}_\epsilon^{(l)}, \tag{4b}$$

subject to

$$-\mathbf{n}^{(j)} \cdot \hat{D}^{(i)} \hat{\nabla} \hat{c}_\epsilon^{(i)} = \hat{T}_\epsilon^{(i,j)} \quad \text{on } \hat{\Gamma}_\epsilon^{(j)}, \tag{4c}$$

$$\begin{aligned} \hat{T}_\epsilon^{(i,j)} = &\sum_{k=1}^{N} (-1)^{p_{SL}^{(i,j,k)}} \hat{\mathcal{K}}_{SL}^{(i,j,k)} \left(\hat{c}_\epsilon^{(k)} - \hat{C}_{SL}^{(i,j,k)} \right) \\ &+ \sum_{k=1}^{N} \sum_{l=k}^{N} (-1)^{p_{SNL}^{(i,j,k,l)}} \hat{\mathcal{K}}_{SNL}^{(i,j,k,l)} \left(\hat{c}_\epsilon^{(k)} \hat{c}_\epsilon^{(l)} - \hat{C}_{SNL}^{(i,j,k,l)^2} \right), \end{aligned} \tag{4d}$$

where $\hat{c}_\epsilon^{(i)} \equiv \hat{c}_\epsilon^{(i)}(\hat{t}, \hat{\mathbf{x}})$ is the concentration of species i at time $\hat{t} > 0$ and spatial coordinate $\hat{\mathbf{x}} \in \hat{\mathcal{B}}_\epsilon$, $\hat{D}^{(i)}$ is the diffusion coefficient of species i, $\hat{R}_\epsilon^{(i)}$ is the sum of all bulk reaction terms for species i, $p_L^{(i,k)}$ and $p_{NL}^{(i,k,l)}$ are either 0 or 1, $\hat{\mathcal{K}}_L^{(i,k)}$ is the reaction rate constant of the linear bulk reaction corresponding to species k in the transport equation for species i, $\hat{\mathcal{K}}_{NL}^{(i,k,l)}$ is the reaction rate constant of the non-linear bulk reaction corresponding to species k and l in the transport equation for species i, $\mathbf{n}^{(j)} \equiv \mathbf{n}^{(j)}(\hat{\mathbf{x}})$ is the normal vector to the liquid-solid interface subsection j pointed towards the solid, $\hat{T}_\epsilon^{(i,j)}$ is the sum of all heterogeneous reaction terms for species i on the liquid-solid interface subsection j, $p_{SL}^{(i,j,k)}$ and $p_{SNL}^{(i,j,k,l)}$ are either 0 or 1, $\hat{\mathcal{K}}_{SL}^{(i,j,k)}$ is the reaction rate constant of the linear reaction at the liquid-solid interface subsection j corresponding to species k in the system of equations for species i, $\hat{C}_{SL}^{(i,j,k)}$ is the threshold concentration for the linear reaction at the liquid-solid interface subsection j for species k in the system of equations for species i (Morse & Arvidson, 2002), $\hat{\mathcal{K}}_{SNL}^{(i,j,k,l)}$ is the reaction rate constant of the non-linear reaction at the liquid-solid interface subsection j corresponding to species k and l in the system of equations for species i, and $\hat{C}_{SNL}^{(i,j,k,l)}$ is the threshold concentration for the non-linear reaction at the liquid-solid interface subsection j for species k and l in the system of equations for species i. Similar to before, we consider these equations far from the boundaries of $\hat{\Omega}_\epsilon$ to eliminate concern of non-local effects from macroscale boundary conditions on $\hat{\Omega}_\epsilon$, and do not assume any specific initial conditions.

2.2 Scaling

To scale systems (2) and (4), we consider the following:

$$\hat{c}_\epsilon^{(i)} = \hat{\mathcal{C}}^{(i)} c_\epsilon^{(i)}, \quad \hat{\nabla} = \frac{1}{\hat{\mathcal{L}}}\nabla, \quad \hat{D}^{(i)} = \hat{\mathcal{D}} D^{(i)}, \quad \hat{\mathbf{u}}_\epsilon = \hat{\mathcal{U}}\mathbf{u}_\epsilon, \quad \hat{p}_\epsilon = \hat{\mathcal{P}} p_\epsilon,$$
$$\hat{t} = \frac{\hat{\mathcal{L}}^2}{\hat{\mathcal{D}}} t, \quad \hat{R}_\epsilon^{(i)} = \frac{\hat{\mathcal{D}}\hat{\mathcal{C}}^{(i)}}{\hat{\mathcal{L}}^2} R_\epsilon^{(i)}, \quad \hat{T}_\epsilon^{(i,j)} = \frac{\hat{\mathcal{D}}\hat{\mathcal{C}}^{(i)}}{\hat{\mathcal{L}}} T_\epsilon^{(i)}, \tag{5}$$

where $\hat{\mathcal{C}}^{(i)}$ is the concentration scale for species i, $\hat{\mathcal{D}}$ is the diffusion coefficient scale, $\hat{\mathcal{U}}$ is the fluid velocity scale, and $\hat{\mathcal{P}}$ is the fluid pressure scale. Applying these scales to system (2) yields

$$A_\epsilon \nabla^2 \mathbf{u}_\epsilon - \nabla p_\epsilon = \mathbf{0} \quad \text{in } \mathcal{B}_\epsilon, \tag{6a}$$

$$\nabla \cdot \mathbf{u}_\epsilon = 0 \quad \text{in } \mathcal{B}_\epsilon, \tag{6b}$$

subject to

$$\mathbf{u}_\epsilon = \mathbf{0} \quad \text{on } \Gamma_\epsilon. \tag{6c}$$

Here, we note that the ratio $A_\epsilon = \hat{\mu}\hat{\mathcal{U}}/(\hat{\mathcal{P}}\hat{\mathcal{L}})$ in equation (6a) is assumed to have a magnitude of $\mathcal{O}(\epsilon^2)$ in the classical homogenization of the Stokes equation (Auriault & Adler, 1995). After applying the defined scales to system (4), we obtain

$$\frac{\partial c_\epsilon^{(i)}}{\partial t} + \nabla \cdot \left(\mathrm{Pe}\mathbf{u}_\epsilon c_\epsilon^{(i)} - D^{(i)} \nabla c_\epsilon^{(i)} \right) = R_\epsilon^{(i)} \quad \text{in } \mathcal{B}_\epsilon, \tag{7a}$$

$$R_\epsilon^{(i)} = \sum_{k=1}^{N} (-1)^{p_L^{(i,k)}} \, \mathrm{Da}_L^{(i,k)} c_\epsilon^{(k)} + \sum_{k=1}^{N}\sum_{l=k}^{N} (-1)^{p_{NL}^{(i,k,l)}} \, \mathrm{Da}_{NL}^{(i,k,l)} c_\epsilon^{(k)} c_\epsilon^{(l)}, \tag{7b}$$

subject to

$$-\mathbf{n}^{(j)} \cdot D^{(i)} \nabla c_\epsilon^{(i)} = T_\epsilon^{(i,j)} \quad \text{on } \Gamma_\epsilon^{(j)}, \tag{7c}$$

$$\begin{aligned} T_\epsilon^{(i,j)} = &\sum_{k=1}^{N} (-1)^{p_{SL}^{(i,j,k)}} \, \mathrm{Da}_{SL}^{(i,j,k)} \left(c_\epsilon^{(k)} - \theta_{SL}^{(i,j,k)} \right) \\ &+ \sum_{k=1}^{N}\sum_{l=k}^{N} (-1)^{p_{SNL}^{(i,j,k,l)}} \, \mathrm{Da}_{SNL}^{(i,j,k,l)} \left(c_\epsilon^{(k)} c_\epsilon^{(l)} - \theta_{SNL}^{(i,j,k,l)} \right), \end{aligned} \tag{7d}$$

where the dimensionless numbers are defined as

$$\mathrm{Pe} = \frac{\hat{\mathcal{U}}\hat{\mathcal{L}}}{\hat{\mathcal{D}}}, \quad \mathrm{Da}_L^{(i,k)} = \frac{\hat{\mathcal{K}}_L^{(i,k)} \hat{\mathcal{L}}^2 \hat{\mathcal{C}}^{(k)}}{\hat{\mathcal{D}}\hat{\mathcal{C}}^{(i)}}, \quad \mathrm{Da}_{NL}^{(i,k,l)} = \frac{\hat{\mathcal{K}}_{NL}^{(i,k,l)} \hat{\mathcal{L}}^2 \hat{\mathcal{C}}^{(k)} \hat{\mathcal{C}}^{(l)}}{\hat{\mathcal{D}}\hat{\mathcal{C}}^{(i)}}, \quad \mathrm{Da}_{SL}^{(i,j,k)} = \frac{\hat{\mathcal{K}}_{SL}^{(i,j,k)} \hat{\mathcal{L}}\hat{\mathcal{C}}^{(k)}}{\hat{\mathcal{D}}\hat{\mathcal{C}}^{(i)}},$$
$$\theta_{SL}^{(i,j,k)} = \frac{\hat{C}_{SL}^{(i,j,k)}}{\hat{\mathcal{C}}^{(k)}}, \quad \mathrm{Da}_{SNL}^{(i,j,k,l)} = \frac{\hat{\mathcal{K}}_{SNL}^{(i,j,k,l)} \hat{\mathcal{L}}\hat{\mathcal{C}}^{(k)} \hat{\mathcal{C}}^{(l)}}{\hat{\mathcal{D}}\hat{\mathcal{C}}^{(i)}}, \quad \theta_{SNL}^{(i,j,k,l)} = \frac{\hat{C}_{SNL}^{(i,j,k,l)^2}}{\hat{\mathcal{C}}^{(k)}\hat{\mathcal{C}}^{(l)}}. \tag{8}$$

Here, Pe is the Péclet number, $\mathrm{Da}_L^{(i,k)}$, $\mathrm{Da}_{NL}^{(i,k,l)}$, $\mathrm{Da}_{SL}^{(i,j,k)}$, and $\mathrm{Da}_{SNL}^{(i,j,k,l)}$ are Damköhler numbers, and $\theta_{SL}^{(i,j,k)}$ and $\theta_{SNL}^{(i,j,k,l)}$ are concentration ratios.

2.3 Unit-Cell Domain Formulation

We define the unit-cell in a similar manner as our previous work (Pietrzyk et al., 2021), and provide the formulation here for completeness. By introducing a spatially-dependent variable $\hat{\boldsymbol{\xi}}(\hat{\mathbf{x}}) \equiv \hat{\mathbf{x}}$, and scaling $\hat{\boldsymbol{\xi}}(\hat{\mathbf{x}})$ by $\hat{\ell}$ and $\hat{\mathbf{x}}$ by $\hat{\mathcal{L}}$, we obtain

$$\boldsymbol{\xi}\left(\mathbf{x}\right) = \epsilon^{-1}\mathbf{x}, \tag{9}$$

where $\boldsymbol{\xi}(\mathbf{x})$ and $\mathbf{x}$ are referred to as "fast" and "slow" variables, respectively (Hornung, 1997). Any spatially-dependent function $f_\epsilon(\mathbf{x})$ is then written as $f_\epsilon(\mathbf{x}) = f(\mathbf{x}, \boldsymbol{\xi}(\mathbf{x}))$, and the chain rule is applied when considering ∇, the total differential operator in space, to write

$$\nabla f_\epsilon \equiv \nabla_{\mathbf{x}} f + \frac{1}{\epsilon}\nabla_{\boldsymbol{\xi}} f. \tag{10}$$

Here, ∇ is shown to be a sum of two differential operators in space: $\nabla_{\mathbf{x}}$ and $\nabla_{\boldsymbol{\xi}}$, which scale with $1/\hat{\mathcal{L}}$ and $1/\hat{\ell}$, respectively.

We now assume $\epsilon \ll 1$ and consider systems with spatial periodicity on the length scale $\hat{\ell}$. Under these constraints, we treat $\boldsymbol{\xi}(\mathbf{x})$ as an independent variable $\boldsymbol{\xi}$, uncoupled from $\mathbf{x}$, that traverses a spatially periodic "unit-cell" domain Y. This domain consists of a pore-space region $\mathcal{B}$ and an impermeable solid region $\mathcal{G}$. A smooth interface $\Gamma = \cup_{j=1}^{N_\Gamma}\Gamma^{(j)}$ consisting of N_Γ subsections $\Gamma^{(j)}$ exists within Y between $\mathcal{B}$ and $\mathcal{G}$. Finally, we note that regions $\mathcal{B}$ and $\mathcal{G}$ should be arranged within Y such that a collection of contiguously placed unit-cell domains Y is representative of how $\hat{\mathcal{B}}_\epsilon$ and $\hat{\mathcal{G}}_\epsilon$ are arranged within $\hat{\Omega}_\epsilon$.

With the provided unit-cell formulation, our intention is to average the reactive transport and fluid flow over the unit-cell domain (Bachmat & Bear, 1986). To do this, we reconsider $\mathbf{x}$ as an element of $\Omega \equiv \Omega_\epsilon = \hat{\Omega}_\epsilon/\hat{\mathcal{L}}^b$, a fictitious model domain treated as an "$\hat{\ell}$-averaged" continuum, and define averaging operators over the unit-cell Y, its pore-space $\mathcal{B}$, the total liquid-solid interface Γ, and the liquid-solid interface subsections $\Gamma^{(j)}$ as

$$\begin{gathered}\langle\cdot\rangle_Y \equiv \frac{1}{|Y|}\int_{\mathcal{B}}(\cdot)\ d\boldsymbol{\xi}, \quad \langle\cdot\rangle_{\mathcal{B}} \equiv \frac{1}{|\mathcal{B}|}\int_{\mathcal{B}}(\cdot)\ d\boldsymbol{\xi}, \quad \langle\cdot\rangle_{\Gamma} \equiv \frac{1}{|\Gamma|}\int_{\Gamma}(\cdot)\ d\boldsymbol{\xi}, \\ \text{and} \quad \langle\cdot\rangle_{\Gamma^{(j)}} \equiv \frac{1}{\left|\Gamma^{(j)}\right|}\int_{\Gamma^{(j)}}(\cdot)\ d\boldsymbol{\xi},\end{gathered} \tag{11}$$

respectively. Depending on b, $|Y|$, $|\mathcal{B}|$, $|\Gamma|$, and $|\Gamma^{(j)}|$ are the volumes, areas, segments, or points of the unit-cell, the pore-space in the unit-cell, the liquid-solid interface in the unit-cell, and the liquid-solid interface subsections in the unit-cell, respectively. Here, we also define $\phi = |\mathcal{B}|/|Y|$ as the porosity of the unit-cell and note that $\langle\cdot\rangle_{\mathcal{B}} = \phi^{-1}\langle\cdot\rangle_Y$.

2.4 Expansions of the Temporal Derivative and Dependent Variables

Similar to the handling of multiple spatial scales, we introduce additional time variables to account for the dynamics occurring on small time scales. Typically, these time variables are introduced based on the dimensionless numbers related to advective and reactive time scales (i.e., Péclet and Damköhler numbers) (Rubinstein & Mauri, 1986; Mei, 1992; Salles et al., 1993; Auriault & Adler, 1995; Battiato & Tartakovsky, 2011; Boso & Battiato, 2013), as these are often the only physical mechanisms appearing in the governing equations besides diffusion. Here, however, we explicitly define the time variables $\tau_m(t) = \epsilon^{-m}t$, where $m \in \{1, 2\}$, to introduce a temporal derivative at each equation order considered during our homogenization procedure. This allows us to clarify the assumptions implied when not considering additional time scales, and ultimately remove ambiguity in the role of additional time scales in the homogenization procedure. We note that while further time variables may be defined in this manner, the time variables introduced here are sufficient for analyzing all small time scale dynamics in our analysis. Any temporally-dependent function $f_\epsilon(t)$ is then written as $f_\epsilon(t) = f(t, \boldsymbol{\tau}(t))$, where $\boldsymbol{\tau}(t)$ is a tuple with components $[\boldsymbol{\tau}(t)]_m = \tau_m(t)$, and the total differential operator in time takes the form

$$\frac{\partial f_\epsilon}{\partial t} \equiv \frac{\partial f}{\partial t} + \epsilon^{-1}\frac{\partial f}{\partial \tau_1} + \epsilon^{-2}\frac{\partial f}{\partial \tau_2}. \tag{12}$$

While simultaneously considering the independent variables in space, dependent variables $c_\epsilon^{(i)}(t,\mathbf{x})$ and $\mathbf{u}_\epsilon(\mathbf{x})$ are now redefined as functions of $\boldsymbol{\xi}$ and $\boldsymbol{\tau}(t)$, and expanded as power series in terms of ϵ such that

$$c_\epsilon^{(i)}(t,\mathbf{x}) \equiv c^{(i)}(t,\mathbf{x},\boldsymbol{\tau}(t),\boldsymbol{\xi}) = \sum_{k=0}^{\infty}\epsilon^k c_k^{(i)}(t,\mathbf{x},\boldsymbol{\tau}(t),\boldsymbol{\xi}), \tag{13a}$$

$$\mathbf{u}_\epsilon(\mathbf{x}) \equiv \mathbf{u}(\mathbf{x},\boldsymbol{\xi}) = \sum_{k=0}^{\infty}\epsilon^k \mathbf{u}_k(\mathbf{x},\boldsymbol{\xi}), \tag{13b}$$

where $c_k^{(i)}(t,\mathbf{x},\boldsymbol{\tau}(t),\boldsymbol{\xi})$ and $\mathbf{u}_k(\mathbf{x},\boldsymbol{\xi})$ are assumed to be periodic in $\boldsymbol{\xi}$.

3 Linear Heterogeneous Reaction: One Species

We now demonstrate our strategy for generalizing the closure form by homogenizing the mass transport of a single species undergoing a linear heterogeneous reaction. We note that a similar problem setup may be found in previous analyses (Pietrzyk et al., 2021; Battiato & Tartakovsky, 2011). While a detailed outline of the applied strategy can be found in Appendix A, we provide a brief description of the problem and homogenized results here. We consider the reactive transport of a single species, whose concentration c_ϵ is governed by

$$\frac{\partial c_\epsilon}{\partial t} + \nabla\cdot(\mathrm{Pe}\mathbf{u}_\epsilon c_\epsilon - D\nabla c_\epsilon) = 0 \quad \text{in } \mathcal{B}_\epsilon, \tag{14a}$$

subject to

$$-\mathbf{n}\cdot D\nabla c_\epsilon = \mathrm{Da}(c_\epsilon - \theta) \quad \text{on } \Gamma_\epsilon, \tag{14b}$$

where the Péclet number Pe, Damköhler number Da, and concentration ratio θ are defined as

$$\mathrm{Pe} = \frac{\hat{\mathcal{U}}\hat{\mathcal{L}}}{\hat{\mathcal{D}}}, \quad \mathrm{Da} = \frac{\hat{\mathcal{K}}\hat{\mathcal{L}}}{\hat{\mathcal{D}}}, \quad \theta = \frac{\hat{C}}{\hat{\mathcal{C}}}. \tag{15}$$

System (14) can be obtained from the general mass transport problem in system (7) by letting $N = 1$, $N_\Gamma = 1$, $i \in \{1\}$, $j \in \{1\}$, $R_\epsilon^{(i)} = 0$, $p_{SL}^{(i,j,k)} = 0$, and $\mathrm{Da}_{SNL}^{(i,j,k,l)} = 0$, and simplifying the notation of the remaining variables to $\{c_\epsilon^{(1)},\ \hat{\mathcal{C}}^{(1)},\ D^{(1)},\ \Gamma_\epsilon^{(1)},\ \mathbf{n}^{(1)},\ \mathrm{Da}_{SL}^{(1,1,1)},\ \hat{\mathcal{K}}_{SL}^{(1,1,1)},\ \theta_{SL}^{(1,1,1)},\ \hat{C}_{SL}^{(1,1,1)}\} = \{c_\epsilon,\ \hat{\mathcal{C}},\ D,\ \Gamma_\epsilon,\ \mathbf{n},\ \mathrm{Da},\ \hat{\mathcal{K}},\ \theta,\ \hat{C}\}$.

We homogenize the system for a moderately reactive case, where diffusive and reactive terms are of similar order, i.e.,

$$\mathrm{Pe} \sim \mathcal{O}(\epsilon^{-1}), \quad \mathrm{Da} \sim \mathcal{O}(\epsilon^0), \quad \theta \sim \mathcal{O}(\epsilon^0). \tag{16}$$

As highlighted in the work of Municchi and Icardi (Municchi & Icardi, 2020), the classical treatment for systems involving heterogeneous reactions is limited to slow reaction rates (i.e., $\mathrm{Da} \leq \mathcal{O}(\epsilon)$), and therefore, cannot be used to homogenize this physical scenario. We also note that a large advective term is considered, but we recover the diffusion-reaction model studied in Bourbatache *et al.* (Bourbatache et al., 2020) by letting $\mathrm{Pe} = 0$ and $\theta = 0$.

3.1 Homogenized Results

With the provided formulation, we show in Appendix A that a homogenized system for $\langle c\rangle_Y = \langle c_0\rangle_Y + \epsilon\langle c_1\rangle_Y + \mathcal{O}(\epsilon^2)$ can be derived for the moderately reactive case with $\mathcal{O}(\epsilon)$ error using the closure form

$$c_1 = \boldsymbol{\chi}^{[1]}\cdot\nabla_{\mathbf{x}} c_0 + (c_0 - \theta)\,\chi^{[2]} + \bar{c}_1, \tag{17}$$

instead of the more classical postulate

$$c_1 = \boldsymbol{\chi} \cdot \nabla_{\mathbf{x}} c_0 + \overline{c}_1, \tag{18}$$

where $\overline{c}_1 \equiv \overline{c}_1(t, \mathbf{x}, \boldsymbol{\tau}(t)) = \phi^{-1}\langle c_1 \rangle_Y$, and $\boldsymbol{\chi}^{[1]}$ and $\chi^{[2]}$ are the closure variables. The resulting homogenized equation is written as

$$\phi \frac{\partial \langle c \rangle_Y}{\partial t} + \mathbf{U} \cdot \nabla_{\mathbf{x}} \langle c \rangle_Y - \nabla_{\mathbf{x}} \cdot (\mathbf{D} \cdot \nabla_{\mathbf{x}} \langle c \rangle_Y) + \mathscr{R} \left(\phi \langle c \rangle_Y - \phi^2 \theta \right) = \mathcal{O}(\epsilon) \quad \text{for } \mathbf{x} \in \Omega, \tag{19a}$$

where the effective parameters are defined as

$$\mathbf{U} = \mathrm{Pe} \langle \mathbf{u} \rangle_Y + \phi \mathrm{Da} \frac{|\Gamma|}{|\mathcal{B}|} \langle \boldsymbol{\chi}^{[1]} \rangle_\Gamma - D \langle \nabla_{\boldsymbol{\xi}} \chi^{[2]} \rangle_Y + \mathrm{Pe}\epsilon \langle \mathbf{u} \chi^{[2]} \rangle_Y, \tag{19b}$$

$$\mathbf{D} = \phi D \mathbf{I} + D \langle \nabla_{\boldsymbol{\xi}} \boldsymbol{\chi}^{[1]} \rangle_Y - \mathrm{Pe}\epsilon \langle \mathbf{u} \otimes \boldsymbol{\chi}^{[1]} \rangle_Y, \tag{19c}$$

$$\mathscr{R} = \mathrm{Da} \frac{|\Gamma|}{|\mathcal{B}|} \left[\epsilon^{-1} + \langle \chi^{[2]} \rangle_\Gamma \right]. \tag{19d}$$

In system (19), the closure variables are found by solving the closure problems

$$\mathrm{Pe}\epsilon \left(\mathbf{u}_0 - \langle \mathbf{u}_0 \rangle_{\mathcal{B}} \right) + \mathrm{Pe}\epsilon \mathbf{u}_0 \cdot \nabla_{\boldsymbol{\xi}} \boldsymbol{\chi}^{[1]} - D \nabla_{\boldsymbol{\xi}} \cdot \left(\mathbf{I} + \nabla_{\boldsymbol{\xi}} \boldsymbol{\chi}^{[1]} \right) = \mathbf{0} \quad \text{for } \boldsymbol{\xi} \in \mathcal{B}, \tag{20a}$$

subject to

$$-\mathbf{n} \cdot D \left(\mathbf{I} + \nabla_{\boldsymbol{\xi}} \boldsymbol{\chi}^{[1]} \right) = \mathbf{0} \quad \text{for } \boldsymbol{\xi} \in \Gamma, \tag{20b}$$

and

$$-\mathrm{Da} \frac{|\Gamma|}{|\mathcal{B}|} + \mathrm{Pe}\epsilon \mathbf{u}_0 \cdot \nabla_{\boldsymbol{\xi}} \chi^{[2]} - D \nabla^2_{\boldsymbol{\xi}} \chi^{[2]} = 0 \quad \text{for } \boldsymbol{\xi} \in \mathcal{B}, \tag{21a}$$

subject to

$$-\mathbf{n} \cdot D \nabla_{\boldsymbol{\xi}} \chi^{[2]} = \mathrm{Da} \quad \text{for } \boldsymbol{\xi} \in \Gamma. \tag{21b}$$

Here, $\langle \boldsymbol{\chi}^{[1]} \rangle_{\mathcal{B}} = \mathbf{0}$ and $\langle \chi^{[2]} \rangle_{\mathcal{B}} = 0$. As shown, by generalizing the assumed closure form of c_1, valid closure problems can be created in scenarios where the traditionally assumed closure form (equation (18)) fails. While an additional closure problem needs to be solved, virtually no mathematical complexity is added to the classical homogenization theory through this strategy.

Upon analyzing the homogenized equation and effective parameters, we find contributions due to the moderate reaction rate in both the effective reaction rate $\mathscr{R}$ and effective velocity $\mathbf{U}$. We notice the product between ϕ and the first term in $\mathscr{R}$ exactly matches the effective reaction rate previously derived for slow heterogeneous reactions (i.e., $\mathrm{Da} \sim \mathcal{O}(\epsilon)$) (Battiato & Tartakovsky, 2011; Boso & Battiato, 2013). As detailed in Appendix A, the second term in $\mathscr{R}$, which contains $\langle \chi^{[2]} \rangle_\Gamma$, acts as the first correction to the effective reaction rate. In light of closure problem in system (21), this correction modifies the effective reaction rate based on the microscopic geometry and high advective flux. Regarding the effective velocity $\mathbf{U}$, three contributions are made due to the moderate reaction rate. This coincides with the results of previous analyses showing reaction-dependent effective velocities (Mikelić et al., 2006). We note that contributions $-D\langle \nabla_{\boldsymbol{\xi}} \chi^{[2]} \rangle_Y$ and $\mathrm{Pe}\epsilon \langle \mathbf{u} \chi^{[2]} \rangle_Y$ are similar to the contributions in the dispersion tensor involving $\boldsymbol{\chi}^{[1]}$ (i.e., $D\langle \nabla_{\boldsymbol{\xi}} \boldsymbol{\chi}^{[1]} \rangle_Y$ and $-\mathrm{Pe}\epsilon \langle \mathbf{u} \otimes \boldsymbol{\chi}^{[1]} \rangle_Y$). Therefore, $-D\langle \nabla_{\boldsymbol{\xi}} \chi^{[2]} \rangle_Y$ and $\mathrm{Pe}\epsilon \langle \mathbf{u} \chi^{[2]} \rangle_Y$ are interpreted analogously as contributions that account for the interactions between (i) the effective reaction

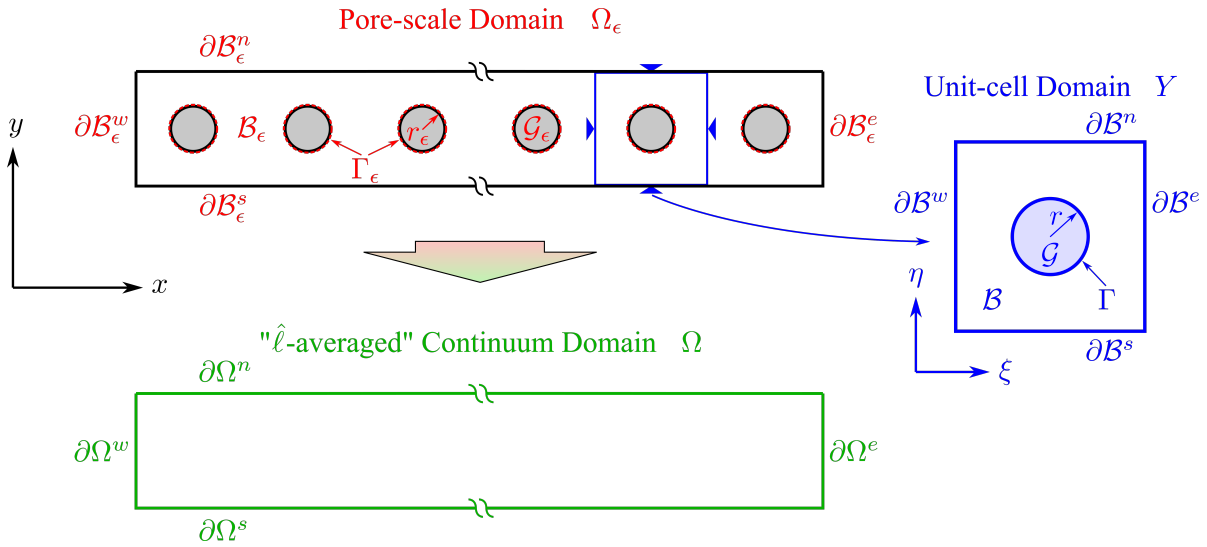

Figure 1. A schematic of the 2D pore-scale, unit-cell, and continuum domains considered for the array of cylinders geometry. Details of the labeled geometric aspects are found in Table 1.

rate correction and the diffusive flux, and (ii) the effective reaction rate correction and the advective flux, respectively. Finally, the third contribution to the effective velocity, $\phi \mathrm{Da} \frac{|\Gamma|}{|\mathcal{B}|} \langle \boldsymbol{\chi}^{[1]} \rangle_\Gamma$, represents the additional reactive flux due to the diffusion flux correction.

We emphasize that the effective velocity remains in the homogenized equation, even if $\mathrm{Pe} = 0$ and $\theta = 0$. Further, the remaining terms in the effective velocity (i.e., $\phi \mathrm{Da} \frac{|\Gamma|}{|\mathcal{B}|} \langle \boldsymbol{\chi}^{[1]} \rangle_\Gamma$ and $-D \langle \nabla_{\boldsymbol{\xi}} \chi^{[2]} \rangle_Y$) represent a coupling between diffusion and reaction, even though the effective reaction rate does not depend on diffusion, and the dispersion tensor does not depend on reaction. This early onset of coupling between diffusion and reaction causes the macroscopic equations to not simply consist of terms similar to those in the microscopic equations, a case warned about in the work of Iliev *et al.* (Iliev et al., 2020). These results advise caution when assuming the form of macroscopic equations to be similar to their microscopic counterparts.

3.2 Numerical Validation

3.2.1 Problem Setup

We now provide validation for the homogenized model derived using the generalized closure form strategy by numerically resolving and comparing the averaged solutions from the pore-scale (system (14)) and homogenized (systems (19), (20), and (21)) models.

To conduct the validation, we consider a 2D array of cylinders geometry in a Cartesian plane (i.e., $\mathbf{x} \equiv [x, y]$ and $\boldsymbol{\xi} \equiv [\xi, \eta]$). Schematics of the considered pore-scale, unit-cell, and continuum domains can be found in Figure 1 with relevant geometric labels, which are detailed in Table 1. We also consider an initial discontinuous concentration profile in the pore-scale simulation, where the concentration is alternatively equal to 0 and 1 in the two halves of the domain. To obtain the corresponding initial condition for the homogenized model, we average the pore-scale initial condition using the averaging operator

$$\langle \cdot \rangle_{\mathcal{W}_\epsilon(\mathbf{x})} \equiv \epsilon^{-2} \frac{1}{|Y|} \int_{\mathcal{W}_\epsilon(\mathbf{x})} (\cdot) \, d\mathbf{y}, \tag{22a}$$

where

$$\mathcal{W}_\epsilon(\mathbf{x}) = \{(x', y') : x - 0.5\epsilon < x' < x + 0.5\epsilon, \; y + 0.5\epsilon < y' < y - 0.5\epsilon, \; \mathbf{x}' \in \mathcal{B}_\epsilon\} \quad \text{for } \mathbf{x} \in \Omega. \tag{22b}$$

Table 1. Specifications for the geometric aspects in the pore-scale, unit-cell, and continuum domains considering the 2D array of cylinders geometry.

Variable	Definition for the 2D Array of Cylinders Geometry
	Dimensional Parameters
$\hat{\ell}$	Unit-cell domain length
$\hat{\mathcal{L}}$	Pore-scale domain length
$\hat{r}_\epsilon$	Cylinder radius
	Pore-scale Domain
r_ϵ	$\hat{r}_\epsilon/\hat{\mathcal{L}}$
Ω_ϵ	$\{(x,y) : -0.5 < x < 0.5,\ -0.5\epsilon < y < 0.5\epsilon\}$
$\mathcal{G}_\epsilon$	$\{(x,y) : (x + 0.5\,(1+\epsilon) - m\epsilon)^2 + y^2 < r_\epsilon^2,\ m \in \mathbb{Z}^+,\ m \leq \epsilon^{-1}\}$
Γ_ϵ	$\{(x,y) : (x + 0.5\,(1+\epsilon) - m\epsilon)^2 + y^2 = r_\epsilon^2,\ m \in \mathbb{Z}^+,\ m \leq \epsilon^{-1}\}$
$\mathcal{B}_\epsilon$	$\Omega_\epsilon \setminus (\mathcal{G}_\epsilon \cup \Gamma_\epsilon)$
$\partial\mathcal{B}_\epsilon^w$	$\{(x,y) : x = -0.5,\ -0.5\epsilon < y < 0.5\epsilon\}$
$\partial\mathcal{B}_\epsilon^e$	$\{(x,y) : x = 0.5,\ -0.5\epsilon < y < 0.5\epsilon\}$
$\partial\mathcal{B}_\epsilon^s$	$\{(x,y) : -0.5 < x < 0.5,\ y = -0.5\epsilon\}$
$\partial\mathcal{B}_\epsilon^n$	$\{(x,y) : -0.5 < x < 0.5,\ y = 0.5\epsilon\}$
	Unit-cell Domain
r	$\hat{r}_\epsilon/\hat{\ell}$
Y	$\{(\xi,\eta) : -0.5 < \xi < 0.5,\ -0.5 < \eta < 0.5\}$
$\mathcal{G}$	$\{(\xi,\eta) : \xi^2 + \eta^2 < r^2\}$
Γ	$\{(\xi,\eta) : \xi^2 + \eta^2 = r^2\}$
$\mathcal{B}$	$\Omega \setminus (\mathcal{G} \cup \Gamma)$
$\partial\mathcal{B}^w$	$\{(\xi,\eta) : \xi = -0.5,\ -0.5 < \eta < 0.5\}$
$\partial\mathcal{B}^e$	$\{(\xi,\eta) : \xi = 0.5,\ -0.5 < \eta < 0.5\}$
$\partial\mathcal{B}^s$	$\{(\xi,\eta) : -0.5 < \xi < 0.5,\ \eta = -0.5\}$
$\partial\mathcal{B}^n$	$\{(\xi,\eta) : -0.5 < \xi < 0.5,\ \eta = 0.5\}$
$\lvert Y\rvert$	1
$\lvert\mathcal{G}\rvert$	πr^2
$\lvert\Gamma\rvert$	$2\pi r$
$\lvert\mathcal{B}\rvert$	$\lvert Y\rvert - \lvert\mathcal{G}\rvert$
ϕ	$\lvert\mathcal{B}\rvert \,/\, \lvert Y\rvert$
	"$\hat{\ell}$-averaged" Continuum Domain
Ω	$\{(x,y) : -0.5 < x < 0.5,\ -0.5\epsilon < y < 0.5\epsilon\}$
$\partial\Omega^w$	$\{(x,y) : x = -0.5,\ -0.5\epsilon < y < 0.5\epsilon\}$
$\partial\Omega^e$	$\{(x,y) : x = 0.5,\ -0.5\epsilon < y < 0.5\epsilon\}$
$\partial\Omega^s$	$\{(x,y) : -0.5 < x < 0.5,\ y = -0.5\epsilon\}$
$\partial\Omega^n$	$\{(x,y) : -0.5 < x < 0.5,\ y = 0.5\epsilon\}$

Table 2. The simulation and mesh parameters used to solve the various models and problems defined on the pore-scale, unit-cell, and continuum domains for the single species system undergoing a linear heterogeneous reaction. Here, $\mathbf{e}_x$ and $\mathbf{e}_\xi$ are the unit vectors in the x-direction and ξ-direction, respectively.

Simulation and Mesh Parameters
General Parameters
$\epsilon = 0.1, \quad D = 1, \quad \mathrm{Pe} = \epsilon^{-1}, \quad \mathrm{Da} = \epsilon^0, \quad \theta = \epsilon^0, \quad \Delta t = 10^{-4}$
Pore-scale Fluid Flow and Mass Transport
$r_\epsilon = 0.02, \quad A_\epsilon = \epsilon^2, \quad \Phi_\epsilon = 8\mathbf{e}_x, \quad N_{elem} = 38287, \quad \max(\Delta x) = 0.0036$
Homogenized Mass Transport
$\phi = 0.8744, \quad N_{elem} = 4006, \quad \max(\Delta x) = 0.0113$
Unit-cell Fluid Flow and Closure Problems
$r = 0.2, \quad A = 1, \quad \Phi = 8\mathbf{e}_\xi, \quad N_{elem} = 44413, \quad \max(\Delta \xi) = 0.0099$

This averaging operator can be considered a "moving-average" that brings pore-scale concentration fields into the continuum domain. We note that the extension of this operator at points near the edges of the continuum domain is trivial when using periodic boundary conditions, as will be considered here. Further details regarding the simulation parameters are provided in Table 2, while details regarding the boundary conditions and initial conditions are provided in Table 3. All numerical calculations are completed using FEniCS, an open-source finite element software (Logg et al., 2012; Alnaes et al., 2015). To minimize the potential for under-resolved results, the spatial and temporal discretizations are refined to show converged solutions to plotting accuracy, and second-order elements are used. Further details regarding the discretizations of each mesh, including the number of elements N_{elem} and maximum spacing between vertices $[\max(\Delta x), \max(\Delta \xi)]$, are presented with the other simulation parameters in Table 2.

To obtain fluid velocity and pressure fields for the pore-scale model, system (6) is resolved for $A_\epsilon = \epsilon^2$, the same value considered in the classical homogenization of the Stokes equation (Auriault & Adler, 1995). To drive the flow, we allow the pressure gradient to be represented as $\nabla p_\epsilon = \Phi_\epsilon + \nabla \tilde{p}_\epsilon$, where Φ_ϵ is physically interpreted as a known, large-scale pressure gradient across the pore-scale domain and $\nabla \tilde{p}_\epsilon$ is interpreted as the gradient of an unknown local pressure field. By choosing an appropriate value for Φ_ϵ, the flow fields $\mathbf{u}_\epsilon$ and $\tilde{p}_\epsilon$ can be solved for such that $|\mathbf{u}_\epsilon| \sim \mathcal{O}(1)$. This ultimately verifies that the value of $\hat{\mathcal{U}}$ calculated using the definition of the Péclet number in equation (15) is consistent with the magnitude of the flow driven by Φ_ϵ.

For the homogenized model, the equations governing fluid flow are directly taken from the classical homogenization of the Stokes equation (equation (20) in (Auriault & Adler, 1995)) and written as

$$A\nabla^2_{\boldsymbol{\xi}}\mathbf{u} - \nabla_{\boldsymbol{\xi}}\tilde{p} - \Phi = \mathbf{0} \quad \text{for } \boldsymbol{\xi} \in \mathcal{B}, \tag{23a}$$

$$\nabla_{\boldsymbol{\xi}} \cdot \mathbf{u} = 0 \quad \text{for } \boldsymbol{\xi} \in \mathcal{B}, \tag{23b}$$

subject to

$$\mathbf{u} = \mathbf{0} \quad \text{for } \boldsymbol{\xi} \in \Gamma, \tag{23c}$$

where we let $A = 1$ and Φ is physically interpreted as a known, large-scale pressure gradient across the unit-cell domain. We note that the flow driven in the unit-cell domain by Φ should be reflective of that driven in the pore-scale domain by Φ_ϵ, i.e., $\Phi = \Phi_\epsilon$. Upon solving system (23) in the unit-cell domain, the velocity field $\mathbf{u}$ can be averaged over the unit-cell and used to calculate the effective parameters (equations (19b)-(19d)).

Table 3. The simulation boundary conditions and initial conditions used to solve the various problems on the pore-scale, unit-cell, and continuum domains for the single species system undergoing a linear heterogeneous reaction. Here, $H(x)$ is the Heaviside function.

Simulation Boundary Conditions

Pore-scale Mass Transport

$$c_\epsilon|_{\partial\mathcal{B}_\epsilon^w} = c_\epsilon|_{\partial\mathcal{B}_\epsilon^e} \qquad \mathbf{n}\cdot\nabla c_\epsilon|_{\partial\mathcal{B}_\epsilon^w} = -\mathbf{n}\cdot\nabla c_\epsilon|_{\partial\mathcal{B}_\epsilon^e}$$
$$c_\epsilon|_{\partial\mathcal{B}_\epsilon^s} = c_\epsilon|_{\partial\mathcal{B}_\epsilon^n} \qquad \mathbf{n}\cdot\nabla c_\epsilon|_{\partial\mathcal{B}_\epsilon^s} = -\mathbf{n}\cdot\nabla c_\epsilon|_{\partial\mathcal{B}_\epsilon^n}$$

Pore-scale Fluid Flow

$$\mathbf{u}_\epsilon|_{\partial\mathcal{B}_\epsilon^w} = \mathbf{u}_\epsilon|_{\partial\mathcal{B}_\epsilon^e} \qquad \mathbf{n}\cdot\nabla\mathbf{u}_\epsilon|_{\partial\mathcal{B}_\epsilon^w} = -\mathbf{n}\cdot\nabla\mathbf{u}_\epsilon|_{\partial\mathcal{B}_\epsilon^e}$$
$$\mathbf{u}_\epsilon|_{\partial\mathcal{B}_\epsilon^s} = \mathbf{u}_\epsilon|_{\partial\mathcal{B}_\epsilon^n} \qquad \mathbf{n}\cdot\nabla\mathbf{u}_\epsilon|_{\partial\mathcal{B}_\epsilon^s} = -\mathbf{n}\cdot\nabla\mathbf{u}_\epsilon|_{\partial\mathcal{B}_\epsilon^n}$$
$$\tilde{p}_\epsilon|_{\partial\mathcal{B}_\epsilon^w} = \tilde{p}_\epsilon|_{\partial\mathcal{B}_\epsilon^e} \qquad \mathbf{n}\cdot\nabla\tilde{p}_\epsilon|_{\partial\mathcal{B}_\epsilon^w} = -\mathbf{n}\cdot\nabla\tilde{p}_\epsilon|_{\partial\mathcal{B}_\epsilon^e}$$
$$\tilde{p}_\epsilon|_{\partial\mathcal{B}_\epsilon^s} = \tilde{p}_\epsilon|_{\partial\mathcal{B}_\epsilon^n} \qquad \mathbf{n}\cdot\nabla\tilde{p}_\epsilon|_{\partial\mathcal{B}_\epsilon^s} = -\mathbf{n}\cdot\nabla\tilde{p}_\epsilon|_{\partial\mathcal{B}_\epsilon^n}$$

Homogenized Mass Transport

$$\langle c\rangle_Y|_{\partial\Omega^w} = \langle c\rangle_Y|_{\partial\Omega^e} \qquad \mathbf{n}\cdot\nabla_{\mathbf{x}}\langle c\rangle_Y|_{\partial\Omega^w} = -\mathbf{n}\cdot\nabla_{\mathbf{x}}\langle c\rangle_Y|_{\partial\Omega^e}$$
$$\langle c\rangle_Y|_{\partial\Omega^s} = \langle c\rangle_Y|_{\partial\Omega^n} \qquad \mathbf{n}\cdot\nabla_{\mathbf{x}}\langle c\rangle_Y|_{\partial\Omega^s} = -\mathbf{n}\cdot\nabla_{\mathbf{x}}\langle c\rangle_Y|_{\partial\Omega^n}$$

Closure Problems

$$\boldsymbol{\chi}^{[1]}\big|_{\partial\mathcal{B}^w} = \boldsymbol{\chi}^{[1]}\big|_{\partial\mathcal{B}^e} \qquad \mathbf{n}\cdot\nabla_{\boldsymbol{\xi}}\boldsymbol{\chi}^{[1]}\big|_{\partial\mathcal{B}^w} = -\mathbf{n}\cdot\nabla_{\boldsymbol{\xi}}\boldsymbol{\chi}^{[1]}\big|_{\partial\mathcal{B}^e}$$
$$\boldsymbol{\chi}^{[1]}\big|_{\partial\mathcal{B}^s} = \boldsymbol{\chi}^{[1]}\big|_{\partial\mathcal{B}^n} \qquad \mathbf{n}\cdot\nabla_{\boldsymbol{\xi}}\boldsymbol{\chi}^{[1]}\big|_{\partial\mathcal{B}^s} = -\mathbf{n}\cdot\nabla_{\boldsymbol{\xi}}\boldsymbol{\chi}^{[1]}\big|_{\partial\mathcal{B}^n}$$
$$\chi^{[2]}\big|_{\partial\mathcal{B}^w} = \chi^{[2]}\big|_{\partial\mathcal{B}^e} \qquad \mathbf{n}\cdot\nabla_{\boldsymbol{\xi}}\chi^{[2]}\big|_{\partial\mathcal{B}^w} = -\mathbf{n}\cdot\nabla_{\boldsymbol{\xi}}\chi^{[2]}\big|_{\partial\mathcal{B}^e}$$
$$\chi^{[2]}\big|_{\partial\mathcal{B}^s} = \chi^{[2]}\big|_{\partial\mathcal{B}^n} \qquad \mathbf{n}\cdot\nabla_{\boldsymbol{\xi}}\chi^{[2]}\big|_{\partial\mathcal{B}^s} = -\mathbf{n}\cdot\nabla_{\boldsymbol{\xi}}\chi^{[2]}\big|_{\partial\mathcal{B}^n}$$

Unit-cell Fluid Flow

$$\mathbf{u}|_{\partial\mathcal{B}^w} = \mathbf{u}|_{\partial\mathcal{B}^e} \qquad \mathbf{n}\cdot\nabla_{\boldsymbol{\xi}}\mathbf{u}|_{\partial\mathcal{B}^w} = -\mathbf{n}\cdot\nabla_{\boldsymbol{\xi}}\mathbf{u}|_{\partial\mathcal{B}^e}$$
$$\mathbf{u}|_{\partial\mathcal{B}^s} = \mathbf{u}|_{\partial\mathcal{B}^n} \qquad \mathbf{n}\cdot\nabla_{\boldsymbol{\xi}}\mathbf{u}|_{\partial\mathcal{B}^s} = -\mathbf{n}\cdot\nabla_{\boldsymbol{\xi}}\mathbf{u}|_{\partial\mathcal{B}^n}$$
$$\tilde{p}|_{\partial\mathcal{B}^w} = \tilde{p}|_{\partial\mathcal{B}^e} \qquad \mathbf{n}\cdot\nabla_{\boldsymbol{\xi}}\tilde{p}|_{\partial\mathcal{B}^w} = -\mathbf{n}\cdot\nabla_{\boldsymbol{\xi}}\tilde{p}|_{\partial\mathcal{B}^e}$$
$$\tilde{p}|_{\partial\mathcal{B}^s} = \tilde{p}|_{\partial\mathcal{B}^n} \qquad \mathbf{n}\cdot\nabla_{\boldsymbol{\xi}}\tilde{p}|_{\partial\mathcal{B}^s} = -\mathbf{n}\cdot\nabla_{\boldsymbol{\xi}}\tilde{p}|_{\partial\mathcal{B}^n}$$

Simulation Initial Conditions

Pore-scale Mass Transport	Homogenized Mass Transport
$c_\epsilon = H(-x) \quad \text{for} \quad (x,y)\in\mathcal{B}_\epsilon,\ t=0$	$\langle c\rangle_Y = \langle c_\epsilon\rangle_{\mathcal{W}_\epsilon(\mathbf{x})} \quad \text{for} \quad (x,y)\in\Omega,\ t=0$

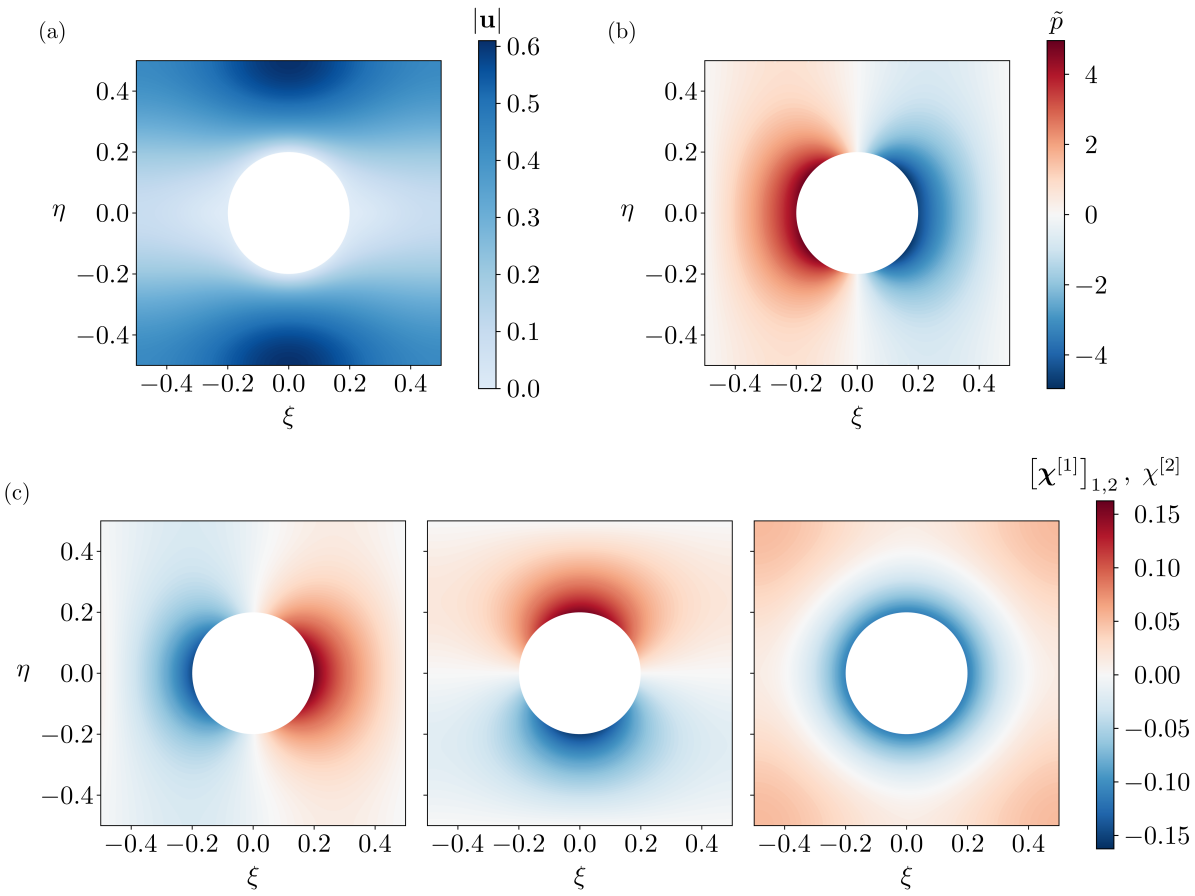

Figure 2. The numerical results of the flow and closure problems in the unit-cell for the single species system undergoing a linear heterogeneous reaction. (a) The magnitude of the resulting flow velocity in the unit-cell. (b) The local pressure of the resulting flow in the unit-cell. (c) The resulting closure solutions $\boldsymbol{\chi}^{[1]}$ and $\chi^{[2]}$. From left to right: $[\boldsymbol{\chi}^{[1]}]_1$ the ξ-component of $\boldsymbol{\chi}^{[1]}$, $[\boldsymbol{\chi}^{[1]}]_2$ the η-component of $\boldsymbol{\chi}^{[1]}$, and $\chi^{[2]}$.

3.2.2 Flow and Closure Problem Results

Prior to solving the homogenized model, solutions to the flow and closure problems must be obtained. The flow problem described in system (6) is solved on the pore-scale domain, and system (23) on the unit-cell domain. The resulting flow velocity magnitude $|\mathbf{u}|$ and local pressure $\tilde{p}$ contours are found in Figures 2(a) and 2(b), respectively. As shown in Figure 2(a), the choice of $\Phi = 8\mathbf{e}_\xi$ (Table 2) is suitable for the current problem due to $|\mathbf{u}| \sim \mathcal{O}(1)$. We also note that only the flow fields in the unit-cell domain are presented, as the pore-scale flow fields result in contiguously placed unit-cell flow fields due to the periodicity of the pore-scale domain. Therefore, no new information is provided by the pore-scale flow fields. Regarding the closure problems, systems (20) and (21) are solved on the unit-cell domain, and the resulting components of $\boldsymbol{\chi}^{[1]}$, $[\boldsymbol{\chi}^{[1]}]_1$ and $[\boldsymbol{\chi}^{[1]}]_2$, are plotted alongside $\chi^{[2]}$ in Figure 2(c). As shown, the contour of $\chi^{[2]}$ has a different appearance than $[\boldsymbol{\chi}^{[1]}]_1$ and $[\boldsymbol{\chi}^{[1]}]_2$, but maintains a similar magnitude for the considered geometry.

3.2.3 Pore-scale and Homogenized Model Results

With the solutions to the closure and flow problems, the pore-scale (system (14)) and homogenized (systems (19), (20), and (21)) models are solved using the simulation parameters, boundary conditions, and initial conditions provided in Tables 2 and 3. Then, the pore-scale solution c_ϵ is averaged using the averaging operator in equation (22a) to obtain the averaged pore-scale solution $\langle c_\epsilon \rangle_{\mathcal{W}_\epsilon(\mathbf{x})}$. To quantitatively compare $\langle c_\epsilon \rangle_{\mathcal{W}_\epsilon(\mathbf{x})}$ to the homogenized solution $\langle c \rangle_Y$, we define the absolute error function

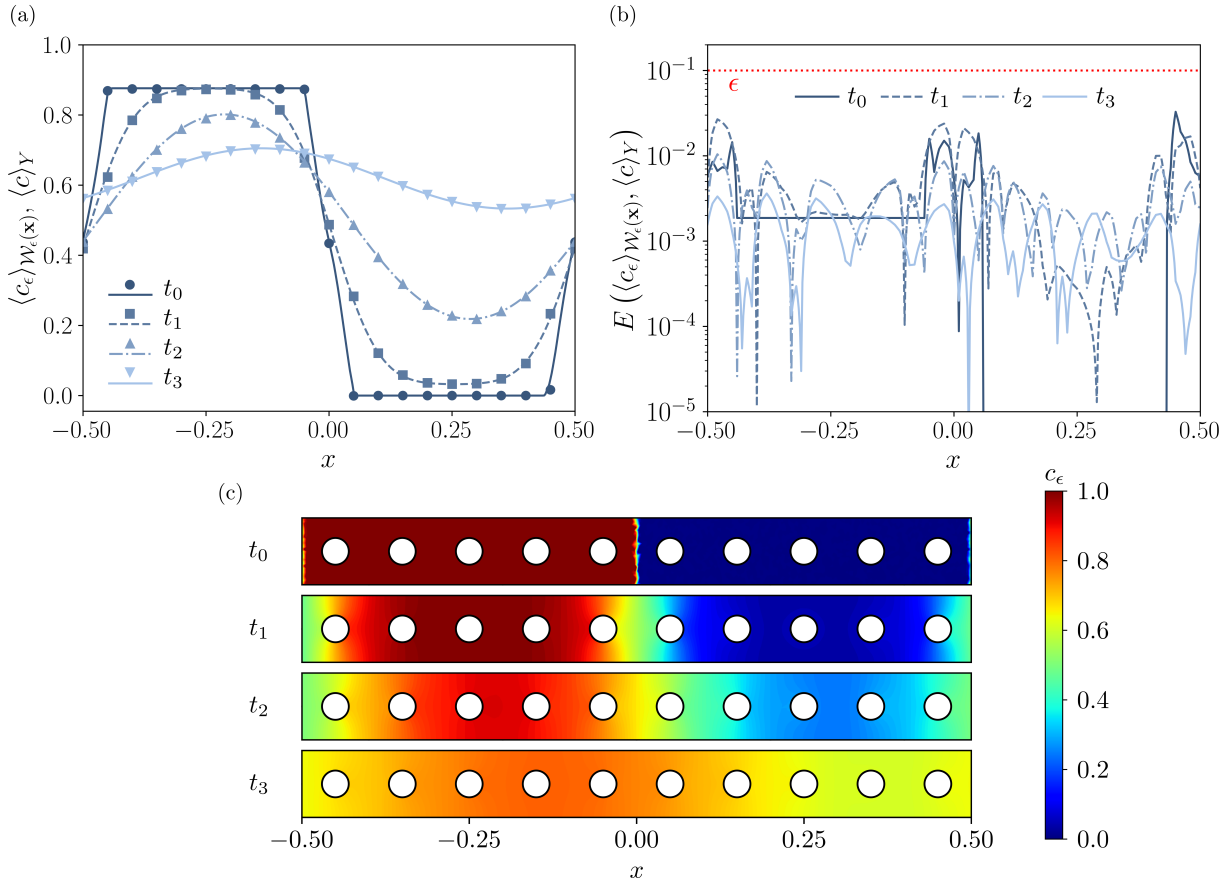

Figure 3. The numerical results for the system involving a single species undergoing a linear heterogeneous reaction. (a) The $\mathcal{W}_\epsilon(\mathbf{x})$-averaged and Y-averaged concentration profiles from the pore-scale (symbols) and homogenized (lines) models, respectively, at various times along the x-direction. (b) The absolute error between the averaged concentration profiles of $\langle c_\epsilon \rangle_{\mathcal{W}_\epsilon(\mathbf{x})}$ and $\langle c \rangle_Y$ at various times along the x-direction. The upper error limit predicted by the homogenized model is displayed by the red dotted line. (c) Contour plots of the pore-scale concentration field c_ϵ at various times. Here, $t_0 = 0$, $t_1 = 0.25 \times 10^{-2}$, $t_2 = 1.25 \times 10^{-2}$, and $t_3 = 3.75 \times 10^{-2}$.

$$E\left(\langle \Psi_\epsilon \rangle_{\mathcal{W}_\epsilon(\mathbf{x})}, \langle \Psi \rangle_Y\right) = \left| \langle \Psi_\epsilon \rangle_{\mathcal{W}_\epsilon(\mathbf{x})} - \langle \Psi \rangle_Y \right|, \tag{24}$$

where $\langle \Psi_\epsilon \rangle_{\mathcal{W}_\epsilon(\mathbf{x})}$ and $\langle \Psi \rangle_Y$ are dummy averaged pore-scale and homogenized solutions, respectively.

In Figure 3, we present the pore-scale, averaged pore-scale, and homogenized model results. The qualitative comparison between $\langle c_\epsilon \rangle_{\mathcal{W}_\epsilon(\mathbf{x})}$ and $\langle c \rangle_Y$ in Figure 3(a) shows the homogenized model is capable of capturing the averaged behavior of the pore-scale model along the x-direction at the recorded times. We note that in conjunction with the periodicity, the prescribed initial condition in this problem causes the evolution of $\langle c_\epsilon \rangle_{\mathcal{W}_\epsilon(\mathbf{x})}$ and $\langle c \rangle_Y$ to be 1D, and therefore, the results in Figure 3(a) are independent of y. We also note that while the prescribed initial condition in the pore-scale simulation is discontinuous at $x = 0$ (as recorded in Table 3 and shown in Figure 3(c) at $t = t_0$), the initial condition of the homogenized model shown at $t = t_0$ in Figure 3(a) displays a sharp slope around $x = 0$. This is due to the averaging of the pore-scale initial condition using equation (22a) that was completed to obtain the appropriate corresponding initial condition for the homogenized model.

In addition to the qualitative comparison, a quantitative comparison between $\langle c_\epsilon \rangle_{\mathcal{W}_\epsilon(\mathbf{x})}$ and $\langle c \rangle_Y$ at the recorded times is provided in Figure 3(b), where the absolute error between the solutions along the x-direction is calculated using equation (24). As shown, the absolute error remains below the upper error limit predicted by the homogenized model ($\sim \mathcal{O}(\epsilon)$; denoted by the red dotted line) for all times. This provides confidence in the validity of the generalized closure form strategy used to derive the homogenized model.

Finally, contours of the pore-scale solution at the recorded times are provided in Figure 3(c). As previously noted, the initial discontinuous concentration profile can be seen in the contour at $t = t_0$. With the progression of time, the solute diffuses to eliminate the discontinuity at $t = t_1$ and $t = t_2$, and advection translates the solute in the positive x-direction. We note that the concentration gradients above and below the cylinders are observed to be slightly y-dependent due to the transport around the cylindrical obstacles. Lastly, in the contour at $t = t_3$, the system is observed to evolve toward a homogeneous state.

With the qualitative and quantitative evidence in Figure 3, we deem the generalized closure form strategy valid for problems involving moderately reactive physics, where diffusive and reactive terms are of similar order. In the next section, this strategy is applied to develop a homogenized model for a more complex case involving two species.

4 Linear Heterogeneous Reaction: Two Species

We now apply the generalized closure form strategy to a system of two species undergoing linear heterogeneous reactions. In particular, we investigate the system presented in the work of Bourbatache *et al.* (Bourbatache et al., 2021) with advection, which is written as

$$\frac{\partial \hat{c}_\epsilon^{(1)}}{\partial \hat{t}} + \hat{\nabla} \cdot \left(\hat{\mathbf{u}}_\epsilon \hat{c}_\epsilon^{(1)} - \hat{D}^{(1)} \hat{\nabla} \hat{c}_\epsilon^{(1)} \right) = 0 \quad \text{in } \hat{\mathcal{B}}_\epsilon, \tag{25a}$$

$$\frac{\partial \hat{c}_\epsilon^{(2)}}{\partial \hat{t}} + \hat{\nabla} \cdot \left(\hat{\mathbf{u}}_\epsilon \hat{c}_\epsilon^{(2)} - \hat{D}^{(2)} \hat{\nabla} \hat{c}_\epsilon^{(2)} \right) = 0 \quad \text{in } \hat{\mathcal{B}}_\epsilon, \tag{25b}$$

subject to

$$-\mathbf{n} \cdot \hat{D}^{(1)} \hat{\nabla} \hat{c}_\epsilon^{(1)} = \hat{\mathcal{K}}_{SL}^{(1)} \hat{c}_\epsilon^{(1)} - \hat{\mathcal{K}}_{SL}^{(2)} \hat{c}_\epsilon^{(2)} \quad \text{on } \hat{\Gamma}_\epsilon, \tag{25c}$$

$$-\mathbf{n} \cdot \hat{D}^{(2)} \hat{\nabla} \hat{c}_\epsilon^{(2)} = \hat{\mathcal{K}}_{SL}^{(2)} \hat{c}_\epsilon^{(2)} - \hat{\mathcal{K}}_{SL}^{(1)} \hat{c}_\epsilon^{(1)} \quad \text{on } \hat{\Gamma}_\epsilon. \tag{25d}$$

These equations can be described using system (4) by letting $N = 2$, $N_\Gamma = 1$, $i \in \{1, 2\}$, $j \in \{1\}$, $\hat{R}_\epsilon^{(i)} = 0$, $\hat{C}_{SL}^{(i,j,k)} = 0$, $\hat{\mathcal{K}}_{SNL}^{(i,j,k,l)} = 0$, $\hat{C}_{SNL}^{(i,j,k,l)} = 0$, $p_{SL}^{(1,1,1)} = p_{SL}^{(2,1,2)} = 0$, $p_{SL}^{(1,1,2)} = p_{SL}^{(2,1,1)} = 1$, $\mathbf{n}^{(1)} = \mathbf{n}$, $\hat{\Gamma}_\epsilon^{(1)} = \hat{\Gamma}_\epsilon$, $\hat{\mathcal{K}}_{SL}^{(n,1,1)} = \hat{\mathcal{K}}_{SL}^{(1)}$ for $n \in \{1, 2\}$, and $\hat{\mathcal{K}}_{SL}^{(n,1,2)} = \hat{\mathcal{K}}_{SL}^{(2)}$ for $n \in \{1, 2\}$. To scale the system, we use the relevant nondimensionalizations in equation (5) to gain

$$\frac{\partial c_\epsilon^{(1)}}{\partial t} + \nabla \cdot \left(\mathrm{Pe} \mathbf{u}_\epsilon c_\epsilon^{(1)} - D^{(1)} \nabla c_\epsilon^{(1)} \right) = 0 \quad \text{in } \mathcal{B}_\epsilon, \tag{26a}$$

$$\frac{\partial c_\epsilon^{(2)}}{\partial t} + \nabla \cdot \left(\mathrm{Pe} \mathbf{u}_\epsilon c_\epsilon^{(2)} - D^{(2)} \nabla c_\epsilon^{(2)} \right) = 0 \quad \text{in } \mathcal{B}_\epsilon, \tag{26b}$$

subject to

$$-\mathbf{n} \cdot D^{(1)} \nabla c_\epsilon^{(1)} = \mathrm{Da}_{SL}^{(1)} c_\epsilon^{(1)} - \mathrm{Da}_{SL}^{(2)} c_\epsilon^{(2)} \quad \text{on } \Gamma_\epsilon, \tag{26c}$$

$$-\mathbf{n} \cdot D^{(2)} \nabla c_\epsilon^{(2)} = \mathrm{Da}_{SL}^{(2)} c_\epsilon^{(2)} - \mathrm{Da}_{SL}^{(1)} c_\epsilon^{(1)} \quad \text{on } \Gamma_\epsilon, \tag{26d}$$

where

$$\mathrm{Pe} = \frac{\hat{\mathcal{U}} \hat{\mathcal{L}}}{\hat{\mathcal{D}}}, \quad \mathrm{Da}_{SL}^{(1)} = \frac{\hat{\mathcal{K}}_{SL}^{(1)} \hat{\mathcal{L}}}{\hat{\mathcal{D}}}, \quad \mathrm{Da}_{SL}^{(2)} = \frac{\hat{\mathcal{K}}_{SL}^{(2)} \hat{\mathcal{L}}}{\hat{\mathcal{D}}}. \tag{27}$$

In addition to the previous syntactic simplifications, we have let $\mathrm{Da}_{SL}^{(n,1,1)} = \mathrm{Da}_{SL}^{(1)}$ and $\mathrm{Da}_{SL}^{(n,1,2)} = \mathrm{Da}_{SL}^{(2)}$ for $n \in \{1, 2\}$ with respect to the notation used in system (7) and equation (8).

In their previous work, Bourbatache *et al.* found that their homogenized models for moderate to high values of Damköhler numbers (i.e., $\mathrm{Da}_{SL}^{(1)} \geq \mathcal{O}(\epsilon^0)$ and $\mathrm{Da}_{SL}^{(2)} \geq \mathcal{O}(\epsilon^0)$) were unable to capture the system dynamics at early times (Bourbatache et al., 2021). Here, we study the case where diffusive and reactive terms are of similar order, namely the moderately reactive regime where

$$\mathrm{Pe} \sim \mathcal{O}\left(\epsilon^{-1}\right), \quad \mathrm{Da}_{SL}^{(1)} \sim \mathcal{O}\left(\epsilon^{0}\right), \quad \mathrm{Da}_{SL}^{(2)} \sim \mathcal{O}\left(\epsilon^{0}\right), \tag{28}$$

and show that the generalized closure form strategy can be used to derive a homogenized model for the system that remains accurate at early times.

4.1 Homogenized Results

With the provided formulation, we show in Appendix B that a homogenized system for $\langle c^{(i)}\rangle_Y = \langle c_0^{(i)}\rangle_Y + \epsilon\langle c_1^{(i)}\rangle_Y + \mathcal{O}(\epsilon^2)$, where $i = \{1, 2\}$, can be derived for the moderately reactive case with $\mathcal{O}(\epsilon)$ error using the closure forms

$$c_1^{(1)} = \boldsymbol{\chi}^{(1)[1]} \cdot \nabla_{\mathbf{x}} c_0^{(1)} + \left(\mathrm{Da}_{SL}^{(1)} c_0^{(1)} - \mathrm{Da}_{SL}^{(2)} c_0^{(2)}\right) \chi^{(1)[2]} + \overline{c}_1^{(1)}, \tag{29a}$$

$$c_1^{(2)} = \boldsymbol{\chi}^{(2)[1]} \cdot \nabla_{\mathbf{x}} c_0^{(2)} + \left(\mathrm{Da}_{SL}^{(2)} c_0^{(2)} - \mathrm{Da}_{SL}^{(1)} c_0^{(1)}\right) \chi^{(2)[2]} + \overline{c}_1^{(2)}, \tag{29b}$$

where $\overline{c}_1^{(i)} \equiv \overline{c}_1^{(i)}(t, \mathbf{x}, \boldsymbol{\tau}(t)) = \phi^{-1}\langle c_1^{(i)}\rangle_Y$, and $\boldsymbol{\chi}^{(i)[1]}$ and $\chi^{(i)[1]}$ are closure variables. The resulting homogenized system is written as

$$\begin{aligned} \phi\frac{\partial\langle c^{(1)}\rangle_Y}{\partial t} + \mathbf{U}^{(1)} \cdot \nabla_{\mathbf{x}}\langle c^{(1)}\rangle_Y - \mathbf{V}^{(1)} \cdot \nabla_{\mathbf{x}}\langle c^{(2)}\rangle_Y - \nabla_{\mathbf{x}} \cdot \left(\mathbf{D}^{(1)} \cdot \nabla_{\mathbf{x}}\langle c^{(1)}\rangle_Y\right) \\ = \mathscr{R}^{(2)}\langle c^{(2)}\rangle_Y - \mathscr{R}^{(1)}\langle c^{(1)}\rangle_Y + \mathcal{O}(\epsilon) \quad \text{for } \mathbf{x} \in \Omega, \end{aligned} \tag{30a}$$

$$\begin{aligned} \phi\frac{\partial\langle c^{(2)}\rangle_Y}{\partial t} + \mathbf{U}^{(2)} \cdot \nabla_{\mathbf{x}}\langle c^{(2)}\rangle_Y - \mathbf{V}^{(2)} \cdot \nabla_{\mathbf{x}}\langle c^{(1)}\rangle_Y - \nabla_{\mathbf{x}} \cdot \left(\mathbf{D}^{(2)} \cdot \nabla_{\mathbf{x}}\langle c^{(2)}\rangle_Y\right) \\ = \mathscr{R}^{(1)}\langle c^{(1)}\rangle_Y - \mathscr{R}^{(2)}\langle c^{(2)}\rangle_Y + \mathcal{O}(\epsilon) \quad \text{for } \mathbf{x} \in \Omega, \end{aligned} \tag{30b}$$

where the effective parameters are defined as

$$\mathbf{U}^{(i)} = \mathrm{Pe}\langle\mathbf{u}\rangle_Y + \mathrm{Da}_{SL}^{(i)}\left[\phi\frac{|\Gamma|}{|\mathcal{B}|}\langle\boldsymbol{\chi}^{(i)[1]}\rangle_\Gamma - D^{(i)}\langle\nabla_{\boldsymbol{\xi}}\chi^{(i)[2]}\rangle_Y + \mathrm{Pe}\epsilon\langle\mathbf{u}\chi^{(i)[2]}\rangle_Y\right], \tag{30c}$$

$$\mathbf{V}^{(1)} = \mathrm{Da}_{SL}^{(2)}\left[\phi\frac{|\Gamma|}{|\mathcal{B}|}\langle\boldsymbol{\chi}^{(2)[1]}\rangle_\Gamma - D^{(1)}\langle\nabla_{\boldsymbol{\xi}}\chi^{(1)[2]}\rangle_Y + \mathrm{Pe}\epsilon\langle\mathbf{u}\chi^{(1)[2]}\rangle_Y\right], \tag{30d}$$

$$\mathbf{V}^{(2)} = \mathrm{Da}_{SL}^{(1)}\left[\phi\frac{|\Gamma|}{|\mathcal{B}|}\langle\boldsymbol{\chi}^{(1)[1]}\rangle_\Gamma - D^{(2)}\langle\nabla_{\boldsymbol{\xi}}\chi^{(2)[2]}\rangle_Y + \mathrm{Pe}\epsilon\langle\mathbf{u}\chi^{(2)[2]}\rangle_Y\right], \tag{30e}$$

$$\mathbf{D}^{(i)} = \phi D^{(i)}\mathbf{I} + D^{(i)}\langle\nabla_{\boldsymbol{\xi}}\boldsymbol{\chi}^{(i)[1]}\rangle_Y - \mathrm{Pe}\epsilon\langle\mathbf{u} \otimes \boldsymbol{\chi}^{(i)[1]}\rangle_Y, \tag{30f}$$

$$\mathscr{R}^{(i)} = \mathrm{Da}_{SL}^{(i)}\mathscr{R}, \tag{30g}$$

$$\mathscr{R} = \phi\frac{|\Gamma|}{|\mathcal{B}|}\left[\epsilon^{-1} + \mathrm{Da}_{SL}^{(1)}\langle\chi^{(1)[2]}\rangle_\Gamma + \mathrm{Da}_{SL}^{(2)}\langle\chi^{(2)[2]}\rangle_\Gamma\right], \tag{30h}$$

for $i \in \{1, 2\}$. In system (30), the four closure variables are found by solving the closure problems

$$\mathrm{Pe}\epsilon\left(\mathbf{u}_0 - \langle \mathbf{u}_0 \rangle_{\mathcal{B}}\right) + \mathrm{Pe}\epsilon \mathbf{u}_0 \cdot \nabla_{\boldsymbol{\xi}} \boldsymbol{\chi}^{(i)[1]} - D^{(i)} \nabla_{\boldsymbol{\xi}} \cdot \left(\mathbf{I} + \nabla_{\boldsymbol{\xi}} \boldsymbol{\chi}^{(i)[1]}\right) = \mathbf{0} \quad \text{for } \boldsymbol{\xi} \in \mathcal{B}, \tag{31a}$$

subject to

$$-\mathbf{n} \cdot D^{(i)} \left(\mathbf{I} + \nabla_{\boldsymbol{\xi}} \boldsymbol{\chi}^{(i)[1]}\right) = \mathbf{0} \quad \text{for } \boldsymbol{\xi} \in \Gamma, \tag{31b}$$

and

$$-\frac{|\Gamma|}{|\mathcal{B}|} + \mathrm{Pe}\epsilon \mathbf{u}_0 \cdot \nabla_{\boldsymbol{\xi}} \chi^{(i)[2]} - D^{(i)} \nabla_{\boldsymbol{\xi}}^2 \chi^{(i)[2]} = 0 \quad \text{for } \boldsymbol{\xi} \in \mathcal{B}, \tag{32a}$$

subject to

$$-\mathbf{n} \cdot D^{(i)} \nabla_{\boldsymbol{\xi}} \chi^{(i)[2]} = 1 \quad \text{for } \boldsymbol{\xi} \in \Gamma. \tag{32b}$$

We note that even for $\mathrm{Pe} = 0$, the homogenized equations differ from those derived in the work of Bourbatache *et al.* (Bourbatache et al., 2020). In comparison to the previous problem, similar contributions to the effective velocities $\mathbf{U}^{(i)}$ are found; however, the effective reaction rates $\mathscr{R}^{(i)}$ contain additional contributions that account for the heterogeneous reactions involving the opposing solute (i.e., $\mathscr{R}^{(1)}$ contains $\mathrm{Da}_{SL}^{(2)} \langle \chi^{(2)[2]} \rangle_\Gamma$ and $\mathscr{R}^{(2)}$ contains $\mathrm{Da}_{SL}^{(1)} \langle \chi^{(1)[2]} \rangle_\Gamma$). As a result, not only do the terms $\mathscr{R}^{(1)} \langle c^{(1)} \rangle_Y$ and $\mathscr{R}^{(2)} \langle c^{(2)} \rangle_Y$ couple the homogenized equations, but the effective reaction rates $\mathscr{R}^{(i)}$ induce a coupling between the averaged reactive mass transport behavior of the solutes through the closure variables.

In addition to the coupling induced by the reaction terms, $\mathbf{V}^{(1)} \cdot \nabla_{\mathbf{x}} \langle c^{(2)} \rangle_Y$ and $\mathbf{V}^{(2)} \cdot \nabla_{\mathbf{x}} \langle c^{(1)} \rangle_Y$ appear in the homogenized equations for $\langle c^{(1)} \rangle_Y$ and $\langle c^{(2)} \rangle_Y$, respectively, due to the moderate reaction rates. These terms induce emergent behaviors in the system through nontrivial couplings within their corresponding homogenized equations, as they consider the gradient of the opposing solute in an advective-like fashion. While $\mathbf{V}^{(1)}$ and $\mathbf{V}^{(2)}$ have similar forms to the reaction induced contributions in the effective velocities $\mathbf{U}^{(i)}$, they each contain contributions that consider the scalar closure variable of the corresponding species (i.e., $\mathbf{V}^{(1)}$ contains $-\mathrm{Da}_{SL}^{(2)} D^{(1)} \langle \nabla_{\boldsymbol{\xi}} \chi^{(1)[2]} \rangle_Y + \mathrm{Da}_{SL}^{(2)} \mathrm{Pe}\epsilon \langle \mathbf{u} \chi^{(1)[2]} \rangle_Y$ and $\mathbf{V}^{(2)}$ contains $-\mathrm{Da}_{SL}^{(1)} D^{(2)} \langle \nabla_{\boldsymbol{\xi}} \chi^{(2)[2]} \rangle_Y + \mathrm{Da}_{SL}^{(1)} \mathrm{Pe}\epsilon \langle \mathbf{u} \chi^{(2)[2]} \rangle_Y$), and a contribution that considers the vector closure variable of the opposing species (i.e., $\mathbf{V}^{(1)}$ contains $\phi \mathrm{Da}_{SL}^{(2)} \frac{|\Gamma|}{|\mathcal{B}|} \langle \boldsymbol{\chi}^{(2)[1]} \rangle_\Gamma$ and $\mathbf{V}^{(2)}$ contains $\phi \mathrm{Da}_{SL}^{(1)} \frac{|\Gamma|}{|\mathcal{B}|} \langle \boldsymbol{\chi}^{(1)[1]} \rangle_\Gamma$). As in the case of the effective reaction rate, these contributions induce a coupling between the averaged reactive mass transport behavior of the solutes through the closure variables in the effective parameters $\mathbf{V}^{(i)}$. Because the contributions have similar forms to those in the previous problem, we interpret them in an analogous manner, and again note that they also demonstrate the early onset of a coupling between advective, diffusive, and reactive physics.

Upon analyzing the homogenized model obtained through the generalized closure form strategy, we reemphasize and add to the point made by Iliev *et al.* (Iliev et al., 2020). The macroscopic equations derived for this problem are considerably different than their microscopic counterparts (system (26)) due to the emergent terms. These terms induce nontrivial couplings between the equations and disallow homogenized models derived for slow reaction rates to accurately model systems with moderate reaction rates by simply fitting effective parameters. Furthermore, we highlight that new effective parameters $\mathbf{V}^{(i)}$ appeared with the emergent terms, and the contributions to $\mathcal{R}^{(i)}$ and $\mathbf{V}^{(i)}$ involve closure variables (i.e., information about the advective, diffusive, and reactive physics) of the opposing solute, as previously noted in our analysis. Therefore, not only can macroscopic equations vastly differ from their microscopic counterparts due to emergent terms, but new effective parameters that inherently couple the macroscopic behavior through the closure variables can appear with the emergent terms. As a result, predicting macroscopic equations from their microscopic counterparts is nontrivial on multiple accounts: the equation forms can differ, the ratio of effective parameters to microscopic coefficients may not be one-to-one, and the effective parameters can be inherently coupled to different physical transport mechanisms in the system through the closure variables (e.g., $\mathbf{V}^{(1)}$, an effective parameter of $\langle c^{(1)} \rangle_Y$, depends on $\boldsymbol{\chi}^{(2)[1]}$, a closure variable of $\langle c^{(2)} \rangle_Y$). Overall, these intricacies greatly support and push the boundary of the point made by Iliev *et al.* (Iliev et al., 2020), and for this reason, we again advise caution when assuming the form of macroscopic equations from the microscopic counterparts.

Table 4. The simulation and mesh parameters used to solve the various models and problems defined on the pore-scale, unit-cell, and continuum domains for the two species system undergoing linear heterogeneous reactions.

Simulation and Mesh Parameters
General Parameters
$\epsilon = 0.05, \quad D^{(1)} = 1, \quad D^{(2)} = 2, \quad \mathrm{Pe} = 0,$
$\mathrm{Da}_{SL}^{(1)} = \epsilon^{-1}/2, \quad \mathrm{Da}_{SL}^{(2)} = \epsilon^{-1}/2, \quad \Delta t = 10^{-4}$
Pore-scale Fluid Flow and Mass Transport
$r_\epsilon = 0.01, \quad N_{elem} = 38617, \quad \max(\Delta x) = 0.0026$
Homogenized Mass Transport
$\phi = 0.8744, \quad N_{elem} = 4054, \quad \max(\Delta x) = 0.0078$
Closure Problems and Unit-cell Fluid Flow
$r = 0.2, \quad N_{elem} = 44413, \quad \max(\Delta \xi) = 0.0099$

4.2 Numerical Validation

4.2.1 Problem Setup

We now provide validation for the derived homogenized model (systems (30), (31), and (32)) by numerically resolving and comparing its solutions to the averaged solutions from the pore-scale model (system (26)). To provide a direct comparison with the work of Bourbatache *et al.*, we consider $\mathrm{Pe} = 0$ for the validation (Bourbatache et al., 2021). Similar to before, we use FEniCS to fully resolve the models on the pore-scale, unit-cell, and continuum domains found in Figure 1, which consider the 2D array of cylinders geometry. The discretization details for each mesh are presented in Table 4 with other simulation parameters. Again, the geometric specifications of each domain are outlined in Table 1; however, we note that $\epsilon = 0.05$ in this validation, which differs from the previous problem.

Regarding initial conditions, we consider discontinuous concentration profiles for each solute in the pore-scale simulation, where the concentrations are alternatively equal to 0 and 1 in the two halves of the domain. The corresponding initial conditions for the homogenized model are then obtained by averaging the pore-scale initial condition using the equation (22a). Further details regarding the simulation parameters, boundary conditions, and initial conditions can be found in Tables 4 and 5.

4.2.2 Closure Problem Results

Similar to before, the four closure problems described in systems (31) and (32) must be solved on the unit-cell domain prior to resolving the homogenized model. As shown in Figure 4, the components of $\boldsymbol{\chi}^{(1)[1]}$, $[\boldsymbol{\chi}^{(1)[1]}]_1$ and $[\boldsymbol{\chi}^{(1)[1]}]_2$, are plotted alongside $\chi^{(1)[2]}$ in Figure 4(a), and the components of $\boldsymbol{\chi}^{(2)[1]}$, $[\boldsymbol{\chi}^{(2)[1]}]_1$ and $[\boldsymbol{\chi}^{(2)[1]}]_2$, are plotted alongside $\chi^{(2)[2]}$ in Figure 4(b). The contours of $[\boldsymbol{\chi}^{(i)[1]}]_1$, $[\boldsymbol{\chi}^{(i)[1]}]_2$, and $\chi^{(i)[2]}$ for $i \in \{1, 2\}$ have similar appearance to those of $[\boldsymbol{\chi}^{[1]}]_1$, $[\boldsymbol{\chi}^{[1]}]_2$, and $\chi^{[2]}$ from the first problem (Figure 2(c)), but the presence of advection in the first problem slightly alters $[\boldsymbol{\chi}^{[1]}]_1$ from $[\boldsymbol{\chi}^{(1)[1]}]_1$ and $[\boldsymbol{\chi}^{(2)[1]}]_1$. Additionally, we note that the magnitudes displayed by $\chi^{(2)[2]}$ are less than those of $\chi^{(1)[2]}$ and $\chi^{[2]}$. We attribute this difference to the high diffusive constant $D^{(2)}$ (Table 4), which is the only difference between the closure problems for $\chi^{(1)[2]}$ and $\chi^{(2)[2]}$ (system (32)).

4.2.3 Pore-scale and Homogenized Model Results

With the closure solutions, the pore-scale (system (26)) and homogenized (systems (30), (31), and (32)) models are solved. Upon doing so, the pore-scale solutions $c_\epsilon^{(1)}$ and $c_\epsilon^{(2)}$ are averaged using the averaging operator in equation (22a) to obtain the averaged pore-scale solutions $\langle c_\epsilon^{(1)} \rangle_{\mathcal{W}_\epsilon(\mathbf{x})}$ and $\langle c_\epsilon^{(2)} \rangle_{\mathcal{W}_\epsilon(\mathbf{x})}$. The absolute errors between the averaged pore-scale solutions and the respective homogenized solutions $\langle c^{(1)} \rangle_Y$ and $\langle c^{(2)} \rangle_Y$ are then calculated using equation (24).

Table 5. The simulation boundary conditions and initial conditions used to solve the various problems on the pore-scale, unit-cell, and continuum domains for the two species system undergoing linear heterogeneous reactions. Here, $H(x)$ is the Heaviside function and $i \in \{1, 2\}$.

Simulation Boundary Conditions	
Pore-scale Mass Transport	
$c_\epsilon^{(i)}\big\vert_{\partial\mathcal{B}_\epsilon^w} = c_\epsilon^{(i)}\big\vert_{\partial\mathcal{B}_\epsilon^e}$	$\mathbf{n}\cdot\nabla c_\epsilon^{(i)}\big\vert_{\partial\mathcal{B}_\epsilon^w} = -\mathbf{n}\cdot\nabla c_\epsilon^{(i)}\big\vert_{\partial\mathcal{B}_\epsilon^e}$
$c_\epsilon^{(i)}\big\vert_{\partial\mathcal{B}_\epsilon^s} = c_\epsilon^{(i)}\big\vert_{\partial\mathcal{B}_\epsilon^n}$	$\mathbf{n}\cdot\nabla c_\epsilon^{(i)}\big\vert_{\partial\mathcal{B}_\epsilon^s} = -\mathbf{n}\cdot\nabla c_\epsilon^{(i)}\big\vert_{\partial\mathcal{B}_\epsilon^n}$
Homogenized Mass Transport	
$\langle c^{(i)}\rangle_Y\big\vert_{\partial\Omega^w} = \langle c^{(i)}\rangle_Y\big\vert_{\partial\Omega^e}$	$\mathbf{n}\cdot\nabla_{\mathbf{x}}\langle c^{(i)}\rangle_Y\big\vert_{\partial\Omega^w} = -\mathbf{n}\cdot\nabla_{\mathbf{x}}\langle c^{(i)}\rangle_Y\big\vert_{\partial\Omega^e}$
$\langle c^{(i)}\rangle_Y\big\vert_{\partial\Omega^s} = \langle c^{(i)}\rangle_Y\big\vert_{\partial\Omega^n}$	$\mathbf{n}\cdot\nabla_{\mathbf{x}}\langle c^{(i)}\rangle_Y\big\vert_{\partial\Omega^s} = -\mathbf{n}\cdot\nabla_{\mathbf{x}}\langle c^{(i)}\rangle_Y\big\vert_{\partial\Omega^n}$
Closure Problems	
$\boldsymbol{\chi}^{(i)[1]}\big\vert_{\partial\mathcal{B}^w} = \boldsymbol{\chi}^{(i)[1]}\big\vert_{\partial\mathcal{B}^e}$	$\mathbf{n}\cdot\nabla_{\boldsymbol{\xi}}\boldsymbol{\chi}^{(i)[1]}\big\vert_{\partial\mathcal{B}^w} = -\mathbf{n}\cdot\nabla_{\boldsymbol{\xi}}\boldsymbol{\chi}^{(i)[1]}\big\vert_{\partial\mathcal{B}^e}$
$\boldsymbol{\chi}^{(i)[1]}\big\vert_{\partial\mathcal{B}^s} = \boldsymbol{\chi}^{(i)[1]}\big\vert_{\partial\mathcal{B}^n}$	$\mathbf{n}\cdot\nabla_{\boldsymbol{\xi}}\boldsymbol{\chi}^{(i)[1]}\big\vert_{\partial\mathcal{B}^s} = -\mathbf{n}\cdot\nabla_{\boldsymbol{\xi}}\boldsymbol{\chi}^{(i)[1]}\big\vert_{\partial\mathcal{B}^n}$
$\chi^{(i)[2]}\big\vert_{\partial\mathcal{B}^w} = \chi^{(i)[2]}\big\vert_{\partial\mathcal{B}^e}$	$\mathbf{n}\cdot\nabla_{\boldsymbol{\xi}}\chi^{(i)[2]}\big\vert_{\partial\mathcal{B}^w} = -\mathbf{n}\cdot\nabla_{\boldsymbol{\xi}}\chi^{(i)[2]}\big\vert_{\partial\mathcal{B}^e}$
$\chi^{(i)[2]}\big\vert_{\partial\mathcal{B}^s} = \chi^{(i)[2]}\big\vert_{\partial\mathcal{B}^n}$	$\mathbf{n}\cdot\nabla_{\boldsymbol{\xi}}\chi^{(i)[2]}\big\vert_{\partial\mathcal{B}^s} = -\mathbf{n}\cdot\nabla_{\boldsymbol{\xi}}\chi^{(i)[2]}\big\vert_{\partial\mathcal{B}^n}$
Simulation Initial Conditions	
Pore-scale Mass Transport	**Homogenized Mass Transport**
$c_\epsilon^{(1)} = H(-x)$ for $(x,y)\in\mathcal{B}_\epsilon,\ t=0$	$\langle c^{(i)}\rangle_Y = \langle c_\epsilon^{(i)}\rangle_{\mathcal{W}_\epsilon(\mathbf{x})}$ for $(x,y)\in\Omega,\ t=0$
$c_\epsilon^{(2)} = H(x)$ for $(x,y)\in\mathcal{B}_\epsilon,\ t=0$	

In a similar manner as before, the pore-scale, averaged pore-scale, and homogenized model results for the first and second solutes are presented in Figures 5 and 6, respectively. The qualitative comparisons found in Figures 5(a) and 6(a) between averaged pore-scale and homogenized solutions show matching profiles along the x-direction, even at simulation times as early as $t = t_1 = 0.625\times10^{-4}$. For similar reasons as before, we note that the results in Figures 5(a) and 6(a) are independent of y, and the initial conditions of the homogenized model (displayed at $t = t_0$) show a sharp slope around $x = 0$ due to the averaging of the discontinuous pore-scale initial conditions using equation (22a).

To provide quantitative comparisons, Figures 5(b) and 6(b) show the absolute errors between the averaged pore-scale and homogenized solutions along the x-direction calculated using equation (24). Despite considering early times, the absolute errors remain below the upper error limits denoted by the red dotted lines for all times. In this regard, we compare our results with those of Bourbatache *et al.* (Bourbatache et al., 2021), who reported discrepancies between their macroscopic and microscopic models for the same problem at early simulation times, and offer the generalized closure form strategy as a solution to deriving homogenized models in the moderately reactive regime. Ultimately, finding the absolute errors within the error limits predicted by homogenization theory provides confidence in the validity of the generalized closure form strategy.

Finally, contours of the pore-scale solutions at various times are presented in Figures 5(c) and 6(c). While the initial discontinuous concentration profiles are seen at $t = t_0$, the reactive and diffusive mechanisms of the problem can be seen at $t = t_1$ through small gradients around the cylinders in the saturated regions and through the diffusion of the discontinuity in the initial concentration profiles, respectively. These mechanisms continue to act into $t = t_2$ until the concentration profiles evolve towards uniform steady-states, as in $t = t_3$.

With the numerical results presented in Figures 5 and 6, we again find that the generalized closure form strategy provides valid homogenized models for moderately reactive systems where diffusive and re-

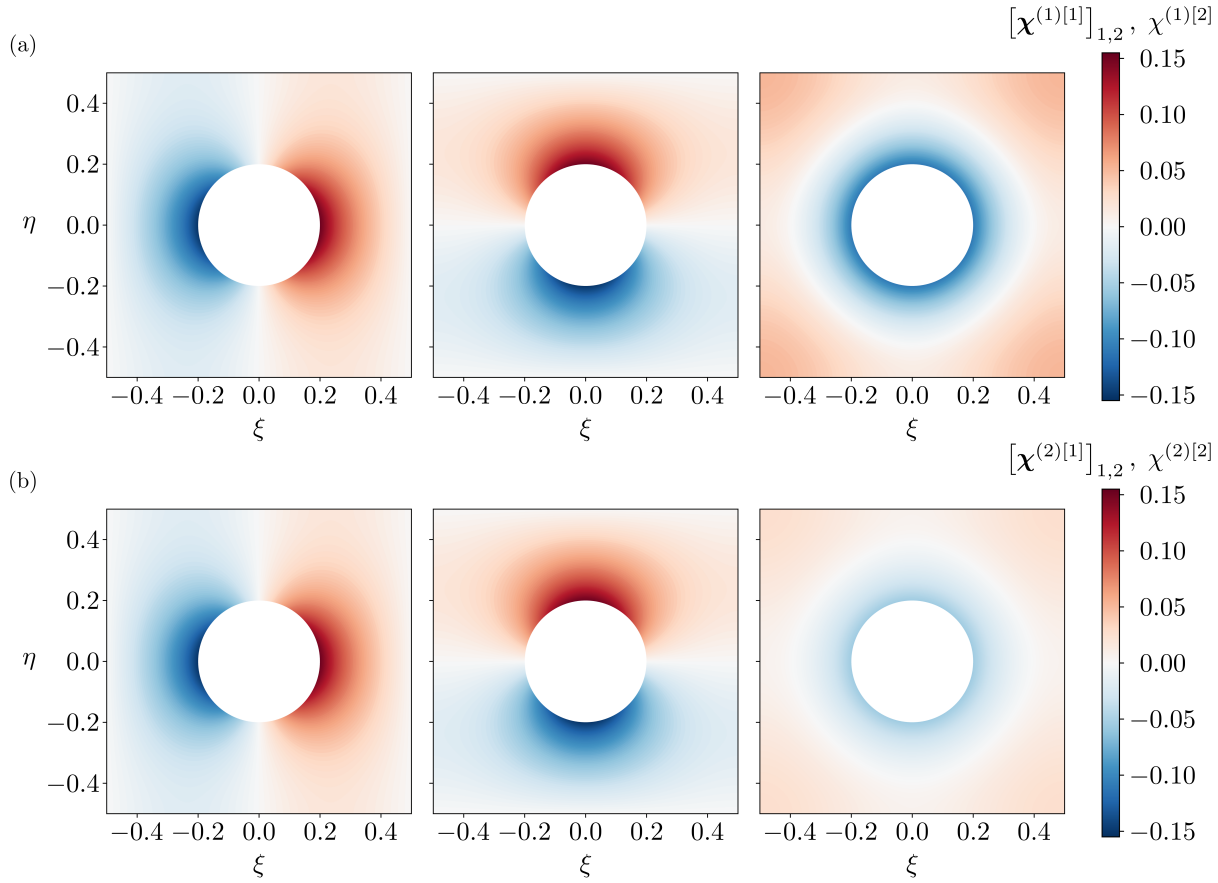

Figure 4. The numerical results of the closure problems for each solute in the system of two species undergoing linear heterogeneous reactions. (a) The resulting closure solutions $\boldsymbol{\chi}^{(1)[1]}$ and $\chi^{(1)[2]}$. From left to right: $[\boldsymbol{\chi}^{(1)[1]}]_1$ the ξ-component of $\boldsymbol{\chi}^{(1)[1]}$, $[\boldsymbol{\chi}^{(1)[1]}]_2$ the η-component of $\boldsymbol{\chi}^{(1)[1]}$, and $\chi^{(1)[2]}$. (b) The resulting closure solutions $\boldsymbol{\chi}^{(2)[1]}$ and $\chi^{(2)[2]}$. From left to right: $[\boldsymbol{\chi}^{(2)[1]}]_1$ the ξ-component of $\boldsymbol{\chi}^{(2)[1]}$, $[\boldsymbol{\chi}^{(2)[1]}]_2$ the η-component of $\boldsymbol{\chi}^{(2)[1]}$, and $\chi^{(2)[2]}$.

active terms are of similar orders, even at early times. Therefore, we offer this method as a more general approach to the classical homogenization procedure.

5 Conclusion

To summarize Part 1 of this series, we introduced a strategy for generalizing the closure form that increases the applicability of classical homogenization theory with only slight deviation from the traditional procedure. As detailed in Appendix A and Appendix B, this strategy involves considering ordered solution forms as linear combinations of closure terms, which are chosen based on the equation for which closure is sought. As a result, multiple closure problems can be defined for a single homogenized equation, whereas classical homogenization theory typically consist of only one closure problem per homogenized equation. In our first problem, we considered a linear heterogeneous reaction with a moderate reaction rate, which cannot be handled by classical homogenization theory, and provided a demonstration for how our strategy can be implemented to homogenize the system. An analysis of the homogenized model then followed, where we emphasized that additional contributions to the effective velocity were found due to interactions between diffusive and reactive fluxes. These contributions do not vanish for $\mathrm{Pe} = 0$ and indicate an early onset of coupling between diffusion and reaction, despite the effective reaction rate being independent of diffusion and the effective dispersion tensor being independent of reaction. We then validated our homogenized model, and ultimately the generalized closure form strategy, by numerically solving the model and comparing the solution to the averaged pore-scale solution. Upon finding the absolute error within the upper error limit predicted by homogenization theory, we deemed the strategy and our homogenized model valid.

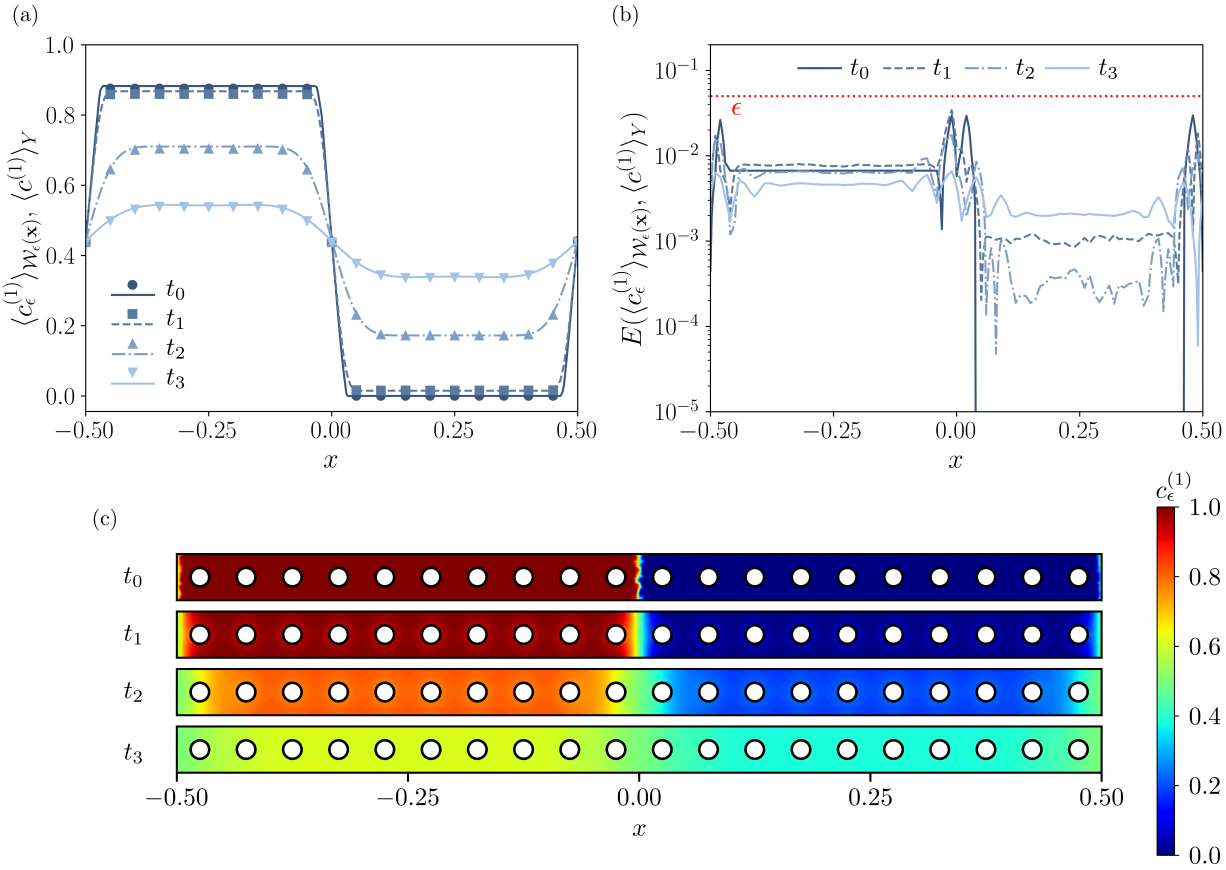

Figure 5. The numerical results of the first concentration in the system involving two species undergoing linear heterogeneous reactions. (a) The $\mathcal{W}_\epsilon(\mathbf{x})$-averaged and Y-averaged concentration profiles from the pore-scale (symbols) and homogenized (lines) models, respectively, at various times along the x-direction. (b) The absolute error between the averaged concentration profiles of $\langle c_\epsilon^{(1)}\rangle_{\mathcal{W}_\epsilon(\mathbf{x})}$ and $\langle c^{(1)}\rangle_Y$ at various times along the x-direction. The upper error limit predicted by the homogenized model is displayed by the red dotted line. (c) Contour plots of the pore-scale concentration field $c_\epsilon^{(1)}$ at various times. Here, $t_0 = 0$, $t_1 = 0.625 \times 10^{-4}$, $t_2 = 9.375 \times 10^{-4}$, and $t_3 = 28.125 \times 10^{-4}$.

In the second problem, we applied the generalized closure form strategy to a system previously investigated by Bourbatache *et al.* (Bourbatache et al., 2021) with advection, which consisted of two species undergoing linear heterogeneous reactions in the moderately reactive regime. After detailing the homogenization procedure using the generalized closure form strategy in Appendix B, we obtained a homogenized model consisting of terms that induce emergent behaviors through nontrivial couplings. The new effective parameters that appeared with these emergent terms rely on the closure variables of both solutes, which indicates an inherent coupling between the new effective parameters and the behavior of the different system components. Ultimately, this furthers the argument that macroscopic equations do not always take the form of their microscopic counterpart and can be nontrivial. Upon numerically solving the homogenized model and comparing its solution to the averaged pore-scale solution, we again found qualitative and quantitative evidence that the homogenized model captures the behavior of the averaged pore-scale solution within the upper error limit predicted by homogenization theory, even for early times. This further validates the presented generalized closure form strategy.

In light of the numerical evidence validating the nontrivial homogenized models and their effective parameters, we deem the generalized closure form strategy valid and offer it as a standard homogenization method that generalizes the classical approach. As we will demonstrate in Part 2 of this series, an algorithmic procedure can be developed for efficient implementation of the strategy using automated (symbolic) upscaling frameworks like Symbolica. By encoding this procedure, automated frameworks will be capable of automatically defining closure forms and closure problems based on the provided equations, with no *a priori* postulations of closure forms and no human interference. We believe this ability will be

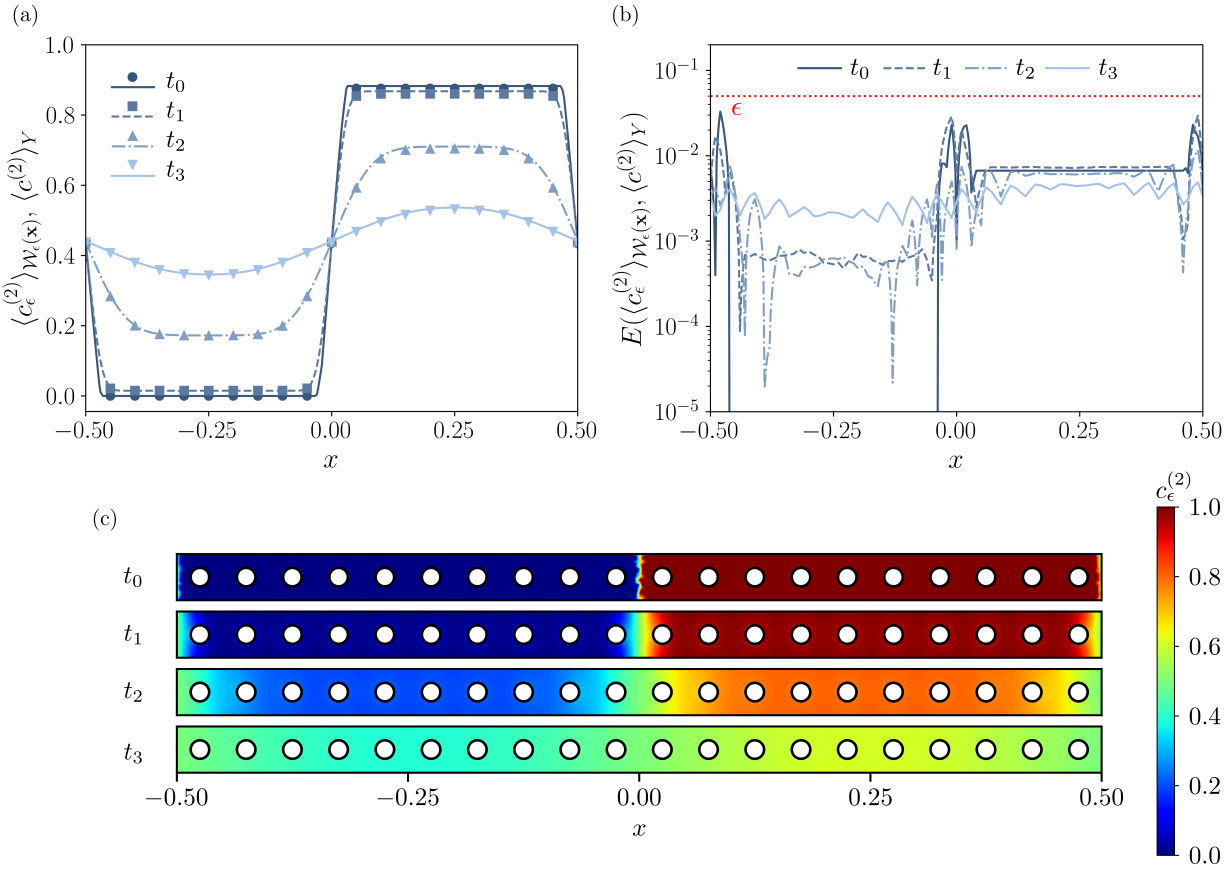

Figure 6. The numerical results of the second concentration in the system involving two species undergoing linear heterogeneous reactions. (a) The $\mathcal{W}_\epsilon(\mathbf{x})$-averaged and Y-averaged concentration profiles from the pore-scale (symbols) and homogenized (lines) models, respectively, at various times along the x-direction. (b) The absolute error between the averaged concentration profiles of $\langle c_\epsilon^{(2)}\rangle_{\mathcal{W}_\epsilon(\mathbf{x})}$ and $\langle c^{(2)}\rangle_Y$ at various times along the x-direction. The upper error limit predicted by the homogenized model is displayed by the red dotted line. (c) Contour plots of the pore-scale concentration field $c_\epsilon^{(2)}$ at various times. Here, $t_0 = 0$, $t_1 = 0.625 \times 10^{-4}$, $t_2 = 9.375 \times 10^{-4}$, and $t_3 = 28.125 \times 10^{-4}$.

invaluable for further development, generalization, and utilization of automated upscaling frameworks that utilize symbolic computing.

Acknowledgments

Support by the Department of Energy under the Early Career award DE-SC0019075 'Multiscale dynamics of reactive fronts in the subsurface' is gratefully acknowledged. KP was also supported by the Stanford Graduate Fellowship in Science and Engineering.

Appendix A Homogenization of a Linear Heterogeneous Reaction: One-Species

In this Appendix, we provide the detailed derivation of the homogenized system (19) from the pore-scale system (14). The strategy to construct a more general closure form for c_1 (equation (17)) is also explicitly discussed.

A1 Homogenization

Upon expanding the spatial operators, temporal operators, and dependent variables using equations (10), (12), and system (13), we simplify system (14) to

$$\begin{aligned}
&\epsilon^{-2}\left[\frac{\partial c_0}{\partial \tau_2}+\nabla_{\boldsymbol{\xi}}\cdot\left(\mathrm{Pe}^{(s)}\mathbf{u}_0c_0-D\nabla_{\boldsymbol{\xi}}c_0\right)\right]\\
&+\epsilon^{-1}\left[\frac{\partial c_0}{\partial \tau_1}+\frac{\partial c_1}{\partial \tau_2}+\nabla_{\mathbf{x}}\cdot\left(\mathrm{Pe}^{(s)}\mathbf{u}_0c_0-D\nabla_{\boldsymbol{\xi}}c_0\right)\right.\\
&\left.+\nabla_{\boldsymbol{\xi}}\cdot\left(\mathrm{Pe}^{(s)}\mathbf{u}_1c_0+\mathrm{Pe}^{(s)}\mathbf{u}_0c_1-D\nabla_{\mathbf{x}}c_0-D\nabla_{\boldsymbol{\xi}}c_1\right)\right]\\
&+\epsilon^{0}\left[\frac{\partial c_0}{\partial t}+\frac{\partial c_1}{\partial \tau_1}+\frac{\partial c_2}{\partial \tau_2}+\nabla_{\mathbf{x}}\cdot\left(\mathrm{Pe}^{(s)}\mathbf{u}_1c_0+\mathrm{Pe}^{(s)}\mathbf{u}_0c_1-D\nabla_{\mathbf{x}}c_0-D\nabla_{\boldsymbol{\xi}}c_1\right)\right.\\
&\left.+\nabla_{\boldsymbol{\xi}}\cdot\left(\mathrm{Pe}^{(s)}\mathbf{u}_2c_0+\mathrm{Pe}^{(s)}\mathbf{u}_1c_1+\mathrm{Pe}^{(s)}\mathbf{u}_0c_2-D\nabla_{\mathbf{x}}c_1-D\nabla_{\boldsymbol{\xi}}c_2\right)\right]\\
&=\mathcal{O}\left(\epsilon\right)\quad\text{for }\mathbf{x}\in\Omega,\ \boldsymbol{\xi}\in\mathcal{B},
\end{aligned}\tag{A1a}$$

subject to

$$\begin{aligned}
&\epsilon^{-1}\left[-\mathbf{n}\cdot D\nabla_{\boldsymbol{\xi}}c_0\right]+\epsilon^{0}\left[-\mathbf{n}\cdot D\left(\nabla_{\mathbf{x}}c_0+\nabla_{\boldsymbol{\xi}}c_1\right)\right]+\epsilon\left[-\mathbf{n}\cdot D\left(\nabla_{\mathbf{x}}c_1+\nabla_{\boldsymbol{\xi}}c_2\right)\right]\\
&=\epsilon^{0}\left[\mathrm{Da}^{(s)}\left(c_0-\theta^{(s)}\right)\right]+\epsilon\left[\mathrm{Da}^{(s)}c_1\right]+\mathcal{O}\left(\epsilon^2\right)\quad\text{for }\mathbf{x}\in\Omega,\ \boldsymbol{\xi}\in\Gamma,
\end{aligned}\tag{A1b}$$

where $\mathrm{Pe}^{(s)}\equiv\mathrm{Pe}\epsilon\sim\mathcal{O}(\epsilon^0)$, $\mathrm{Da}^{(s)}\equiv\mathrm{Da}\sim\mathcal{O}(\epsilon^0)$, and $\theta^{(s)}\equiv\theta\sim\mathcal{O}(\epsilon^0)$ are used to track where the dimensionless numbers appear in the final homogenized model. In addition to the mass transport equation, we find it useful to simplify equation (6b) using equations (10) and (13b), such that

$$\epsilon^{-1}\left[\nabla_{\boldsymbol{\xi}}\cdot\mathbf{u}_0\right]+\epsilon^{0}\left[\nabla_{\mathbf{x}}\cdot\mathbf{u}_0+\nabla_{\boldsymbol{\xi}}\cdot\mathbf{u}_1\right]+\epsilon\left[\nabla_{\mathbf{x}}\cdot\mathbf{u}_1+\nabla_{\boldsymbol{\xi}}\cdot\mathbf{u}_2\right]=\mathcal{O}\left(\epsilon^2\right)\quad\text{for }\mathbf{x}\in\Omega,\ \boldsymbol{\xi}\in\mathcal{B}.\tag{A2}$$

We now create a system of differential equations from system (A1) by considering the terms at each order of ϵ independently.

A11 Terms of Order $\mathcal{O}\left(\epsilon^{-2}\right)$

After collecting the leading order terms in system (A1), we gain

$$\frac{\partial c_0}{\partial \tau_2}+\nabla_{\boldsymbol{\xi}}\cdot\left(\mathrm{Pe}^{(s)}\mathbf{u}_0c_0-D\nabla_{\boldsymbol{\xi}}c_0\right)=0\quad\text{for }\mathbf{x}\in\Omega,\ \boldsymbol{\xi}\in\mathcal{B},\tag{A3a}$$

subject to the leading order boundary condition (i.e., at $\mathcal{O}(\epsilon^{-1})$)

$$-\mathbf{n}\cdot D\nabla_{\boldsymbol{\xi}}c_0=0\quad\text{for }\mathbf{x}\in\Omega,\ \boldsymbol{\xi}\in\Gamma.\tag{A3b}$$

By applying the averaging operator $\langle\cdot\rangle_{\mathcal{B}}$ (equation (11)) to equation (A3a), we implement the divergence theorem on both the diffusive and advective flux terms. While the boundary condition (equation (A3b)) is applied through the diffusive flux, we enforce the no-slip condition and consider that $\mathbf{u}_0$ and c_0 are periodic in $\boldsymbol{\xi}$ to simplify the advective flux and gain

$$\frac{\partial\langle c_0\rangle_{\mathcal{B}}}{\partial \tau_2}=0\quad\text{for }\mathbf{x}\in\Omega.\tag{A4}$$

As shown in equation (A4), if our hypotheses regarding the magnitudes of the dimensionless parameters and periodicity of the system are correct, we find that the zeroth order average concentration should not vary on the smallest time scale according to homogenization theory (i.e., vary with $\tau_2(t)$). We emphasize that this is not a limitation of homogenization theory, but rather a result of upholding our initial hypotheses and remaining within the applicability conditions considered. This highlights the importance of ensuring that the dynamics of a system do not violate the underlying hypotheses at any time; otherwise, the homogenized model will be invalid for analyzing the system.

After briefly analyzing equation (A2) to obtain $\nabla_{\boldsymbol{\xi}} \cdot \mathbf{u}_0 = 0$ from the $\mathcal{O}(\epsilon^{-1})$ terms, we rewrite system (A3) as

$$\frac{\partial c_0}{\partial \tau_2} + \mathrm{Pe}^{(s)} \mathbf{u}_0 \cdot \nabla_{\boldsymbol{\xi}} c_0 - \nabla_{\boldsymbol{\xi}} \cdot (D \nabla_{\boldsymbol{\xi}} c_0) = 0 \quad \text{for } \mathbf{x} \in \Omega,\ \boldsymbol{\xi} \in \mathcal{B}, \tag{A5a}$$

subject to

$$-\mathbf{n} \cdot D \nabla_{\boldsymbol{\xi}} c_0 = 0 \quad \text{for } \mathbf{x} \in \Omega,\ \boldsymbol{\xi} \in \Gamma. \tag{A5b}$$

Considering initial conditions for c_0 that are independent of $\boldsymbol{\xi}$, we find c_0 to be independent of τ_2. It then follows from the homogeneity of the system that c_0 is independent of $\boldsymbol{\xi}$, and therefore $c_0 \equiv c_0(t, \mathbf{x}, \tau_1(t))$. This coincides with the familiar leading order result of classical homogenization theory, where the fastest time variable (i.e., $\tau_2(t)$) is typically not introduced for the sake of brevity.

A12 Terms of Order $\mathcal{O}(\epsilon^{-1})$

At the following order, we collect terms from system (A1) to write

$$\begin{aligned} &\frac{\partial c_0}{\partial \tau_1} + \frac{\partial c_1}{\partial \tau_2} + \nabla_{\mathbf{x}} \cdot \left(\mathrm{Pe}^{(s)} \mathbf{u}_0 c_0 - D \nabla_{\boldsymbol{\xi}} c_0 \right) \\ &+ \nabla_{\boldsymbol{\xi}} \cdot \left(\mathrm{Pe}^{(s)} \mathbf{u}_1 c_0 + \mathrm{Pe}^{(s)} \mathbf{u}_0 c_1 - D \nabla_{\mathbf{x}} c_0 - D \nabla_{\boldsymbol{\xi}} c_1 \right) = 0 \quad \text{for } \mathbf{x} \in \Omega,\ \boldsymbol{\xi} \in \mathcal{B}, \end{aligned} \tag{A6a}$$

subject to the boundary condition (i.e., at $\mathcal{O}(\epsilon^0)$)

$$-\mathbf{n} \cdot D \left(\nabla_{\mathbf{x}} c_0 + \nabla_{\boldsymbol{\xi}} c_1 \right) = \mathrm{Da}^{(s)} \left(c_0 - \theta^{(s)} \right) \quad \text{for } \mathbf{x} \in \Omega,\ \boldsymbol{\xi} \in \Gamma. \tag{A6b}$$

Again, we apply the averaging operator $\langle \cdot \rangle_{\mathcal{B}}$ (equation (11)) to equation (A6a), implement the divergence theorem, and apply the boundary condition (equation (A6b)) and no-slip condition to the equation. We also consider that $\mathbf{u}_0$, $\mathbf{u}_1$, and c_1 are periodic in $\boldsymbol{\xi}$ to simplify the equation to

$$\frac{\partial c_0}{\partial \tau_1} + \frac{\partial \langle c_1 \rangle_{\mathcal{B}}}{\partial \tau_2} + \mathrm{Pe}^{(s)} \langle \mathbf{u}_0 \rangle_{\mathcal{B}} \cdot \nabla_{\mathbf{x}} c_0 + \mathrm{Da}^{(s)} \frac{|\Gamma|}{|\mathcal{B}|} \left(c_0 - \theta^{(s)} \right) = 0 \quad \text{for } \mathbf{x} \in \Omega. \tag{A7}$$

As shown, equation (A7) describes how c_0 and $\langle c_1 \rangle_{\mathcal{B}}$ vary with fast time variables $\tau_1(t)$ and $\tau_2(t)$, respectively.

Now, we return to equation (A2) and conclude that $\nabla_{\mathbf{x}} \cdot \mathbf{u}_0 = 0$ from the $\mathcal{O}(\epsilon^0)$ terms after applying the averaging operator $\langle \cdot \rangle_{\mathcal{B}}$, the divergence theorem, and assuming $\mathbf{u}_1$ is periodic in $\boldsymbol{\xi}$ with the no-slip condition. Ultimately, this leads to $\nabla_{\boldsymbol{\xi}} \cdot \mathbf{u}_1 = 0$ as well. After subtracting equation (A7) from equation (A6a), we gain

$$\begin{aligned} &\frac{\partial c_1}{\partial \tau_2} - \frac{\partial \langle c_1 \rangle_{\mathcal{B}}}{\partial \tau_2} + \mathrm{Pe}^{(s)} \left(\mathbf{u}_0 - \langle \mathbf{u}_0 \rangle_{\mathcal{B}} \right) \cdot \nabla_{\mathbf{x}} c_0 - \mathrm{Da}^{(s)} \frac{|\Gamma|}{|\mathcal{B}|} \left(c_0 - \theta^{(s)} \right) \\ &+ \mathrm{Pe}^{(s)} \mathbf{u}_0 \cdot \nabla_{\boldsymbol{\xi}} c_1 - D \nabla_{\boldsymbol{\xi}} \cdot \left(\nabla_{\mathbf{x}} c_0 + \nabla_{\boldsymbol{\xi}} c_1 \right) = 0 \quad \text{for } \mathbf{x} \in \Omega,\ \boldsymbol{\xi} \in \mathcal{B}, \end{aligned} \tag{A8}$$

subject to the boundary condition previously presented in equation (A6b). Here, we note that through brief analysis of equations (A8) and (A6b), the traditionally used closure form $c_1 = \boldsymbol{\chi} \cdot \nabla_{\mathbf{x}} c_0 + \bar{c}_1$, where

$\boldsymbol{\chi} \equiv \boldsymbol{\chi}(\boldsymbol{\xi})$ is the *closure variable* and $\overline{c}_1 \equiv \overline{c}_1(t, \mathbf{x}, \boldsymbol{\tau}(t)) = \langle c_1 \rangle_{\mathcal{B}}$ is the average of the first-order concentration over $\mathcal{B}$ (which implies $\langle \boldsymbol{\chi} \rangle_{\mathcal{B}} = \mathbf{0}$), cannot be used to separate scales and create a valid closure problem, i.e., a problem where the only independent variable is $\boldsymbol{\xi}$. This is due to the reaction terms that exist in both the equation and boundary condition, which are not dotted with $\nabla_{\mathbf{x}} c_0$. However, due to the linearity of equations (A8) and (A6b), we can simply assume a solution of the form $c_1 = c_1^{[1]} + c_1^{[2]}$ and linearly separate the system to consider the terms multiplied by $(c_0 - \theta^{(s)})$ and the terms dotted with $\nabla_{\mathbf{x}} c_0$ independently. In doing so, we obtain

$$\begin{aligned} \frac{\partial c_1^{[1]}}{\partial \tau_2} - \frac{\partial \langle c_1^{[1]} \rangle_{\mathcal{B}}}{\partial \tau_2} + \mathrm{Pe}^{(s)} \left(\mathbf{u}_0 - \langle \mathbf{u}_0 \rangle_{\mathcal{B}} \right) \cdot \nabla_{\mathbf{x}} c_0 + \mathrm{Pe}^{(s)} \mathbf{u}_0 \cdot \nabla_{\boldsymbol{\xi}} c_1^{[1]} \\ - D \nabla_{\boldsymbol{\xi}} \cdot \left(\nabla_{\mathbf{x}} c_0 + \nabla_{\boldsymbol{\xi}} c_1^{[1]} \right) = 0 \quad \text{for } \mathbf{x} \in \Omega,\ \boldsymbol{\xi} \in \mathcal{B}, \end{aligned} \tag{A9a}$$

subject to

$$-\mathbf{n} \cdot D \left(\nabla_{\mathbf{x}} c_0 + \nabla_{\boldsymbol{\xi}} c_1^{[1]} \right) = 0 \quad \text{for } \mathbf{x} \in \Omega,\ \boldsymbol{\xi} \in \Gamma, \tag{A9b}$$

which considers the terms dotted by $\nabla_{\mathbf{x}} c_0$, and

$$\frac{\partial c_1^{[2]}}{\partial \tau_2} - \frac{\partial \langle c_1^{[2]} \rangle_{\mathcal{B}}}{\partial \tau_2} - \mathrm{Da}^{(s)} \frac{|\Gamma|}{|\mathcal{B}|} \left(c_0 - \theta^{(s)} \right) + \mathrm{Pe}^{(s)} \mathbf{u}_0 \cdot \nabla_{\boldsymbol{\xi}} c_1^{[2]} - D \nabla_{\boldsymbol{\xi}}^2 c_1^{[2]} = 0 \quad \text{for } \mathbf{x} \in \Omega,\ \boldsymbol{\xi} \in \mathcal{B}, \tag{A10a}$$

subject to

$$-\mathbf{n} \cdot D \nabla_{\boldsymbol{\xi}} c_1^{[2]} = \mathrm{Da}^{(s)} \left(c_0 - \theta^{(s)} \right) \quad \text{for } \mathbf{x} \in \Omega,\ \boldsymbol{\xi} \in \Gamma, \tag{A10b}$$

which considers the terms multiplied by $(c_0 - \theta^{(s)})$. By assuming different closure forms for $c_1^{[1]}$ and $c_1^{[2]}$, two closure problems can be created (i.e., one from system (A9) and one from system (A10)) to accommodate all terms in equations (A8) and (A6b). Here, we let

$$c_1^{[1]} = \boldsymbol{\chi}^{[1]} \cdot \nabla_{\mathbf{x}} c_0 + \overline{c}_1^{[1]}, \tag{A11a}$$

$$c_1^{[2]} = \left(c_0 - \theta^{(s)} \right) \chi^{[2]} + \overline{c}_1^{[2]}, \tag{A11b}$$

where $\boldsymbol{\chi}^{[1]} \equiv \boldsymbol{\chi}^{[1]}(\boldsymbol{\xi})$ is the vector closure variable for $c_1^{[1]}$, $\chi^{[2]} \equiv \chi^{[2]}(\boldsymbol{\xi})$ is the scalar closure variable for $c_1^{[2]}$, $\overline{c}_1^{[1]} \equiv \overline{c}_1^{[1]}(t, \mathbf{x}, \boldsymbol{\tau}(t)) = \langle c_1^{[1]} \rangle_{\mathcal{B}}$ is the average of the first component to the first-order concentration over $\mathcal{B}$, and $\overline{c}_1^{[2]} \equiv \overline{c}_1^{[2]}(t, \mathbf{x}, \boldsymbol{\tau}(t)) = \langle c_1^{[2]} \rangle_{\mathcal{B}}$ is the average of the second component to the first-order concentration over $\mathcal{B}$. Similar to before, we note that $\langle \boldsymbol{\chi}^{[1]} \rangle_{\mathcal{B}} = \mathbf{0}$ and $\langle \chi^{[2]} \rangle_{\mathcal{B}} = 0$. We also note that due to the lack of dependency on τ_2 in the equations, we find it suitable to assume $\overline{c}_1^{[1]}$ and $\overline{c}_1^{[2]}$ are the only parts of $c_1^{[1]}$ and $c_1^{[2]}$ that depend on τ_2. Upon substituting equation (A11a) into system (A9) and equation (A11b) into system (A10), we can write the closure problems as

$$\mathrm{Pe}^{(s)} \left(\mathbf{u}_0 - \langle \mathbf{u}_0 \rangle_{\mathcal{B}} \right) + \mathrm{Pe}^{(s)} \mathbf{u}_0 \cdot \nabla_{\boldsymbol{\xi}} \boldsymbol{\chi}^{[1]} - D \nabla_{\boldsymbol{\xi}} \cdot \left(\mathbf{I} + \nabla_{\boldsymbol{\xi}} \boldsymbol{\chi}^{[1]} \right) = \mathbf{0} \quad \text{for } \boldsymbol{\xi} \in \mathcal{B}, \tag{A12a}$$

subject to

$$-\mathbf{n} \cdot D \left(\mathbf{I} + \nabla_{\boldsymbol{\xi}} \boldsymbol{\chi}^{[1]} \right) = \mathbf{0} \quad \text{for } \boldsymbol{\xi} \in \Gamma, \tag{A12b}$$

and

$$-\mathrm{Da}^{(s)} \frac{|\Gamma|}{|\mathcal{B}|} + \mathrm{Pe}^{(s)} \mathbf{u}_0 \cdot \nabla_{\boldsymbol{\xi}} \chi^{[2]} - D \nabla_{\boldsymbol{\xi}}^2 \chi^{[2]} = 0 \quad \text{for } \boldsymbol{\xi} \in \mathcal{B}, \tag{A13a}$$

subject to

$$-\mathbf{n}\cdot D\nabla_{\boldsymbol{\xi}}\chi^{[2]} = \mathrm{Da}^{(s)} \quad \text{for } \boldsymbol{\xi}\in\Gamma. \tag{A13b}$$

From the derived closure problems, we physically interpret $\chi^{[2]}$ as a function that provides correction to the reactive flux due to the presence of microscopic geometry and high advection, similar to how $\boldsymbol{\chi}^{[1]}$ provides correction to the diffusive flux. Finally, we note that the full closure form of c_1 to be used throughout the rest of the homogenization procedure is written as

$$c_1 = \boldsymbol{\chi}^{[1]}\cdot\nabla_{\mathbf{x}}c_0 + \left(c_0-\theta^{(s)}\right)\chi^{[2]} + \overline{c}_1, \tag{A14}$$

where $\overline{c}_1 \equiv \overline{c}_1^{[1]} + \overline{c}_1^{[2]}$. As demonstrated, linearly separating equations (A8) and (A6b) and generalizing the assumed closure form of c_1 as a linear combination of closure terms allows for valid closure problems to be created in scenarios where the traditionally assumed closure form fails.

A13 Terms of Order $\mathcal{O}(\epsilon^0)$

Finally, we collect terms of $\mathcal{O}(\epsilon^0)$ from system (A1) to write

$$\begin{aligned}&\frac{\partial c_0}{\partial t}+\frac{\partial c_1}{\partial \tau_1}+\frac{\partial c_2}{\partial \tau_2}+\nabla_{\mathbf{x}}\cdot\left(\mathrm{Pe}^{(s)}\mathbf{u}_1c_0+\mathrm{Pe}^{(s)}\mathbf{u}_0c_1-D\nabla_{\mathbf{x}}c_0-D\nabla_{\boldsymbol{\xi}}c_1\right)\\ &+\nabla_{\boldsymbol{\xi}}\cdot\left(\mathrm{Pe}^{(s)}\mathbf{u}_2c_0+\mathrm{Pe}^{(s)}\mathbf{u}_1c_1+\mathrm{Pe}^{(s)}\mathbf{u}_0c_2-D\nabla_{\mathbf{x}}c_1-D\nabla_{\boldsymbol{\xi}}c_2\right)=0 \quad \text{for } \mathbf{x}\in\Omega,\ \boldsymbol{\xi}\in\mathcal{B},\end{aligned} \tag{A15a}$$

subject to the boundary condition (i.e., at $\mathcal{O}(\epsilon)$)

$$-\mathbf{n}\cdot D\left(\nabla_{\mathbf{x}}c_1+\nabla_{\boldsymbol{\xi}}c_2\right)=\mathrm{Da}^{(s)}c_1 \quad \text{for } \mathbf{x}\in\Omega,\ \boldsymbol{\xi}\in\Gamma. \tag{A15b}$$

After substituting in the solution for c_1 (equation (A14)), we again apply the averaging operator $\langle\cdot\rangle_{\mathcal{B}}$ (equation (11)) to equation (A15a) and implement the divergence theorem to incorporate the boundary condition (equation (A15b)) and apply the no-slip condition. Further simplifications regarding the periodicity of the dependent variables in $\boldsymbol{\xi}$ are also made to write equation (A15a) as

$$\begin{aligned}&\frac{\partial c_0}{\partial t}+\frac{\partial \overline{c}_1}{\partial \tau_1}+\frac{\partial\langle c_2\rangle_{\mathcal{B}}}{\partial\tau_2}\\ &+\left[\mathrm{Pe}^{(s)}\left(\langle\mathbf{u}_1\rangle_{\mathcal{B}}+\langle\mathbf{u}_0\chi^{[2]}\rangle_{\mathcal{B}}\right)+\mathrm{Da}^{(s)}\frac{|\Gamma|}{|\mathcal{B}|}\langle\boldsymbol{\chi}^{[1]}\rangle_{\Gamma}-D\langle\nabla_{\boldsymbol{\xi}}\chi^{[2]}\rangle_{\mathcal{B}}\right]\cdot\nabla_{\mathbf{x}}c_0\\ &+\mathrm{Pe}^{(s)}\langle\mathbf{u}_0\rangle_{\mathcal{B}}\cdot\nabla_{\mathbf{x}}\overline{c}_1\\ &-\nabla_{\mathbf{x}}\cdot\left[\left(D\mathbf{I}+D\langle\nabla_{\boldsymbol{\xi}}\boldsymbol{\chi}^{[1]}\rangle_{\mathcal{B}}-\mathrm{Pe}^{(s)}\langle\mathbf{u}_0\otimes\boldsymbol{\chi}^{[1]}\rangle_{\mathcal{B}}\right)\cdot\nabla_{\mathbf{x}}c_0\right]\\ &+\mathrm{Da}^{(s)}\frac{|\Gamma|}{|\mathcal{B}|}\left[\left(c_0-\theta^{(s)}\right)\langle\chi^{[2]}\rangle_{\Gamma}+\overline{c}_1\right]=0 \quad \text{for } \mathbf{x}\in\Omega.\end{aligned} \tag{A16}$$

We now add equations (A4), (A7), and (A16), and make the substitutions $\mathrm{Pe}^{(s)}=\mathrm{Pe}\epsilon$, $\mathrm{Da}^{(s)}=\mathrm{Da}$, and $\theta^{(s)}=\theta$, to obtain

$$\begin{aligned}&\epsilon^{-2}\frac{\partial c_0}{\partial\tau_2}+\epsilon^{-1}\left(\frac{\partial c_0}{\partial\tau_1}+\frac{\partial\overline{c}_1}{\partial\tau_2}\right)+\frac{\partial c_0}{\partial t}+\frac{\partial\overline{c}_1}{\partial\tau_1}+\frac{\partial\langle c_2\rangle_{\mathcal{B}}}{\partial\tau_2}\\ &+\mathrm{Pe}\left[\langle\mathbf{u}_0\rangle_{\mathcal{B}}\cdot\nabla_{\mathbf{x}}c_0+\epsilon\left(\langle\mathbf{u}_1\rangle_{\mathcal{B}}\cdot\nabla_{\mathbf{x}}c_0+\langle\mathbf{u}_0\rangle_{\mathcal{B}}\cdot\nabla_{\mathbf{x}}\overline{c}_1\right)\right]\\ &+\left[\mathrm{Da}\frac{|\Gamma|}{|\mathcal{B}|}\langle\boldsymbol{\chi}^{[1]}\rangle_{\Gamma}-D\langle\nabla_{\boldsymbol{\xi}}\chi^{[2]}\rangle_{\mathcal{B}}+\mathrm{Pe}\epsilon\langle\mathbf{u}_0\chi^{[2]}\rangle_{\mathcal{B}}\right]\cdot\nabla_{\mathbf{x}}c_0\\ &-\nabla_{\mathbf{x}}\cdot\left[\left(D\mathbf{I}+D\langle\nabla_{\boldsymbol{\xi}}\boldsymbol{\chi}^{[1]}\rangle_{\mathcal{B}}-\mathrm{Pe}\epsilon\langle\mathbf{u}_0\otimes\boldsymbol{\chi}^{[1]}\rangle_{\mathcal{B}}\right)\cdot\nabla_{\mathbf{x}}c_0\right]\\ &+\mathrm{Da}\frac{|\Gamma|}{|\mathcal{B}|}\left[\left(c_0-\theta\right)\langle\chi^{[2]}\rangle_{\Gamma}+\left(\frac{1}{\epsilon}c_0+\overline{c}_1\right)-\frac{1}{\epsilon}\theta\right]=0 \quad \text{for } \mathbf{x}\in\Omega.\end{aligned} \tag{A17}$$

Considering the expansions

$$\frac{\partial\langle c\rangle_{\mathcal{B}}}{\partial t} = \epsilon^{-2}\frac{\partial c_0}{\partial \tau_2} + \epsilon^{-1}\left(\frac{\partial c_0}{\partial \tau_1} + \frac{\partial \overline{c}_1}{\partial \tau_2}\right) + \frac{\partial c_0}{\partial t} + \frac{\partial \overline{c}_1}{\partial \tau_1} + \frac{\partial \langle c_2\rangle_{\mathcal{B}}}{\partial \tau_2} + \mathcal{O}\left(\epsilon\right), \tag{A18a}$$

$$\mathrm{Pe}\langle \mathbf{u}\rangle_{\mathcal{B}} \cdot \nabla_{\mathbf{x}}\langle c\rangle_{\mathcal{B}} = \mathrm{Pe}\left[\langle \mathbf{u}_0\rangle_{\mathcal{B}} \cdot \nabla_{\mathbf{x}} c_0 + \epsilon\left(\langle \mathbf{u}_1\rangle_{\mathcal{B}} \cdot \nabla_{\mathbf{x}} c_0 + \langle \mathbf{u}_0\rangle_{\mathcal{B}} \cdot \nabla_{\mathbf{x}} \overline{c}_1\right)\right] + \mathcal{O}\left(\epsilon\right), \tag{A18b}$$

$$\langle c\rangle_{\mathcal{B}} = c_0 + \epsilon \overline{c}_1 + \mathcal{O}\left(\epsilon^2\right), \tag{A18c}$$

$$\langle \mathbf{u}\rangle_{\mathcal{B}} = \mathbf{u}_0 + \mathcal{O}\left(\epsilon\right), \tag{A18d}$$

obtained using equations (10), (12), and system (13), we can simplify equation (A17) to write the homogenized model in system (19) as

$$\phi\frac{\partial\langle c\rangle_Y}{\partial t} + \mathbf{U}\cdot\nabla_{\mathbf{x}}\langle c\rangle_Y - \nabla_{\mathbf{x}}\cdot\left(\mathbf{D}\cdot\nabla_{\mathbf{x}}\langle c\rangle_Y\right) + \mathscr{R}\left(\phi\langle c\rangle_Y - \phi^2\theta\right) = \mathcal{O}\left(\epsilon\right) \quad \text{for } \mathbf{x}\in\Omega, \tag{A19a}$$

$$\mathbf{U} = \mathrm{Pe}\langle \mathbf{u}\rangle_Y + \phi\mathrm{Da}\frac{|\Gamma|}{|\mathcal{B}|}\langle \boldsymbol{\chi}^{[1]}\rangle_\Gamma - D\langle \nabla_{\boldsymbol{\xi}}\chi^{[2]}\rangle_Y + \mathrm{Pe}\epsilon\langle \mathbf{u}\chi^{[2]}\rangle_Y, \tag{A19b}$$

$$\mathbf{D} = \phi D\mathbf{I} + D\langle \nabla_{\boldsymbol{\xi}}\boldsymbol{\chi}^{[1]}\rangle_Y - \mathrm{Pe}\epsilon\langle \mathbf{u}\otimes\boldsymbol{\chi}^{[1]}\rangle_Y, \tag{A19c}$$

$$\mathscr{R} = \mathrm{Da}\frac{|\Gamma|}{|\mathcal{B}|}\left[\epsilon^{-1} + \langle\chi^{[2]}\rangle_\Gamma\right], \tag{A19d}$$

where $\boldsymbol{\chi}^{[1]}$ is found by solving system (A12), $\chi^{[2]}$ is found by solving system (A13), and we have used $\langle\cdot\rangle_{\mathcal{B}} = \phi^{-1}\langle\cdot\rangle_Y$ to convert the averaging operators. We emphasize that these equations are valid when $\mathrm{Pe}\sim\mathcal{O}(\epsilon^{-1})$, $\mathrm{Da}\sim\mathcal{O}(\epsilon^0)$, and $\theta\sim\mathcal{O}(\epsilon^0)$.

With the homogenized model, we reiterate that generalizing the closure form as a linear combination of closure terms allowed the moderately reactive case considered to be homogenized. While the classical treatment of heterogeneous reactions is limited to slow reaction rates (i.e., $\mathrm{Da}\leq\mathcal{O}(\epsilon)$) (Municchi & Icardi, 2020), we were able to linearly separate the inhomogeneous terms of equations (A8) and (A6b) such that two valid closure problems could be defined with an appropriate closure form for c_1. The homogenization procedure could then be completed with little deviation from the classical treatment.

Appendix B Homogenization of a Linear Heterogeneous Reaction: Two-Species

In this Appendix, we provide the detailed derivation of the homogenized system (30) from the pore-scale system (26). Again, the strategy to construct general closure forms for $c_1^{(1)}$ and $c_1^{(2)}$ (system (29)) is explicitly discussed in detail.

B1 Homogenization

Upon expanding the spatial operators, temporal operators, and dependent variables using equations (10), (12), and system (13), we simplify system (26) to

$$
\begin{aligned}
&\epsilon^{-2}\left[\frac{\partial c_0^{(1)}}{\partial \tau_2}+\nabla_{\boldsymbol{\xi}}\cdot\left(\mathrm{Pe}^{(s)}\mathbf{u}_0c_0^{(1)}-D^{(1)}\nabla_{\boldsymbol{\xi}}c_0^{(1)}\right)\right]\\
&+\epsilon^{-1}\left[\frac{\partial c_0^{(1)}}{\partial \tau_1}+\frac{\partial c_1^{(1)}}{\partial \tau_2}+\nabla_{\mathbf{x}}\cdot\left(\mathrm{Pe}^{(s)}\mathbf{u}_0c_0^{(1)}-D^{(1)}\nabla_{\boldsymbol{\xi}}c_0^{(1)}\right)\right.\\
&\left.+\nabla_{\boldsymbol{\xi}}\cdot\left(\mathrm{Pe}^{(s)}\mathbf{u}_1c_0^{(1)}+\mathrm{Pe}^{(s)}\mathbf{u}_0c_1^{(1)}-D^{(1)}\nabla_{\mathbf{x}}c_0^{(1)}-D^{(1)}\nabla_{\boldsymbol{\xi}}c_1^{(1)}\right)\right]\\
&+\epsilon^{0}\left[\frac{\partial c_0^{(1)}}{\partial t}+\frac{\partial c_1^{(1)}}{\partial \tau_1}+\frac{\partial c_2^{(1)}}{\partial \tau_2}+\nabla_{\mathbf{x}}\cdot\left(\mathrm{Pe}^{(s)}\mathbf{u}_1c_0^{(1)}+\mathrm{Pe}^{(s)}\mathbf{u}_0c_1^{(1)}-D^{(1)}\nabla_{\mathbf{x}}c_0^{(1)}-D^{(1)}\nabla_{\boldsymbol{\xi}}c_1^{(1)}\right)\right.\\
&\left.+\nabla_{\boldsymbol{\xi}}\cdot\left(\mathrm{Pe}^{(s)}\mathbf{u}_2c_0^{(1)}+\mathrm{Pe}^{(s)}\mathbf{u}_1c_1^{(1)}+\mathrm{Pe}^{(s)}\mathbf{u}_0c_2^{(1)}-D^{(1)}\nabla_{\mathbf{x}}c_1^{(1)}-D^{(1)}\nabla_{\boldsymbol{\xi}}c_2^{(1)}\right)\right]\\
&=\mathcal{O}\left(\epsilon\right)\quad\text{for }\mathbf{x}\in\Omega,\ \boldsymbol{\xi}\in\mathcal{B},
\end{aligned}
\tag{B1a}
$$

$$
\begin{aligned}
&\epsilon^{-2}\left[\frac{\partial c_0^{(2)}}{\partial \tau_2}+\nabla_{\boldsymbol{\xi}}\cdot\left(\mathrm{Pe}^{(s)}\mathbf{u}_0c_0^{(2)}-D^{(2)}\nabla_{\boldsymbol{\xi}}c_0^{(2)}\right)\right]\\
&+\epsilon^{-1}\left[\frac{\partial c_0^{(2)}}{\partial \tau_1}+\frac{\partial c_1^{(2)}}{\partial \tau_2}+\nabla_{\mathbf{x}}\cdot\left(\mathrm{Pe}^{(s)}\mathbf{u}_0c_0^{(2)}-D^{(2)}\nabla_{\boldsymbol{\xi}}c_0^{(2)}\right)\right.\\
&\left.+\nabla_{\boldsymbol{\xi}}\cdot\left(\mathrm{Pe}^{(s)}\mathbf{u}_1c_0^{(2)}+\mathrm{Pe}^{(s)}\mathbf{u}_0c_1^{(2)}-D^{(2)}\nabla_{\mathbf{x}}c_0^{(2)}-D^{(2)}\nabla_{\boldsymbol{\xi}}c_1^{(2)}\right)\right]\\
&+\epsilon^{0}\left[\frac{\partial c_0^{(2)}}{\partial t}+\frac{\partial c_1^{(2)}}{\partial \tau_1}+\frac{\partial c_2^{(2)}}{\partial \tau_2}+\nabla_{\mathbf{x}}\cdot\left(\mathrm{Pe}^{(s)}\mathbf{u}_1c_0^{(2)}+\mathrm{Pe}^{(s)}\mathbf{u}_0c_1^{(2)}-D^{(2)}\nabla_{\mathbf{x}}c_0^{(2)}-D^{(2)}\nabla_{\boldsymbol{\xi}}c_1^{(2)}\right)\right.\\
&\left.+\nabla_{\boldsymbol{\xi}}\cdot\left(\mathrm{Pe}^{(s)}\mathbf{u}_2c_0^{(2)}+\mathrm{Pe}^{(s)}\mathbf{u}_1c_1^{(2)}+\mathrm{Pe}^{(s)}\mathbf{u}_0c_2^{(2)}-D^{(2)}\nabla_{\mathbf{x}}c_1^{(2)}-D^{(2)}\nabla_{\boldsymbol{\xi}}c_2^{(2)}\right)\right]\\
&=\mathcal{O}\left(\epsilon\right)\quad\text{for }\mathbf{x}\in\Omega,\ \boldsymbol{\xi}\in\mathcal{B},
\end{aligned}
\tag{B1b}
$$

subject to

$$
\begin{aligned}
&\epsilon^{-1}\left[-\mathbf{n}\cdot D^{(1)}\nabla_{\boldsymbol{\xi}}c_0^{(1)}\right]+\epsilon^{0}\left[-\mathbf{n}\cdot D^{(1)}\left(\nabla_{\mathbf{x}}c_0^{(1)}+\nabla_{\boldsymbol{\xi}}c_1^{(1)}\right)\right]+\epsilon\left[-\mathbf{n}\cdot D^{(1)}\left(\nabla_{\mathbf{x}}c_1^{(1)}+\nabla_{\boldsymbol{\xi}}c_2^{(1)}\right)\right]\\
&=\epsilon^{0}\left[\mathrm{Da}_{SL}^{(1,s)}c_0^{(1)}-\mathrm{Da}_{SL}^{(2,s)}c_0^{(2)}\right]+\epsilon\left[\mathrm{Da}_{SL}^{(1,s)}c_1^{(1)}-\mathrm{Da}_{SL}^{(2,s)}c_1^{(2)}\right]+\mathcal{O}\left(\epsilon^2\right)\quad\text{for }\mathbf{x}\in\Omega,\ \boldsymbol{\xi}\in\Gamma,
\end{aligned}
\tag{B1c}
$$

$$
\begin{aligned}
&\epsilon^{-1}\left[-\mathbf{n}\cdot D^{(2)}\nabla_{\boldsymbol{\xi}}c_0^{(2)}\right]+\epsilon^{0}\left[-\mathbf{n}\cdot D^{(2)}\left(\nabla_{\mathbf{x}}c_0^{(2)}+\nabla_{\boldsymbol{\xi}}c_1^{(2)}\right)\right]+\epsilon\left[-\mathbf{n}\cdot D^{(2)}\left(\nabla_{\mathbf{x}}c_1^{(2)}+\nabla_{\boldsymbol{\xi}}c_2^{(2)}\right)\right]\\
&=\epsilon^{0}\left[\mathrm{Da}_{SL}^{(2,s)}c_0^{(2)}-\mathrm{Da}_{SL}^{(1,s)}c_0^{(1)}\right]+\epsilon\left[\mathrm{Da}_{SL}^{(2,s)}c_1^{(2)}-\mathrm{Da}_{SL}^{(1,s)}c_1^{(1)}\right]+\mathcal{O}\left(\epsilon^2\right)\quad\text{for }\mathbf{x}\in\Omega,\ \boldsymbol{\xi}\in\Gamma,
\end{aligned}
\tag{B1d}
$$

where $\mathrm{Pe}^{(s)}\equiv\mathrm{Pe}\epsilon\sim\mathcal{O}(\epsilon^0)$, $\mathrm{Da}_{SL}^{(1,s)}\equiv\mathrm{Da}_{SL}^{(1)}\sim\mathcal{O}(\epsilon^0)$, and $\mathrm{Da}_{SL}^{(2,s)}\equiv\mathrm{Da}_{SL}^{(2)}\sim\mathcal{O}(\epsilon^0)$ are used to track where the dimensionless numbers appear in the final homogenized model. Similar to before, we simplify equation (6b) using equations (10) and (13b), such that

$$
\epsilon^{-1}\left[\nabla_{\boldsymbol{\xi}}\cdot\mathbf{u}_0\right]+\epsilon^{0}\left[\nabla_{\mathbf{x}}\cdot\mathbf{u}_0+\nabla_{\boldsymbol{\xi}}\cdot\mathbf{u}_1\right]+\epsilon\left[\nabla_{\mathbf{x}}\cdot\mathbf{u}_1+\nabla_{\boldsymbol{\xi}}\cdot\mathbf{u}_2\right]=\mathcal{O}\left(\epsilon^2\right)\quad\text{for }\mathbf{x}\in\Omega,\ \boldsymbol{\xi}\in\mathcal{B}.
\tag{B2}
$$

We now create a system of differential equations from system (B1) by considering the terms at each order of ϵ independently.

B11 Terms of Order $\mathcal{O}\left(\epsilon^{-2}\right)$

After collecting the leading order terms in system (B1), we gain

$$
\frac{\partial c_0^{(1)}}{\partial \tau_2}+\nabla_{\boldsymbol{\xi}}\cdot\left(\mathrm{Pe}^{(s)}\mathbf{u}_0c_0^{(1)}-D^{(1)}\nabla_{\boldsymbol{\xi}}c_0^{(1)}\right)=0\quad\text{for }\mathbf{x}\in\Omega,\ \boldsymbol{\xi}\in\mathcal{B},
\tag{B3a}
$$

$$\frac{\partial c_0^{(2)}}{\partial \tau_2} + \nabla_{\boldsymbol{\xi}} \cdot \left(\mathrm{Pe}^{(s)} \mathbf{u}_0 c_0^{(2)} - D^{(2)} \nabla_{\boldsymbol{\xi}} c_0^{(2)} \right) = 0 \quad \text{for } \mathbf{x} \in \Omega,\ \boldsymbol{\xi} \in \mathcal{B}, \tag{B3b}$$

subject to the leading order boundary conditions (i.e., at $\mathcal{O}(\epsilon^{-1})$)

$$-\mathbf{n} \cdot D^{(1)} \nabla_{\boldsymbol{\xi}} c_0^{(1)} = 0 \quad \text{for } \mathbf{x} \in \Omega,\ \boldsymbol{\xi} \in \Gamma, \tag{B3c}$$

$$-\mathbf{n} \cdot D^{(2)} \nabla_{\boldsymbol{\xi}} c_0^{(2)} = 0 \quad \text{for } \mathbf{x} \in \Omega,\ \boldsymbol{\xi} \in \Gamma. \tag{B3d}$$

Similar to before, we apply the averaging operator $\langle \cdot \rangle_{\mathcal{B}}$ (equation (11)) to equations (B3a)-(B3b) and implement the divergence theorem on both the diffusive and advective flux terms. While the boundary conditions (equations (B3c)-(B3d)) are applied through the diffusive flux, we enforce the no-slip condition and consider that $\mathbf{u}_0$ and c_0 are periodic in $\boldsymbol{\xi}$ to simplify the advective flux and gain

$$\frac{\partial \langle c_0^{(1)} \rangle_{\mathcal{B}}}{\partial \tau_2} = 0 \quad \text{for } \mathbf{x} \in \Omega, \tag{B4a}$$

$$\frac{\partial \langle c_0^{(2)} \rangle_{\mathcal{B}}}{\partial \tau_2} = 0 \quad \text{for } \mathbf{x} \in \Omega. \tag{B4b}$$

Again, we find these equations to be results of upholding the initial hypotheses regarding the magnitudes of the dimensionless parameters and the periodicity of the system. Then, considering $\nabla_{\boldsymbol{\xi}} \cdot \mathbf{u}_0 = 0$ from the $\mathcal{O}(\epsilon^{-1})$ terms of equation (B2), initial conditions that are independent of $\boldsymbol{\xi}$, and the homogeneity of the system, we find $c_0^{(1)} = c_0^{(1)}(t, \mathbf{x}, \tau_1(t))$ and $c_0^{(2)} = c_0^{(2)}(t, \mathbf{x}, \tau_1(t))$.

B12 Terms of Order $\mathcal{O}(\epsilon^{-1})$

At the following order, we collect terms from system (B1) to write

$$\begin{aligned} &\frac{\partial c_0^{(1)}}{\partial \tau_1} + \frac{\partial c_1^{(1)}}{\partial \tau_2} + \nabla_{\mathbf{x}} \cdot \left(\mathrm{Pe}^{(s)} \mathbf{u}_0 c_0^{(1)} - D^{(1)} \nabla_{\boldsymbol{\xi}} c_0^{(1)} \right) \\ &+ \nabla_{\boldsymbol{\xi}} \cdot \left(\mathrm{Pe}^{(s)} \mathbf{u}_1 c_0^{(1)} + \mathrm{Pe}^{(s)} \mathbf{u}_0 c_1^{(1)} - D^{(1)} \nabla_{\mathbf{x}} c_0^{(1)} - D^{(1)} \nabla_{\boldsymbol{\xi}} c_1^{(1)} \right) = 0 \quad \text{for } \mathbf{x} \in \Omega,\ \boldsymbol{\xi} \in \mathcal{B}, \end{aligned} \tag{B5a}$$

$$\begin{aligned} &\frac{\partial c_0^{(2)}}{\partial \tau_1} + \frac{\partial c_1^{(2)}}{\partial \tau_2} + \nabla_{\mathbf{x}} \cdot \left(\mathrm{Pe}^{(s)} \mathbf{u}_0 c_0^{(2)} - D^{(2)} \nabla_{\boldsymbol{\xi}} c_0^{(2)} \right) \\ &+ \nabla_{\boldsymbol{\xi}} \cdot \left(\mathrm{Pe}^{(s)} \mathbf{u}_1 c_0^{(2)} + \mathrm{Pe}^{(s)} \mathbf{u}_0 c_1^{(2)} - D^{(2)} \nabla_{\mathbf{x}} c_0^{(2)} - D^{(2)} \nabla_{\boldsymbol{\xi}} c_1^{(2)} \right) = 0 \quad \text{for } \mathbf{x} \in \Omega,\ \boldsymbol{\xi} \in \mathcal{B}, \end{aligned} \tag{B5b}$$

subject to the boundary conditions (i.e., at $\mathcal{O}(\epsilon^0)$)

$$-\mathbf{n} \cdot D^{(1)} \left(\nabla_{\mathbf{x}} c_0^{(1)} + \nabla_{\boldsymbol{\xi}} c_1^{(1)} \right) = \mathrm{Da}_{SL}^{(1,s)} c_0^{(1)} - \mathrm{Da}_{SL}^{(2,s)} c_0^{(2)} \quad \text{for } \mathbf{x} \in \Omega,\ \boldsymbol{\xi} \in \Gamma, \tag{B5c}$$

$$-\mathbf{n} \cdot D^{(2)} \left(\nabla_{\mathbf{x}} c_0^{(2)} + \nabla_{\boldsymbol{\xi}} c_1^{(2)} \right) = \mathrm{Da}_{SL}^{(2,s)} c_0^{(2)} - \mathrm{Da}_{SL}^{(1,s)} c_0^{(1)} \quad \text{for } \mathbf{x} \in \Omega,\ \boldsymbol{\xi} \in \Gamma. \tag{B5d}$$

Again, we apply the averaging operator $\langle \cdot \rangle_{\mathcal{B}}$ (equation (11)) to equations (B5a)-(B5b), implement the divergence theorem, and apply the boundary conditions (equations (B5c)-(B5d)) and no-slip condition to the equations. In doing so, we consider $\mathbf{u}_0$, $\mathbf{u}_1$, and c_1 as periodic in $\boldsymbol{\xi}$ to simplify the system to

$$\frac{\partial c_0^{(1)}}{\partial \tau_1} + \frac{\partial \langle c_1^{(1)} \rangle_{\mathcal{B}}}{\partial \tau_2} + \mathrm{Pe}^{(s)} \langle \mathbf{u}_0 \rangle_{\mathcal{B}} \cdot \nabla_{\mathbf{x}} c_0^{(1)} + \frac{|\Gamma|}{|\mathcal{B}|} \left(\mathrm{Da}_{SL}^{(1,s)} c_0^{(1)} - \mathrm{Da}_{SL}^{(2,s)} c_0^{(2)} \right) = 0 \quad \text{for } \mathbf{x} \in \Omega, \tag{B6a}$$

$$\frac{\partial c_0^{(2)}}{\partial \tau_1} + \frac{\partial \langle c_1^{(2)} \rangle_{\mathcal{B}}}{\partial \tau_2} + \mathrm{Pe}^{(s)} \langle \mathbf{u}_0 \rangle_{\mathcal{B}} \cdot \nabla_{\mathbf{x}} c_0^{(2)} + \frac{|\Gamma|}{|\mathcal{B}|} \left(\mathrm{Da}_{SL}^{(2,s)} c_0^{(2)} - \mathrm{Da}_{SL}^{(1,s)} c_0^{(1)} \right) = 0 \quad \text{for } \mathbf{x} \in \Omega. \tag{B6b}$$

Similar to before, system (B6) describes how the zeroth and averaged first order concentrations vary with fast time variables $\tau_1(t)$ and $\tau_2(t)$, respectively. It is worth noting that a steady state can exist (i.e., when $\partial c_0^{(i)}/\partial \tau_1 = 0$ and $\partial \langle c_1^{(i)} \rangle_{\mathcal{B}}/\partial \tau_2 = 0$ for $i \in \{1, 2\}$), but is not required for all times, as implied by equation (30) in the work of Bourbatache *et al.* (Bourbatache et al., 2020). This difference is a result of considering additional time scales in the derivation.

Returning to equation (B2), we apply the averaging operator $\langle \cdot \rangle_{\mathcal{B}}$ and the divergence theorem to the $\mathcal{O}(\epsilon^0)$ terms, and assume $\mathbf{u}_1$ is periodic in $\boldsymbol{\xi}$ with the no-slip condition to conclude that $\nabla_{\mathbf{x}} \cdot \mathbf{u}_0 = 0$. Ultimately, this lead to $\nabla_{\boldsymbol{\xi}} \cdot \mathbf{u}_1 = 0$ as well. Then, we subtract equation (B6a) from equation (B5a), and equation (B6b) from equation (B5b) to gain

$$\begin{aligned} &\frac{\partial c_1^{(1)}}{\partial \tau_2} - \frac{\partial \langle c_1^{(1)} \rangle_{\mathcal{B}}}{\partial \tau_2} + \mathrm{Pe}^{(s)} \left(\mathbf{u}_0 - \langle \mathbf{u}_0 \rangle_{\mathcal{B}} \right) \cdot \nabla_{\mathbf{x}} c_0^{(1)} - \frac{|\Gamma|}{|\mathcal{B}|} \left(\mathrm{Da}_{SL}^{(1,s)} c_0^{(1)} - \mathrm{Da}_{SL}^{(2,s)} c_0^{(2)} \right) \\ &+ \mathrm{Pe}^{(s)} \mathbf{u}_0 \cdot \nabla_{\boldsymbol{\xi}} c_1^{(1)} - \nabla_{\boldsymbol{\xi}} \cdot \left(D^{(1)} \nabla_{\mathbf{x}} c_0^{(1)} + D^{(1)} \nabla_{\boldsymbol{\xi}} c_1^{(1)} \right) = 0 \quad \text{for } \mathbf{x} \in \Omega,\ \boldsymbol{\xi} \in \mathcal{B}, \end{aligned} \tag{B7a}$$

$$\begin{aligned} &\frac{\partial c_1^{(2)}}{\partial \tau_2} - \frac{\partial \langle c_1^{(2)} \rangle_{\mathcal{B}}}{\partial \tau_2} + \mathrm{Pe}^{(s)} \left(\mathbf{u}_0 - \langle \mathbf{u}_0 \rangle_{\mathcal{B}} \right) \cdot \nabla_{\mathbf{x}} c_0^{(2)} - \frac{|\Gamma|}{|\mathcal{B}|} \left(\mathrm{Da}_{SL}^{(2,s)} c_0^{(2)} - \mathrm{Da}_{SL}^{(1,s)} c_0^{(1)} \right) \\ &+ \mathrm{Pe}^{(s)} \mathbf{u}_0 \cdot \nabla_{\boldsymbol{\xi}} c_1^{(2)} - \nabla_{\boldsymbol{\xi}} \cdot \left(D^{(2)} \nabla_{\mathbf{x}} c_0^{(2)} + D^{(2)} \nabla_{\boldsymbol{\xi}} c_1^{(2)} \right) = 0 \quad \text{for } \mathbf{x} \in \Omega,\ \boldsymbol{\xi} \in \mathcal{B}, \end{aligned} \tag{B7b}$$

subject to the boundary conditions in equations (B5c)-(B5d). Due to the linearity of the system, we again assume solutions of the form $c_1^{(i)} = c_1^{(i)[1]} + c_1^{(i)[2]}$, for $i \in \{1, 2\}$, and linearly separate the systems. While the separated equations for $c_1^{(i)[1]}$ and $c_1^{(i)[2]}$ may be found in Appendix C, we provide the assumed solution forms as

$$c_1^{(1)} = \boldsymbol{\chi}^{(1)[1]} \cdot \nabla_{\mathbf{x}} c_0^{(1)} + \left(\mathrm{Da}_{SL}^{(1,s)} c_0^{(1)} - \mathrm{Da}_{SL}^{(2,s)} c_0^{(2)} \right) \chi^{(1)[2]} + \overline{c}_1^{(1)}, \tag{B8a}$$

$$c_1^{(2)} = \boldsymbol{\chi}^{(2)[1]} \cdot \nabla_{\mathbf{x}} c_0^{(2)} + \left(\mathrm{Da}_{SL}^{(2,s)} c_0^{(2)} - \mathrm{Da}_{SL}^{(1,s)} c_0^{(1)} \right) \chi^{(2)[2]} + \overline{c}_1^{(2)}, \tag{B8b}$$

and the closure problems for the four closure variables as

$$\mathrm{Pe}^{(s)} \left(\mathbf{u}_0 - \langle \mathbf{u}_0 \rangle_{\mathcal{B}} \right) + \mathrm{Pe}^{(s)} \mathbf{u}_0 \cdot \nabla_{\boldsymbol{\xi}} \boldsymbol{\chi}^{(i)[1]} - D^{(i)} \nabla_{\boldsymbol{\xi}} \cdot \left(\mathbf{I} + \nabla_{\boldsymbol{\xi}} \boldsymbol{\chi}^{(i)[1]} \right) = \mathbf{0} \quad \text{for } \boldsymbol{\xi} \in \mathcal{B}, \tag{B9a}$$

subject to

$$-\mathbf{n} \cdot D^{(i)} \left(\mathbf{I} + \nabla_{\boldsymbol{\xi}} \boldsymbol{\chi}^{(i)[1]} \right) = \mathbf{0} \quad \text{for } \boldsymbol{\xi} \in \Gamma, \tag{B9b}$$

and

$$-\frac{|\Gamma|}{|\mathcal{B}|} + \mathrm{Pe}^{(s)} \mathbf{u}_0 \cdot \nabla_{\boldsymbol{\xi}} \chi^{(i)[2]} - D^{(i)} \nabla_{\boldsymbol{\xi}}^2 \chi^{(i)[2]} = 0 \quad \text{for } \boldsymbol{\xi} \in \mathcal{B}, \tag{B10a}$$

subject to

$$-\mathbf{n} \cdot D^{(i)} \nabla_{\boldsymbol{\xi}} \chi^{(i)[2]} = 1 \quad \text{for } \boldsymbol{\xi} \in \Gamma. \tag{B10b}$$

B13 Terms of Order $\mathcal{O}(\epsilon^0)$

Finally, we collect terms of $\mathcal{O}(\epsilon^0)$ from system (B1) to write

$$\begin{aligned}\frac{\partial c_0^{(1)}}{\partial t}+\frac{\partial c_1^{(1)}}{\partial \tau_1}+\frac{\partial c_2^{(1)}}{\partial \tau_2}+\nabla_{\mathbf{x}}\cdot\left(\mathrm{Pe}^{(s)}\mathbf{u}_1c_0^{(1)}+\mathrm{Pe}^{(s)}\mathbf{u}_0c_1^{(1)}-D^{(1)}\nabla_{\mathbf{x}}c_0^{(1)}-D^{(1)}\nabla_{\boldsymbol{\xi}}c_1^{(1)}\right)\\ +\nabla_{\boldsymbol{\xi}}\cdot\left(\mathrm{Pe}^{(s)}\mathbf{u}_2c_0^{(1)}+\mathrm{Pe}^{(s)}\mathbf{u}_1c_1^{(1)}+\mathrm{Pe}^{(s)}\mathbf{u}_0c_2^{(1)}-D^{(1)}\nabla_{\mathbf{x}}c_1^{(1)}-D^{(1)}\nabla_{\boldsymbol{\xi}}c_2^{(1)}\right)\\ =0\quad\text{for }\mathbf{x}\in\Omega,\ \boldsymbol{\xi}\in\mathcal{B},\end{aligned}\tag{B11a}$$

$$\begin{aligned}\frac{\partial c_0^{(2)}}{\partial t}+\frac{\partial c_1^{(2)}}{\partial \tau_1}+\frac{\partial c_2^{(2)}}{\partial \tau_2}+\nabla_{\mathbf{x}}\cdot\left(\mathrm{Pe}^{(s)}\mathbf{u}_1c_0^{(2)}+\mathrm{Pe}^{(s)}\mathbf{u}_0c_1^{(2)}-D^{(2)}\nabla_{\mathbf{x}}c_0^{(2)}-D^{(2)}\nabla_{\boldsymbol{\xi}}c_1^{(2)}\right)\\ +\nabla_{\boldsymbol{\xi}}\cdot\left(\mathrm{Pe}^{(s)}\mathbf{u}_2c_0^{(2)}+\mathrm{Pe}^{(s)}\mathbf{u}_1c_1^{(2)}+\mathrm{Pe}^{(s)}\mathbf{u}_0c_2^{(2)}-D^{(2)}\nabla_{\mathbf{x}}c_1^{(2)}-D^{(2)}\nabla_{\boldsymbol{\xi}}c_2^{(2)}\right)\\ =0\quad\text{for }\mathbf{x}\in\Omega,\ \boldsymbol{\xi}\in\mathcal{B},\end{aligned}\tag{B11b}$$

subject to the boundary conditions (i.e., at $\mathcal{O}(\epsilon)$)

$$-\mathbf{n}\cdot D^{(1)}\left(\nabla_{\mathbf{x}}c_1^{(1)}+\nabla_{\boldsymbol{\xi}}c_2^{(1)}\right)=\mathrm{Da}_{SL}^{(1,s)}c_1^{(1)}-\mathrm{Da}_{SL}^{(2,s)}c_1^{(2)}\quad\text{for }\mathbf{x}\in\Omega,\ \boldsymbol{\xi}\in\Gamma,\tag{B11c}$$

$$-\mathbf{n}\cdot D^{(2)}\left(\nabla_{\mathbf{x}}c_1^{(2)}+\nabla_{\boldsymbol{\xi}}c_2^{(2)}\right)=\mathrm{Da}_{SL}^{(2,s)}c_1^{(2)}-\mathrm{Da}_{SL}^{(1,s)}c_1^{(1)}\quad\text{for }\mathbf{x}\in\Omega,\ \boldsymbol{\xi}\in\Gamma.\tag{B11d}$$

After substituting in the solutions for $c_1^{(i)}$ (system (B8)), we again apply the averaging operator $\langle\cdot\rangle_{\mathcal{B}}$ (equation (11)) to equations (B11a)-(B11b), and implement the divergence theorem to incorporate the boundary conditions (equations (B11c)-(B11d)) and the no-slip condition. Further simplifications regarding the periodicity of the dependent variables in $\boldsymbol{\xi}$ are also made to write

$$\begin{aligned}\frac{\partial c_0^{(1)}}{\partial t}+\frac{\partial \overline{c}_1^{(1)}}{\partial \tau_1}+\frac{\partial \langle c_2^{(1)}\rangle_{\mathcal{B}}}{\partial \tau_2}+\Big[\mathrm{Pe}^{(s)}\left(\langle\mathbf{u}_1\rangle_{\mathcal{B}}+\mathrm{Da}_{SL}^{(1,s)}\langle\mathbf{u}_0\chi^{(1)[2]}\rangle_{\mathcal{B}}\right)\\ +\mathrm{Da}_{SL}^{(1,s)}\frac{|\Gamma|}{|\mathcal{B}|}\langle\boldsymbol{\chi}^{(1)[1]}\rangle_{\Gamma}-\mathrm{Da}_{SL}^{(1,s)}D^{(1)}\langle\nabla_{\boldsymbol{\xi}}\chi^{(1)[2]}\rangle_{\mathcal{B}}\Big]\cdot\nabla_{\mathbf{x}}c_0^{(1)}+\mathrm{Pe}^{(s)}\langle\mathbf{u}_0\rangle_{\mathcal{B}}\cdot\nabla_{\mathbf{x}}\overline{c}_1^{(1)}\\ -\mathrm{Da}_{SL}^{(2,s)}\left[\frac{|\Gamma|}{|\mathcal{B}|}\langle\boldsymbol{\chi}^{(2)[1]}\rangle_{\Gamma}-D^{(1)}\langle\nabla_{\boldsymbol{\xi}}\chi^{(1)[2]}\rangle_{\mathcal{B}}+\mathrm{Pe}^{(s)}\langle\mathbf{u}_0\chi^{(1)[2]}\rangle_{\mathcal{B}}\right]\cdot\nabla_{\mathbf{x}}c_0^{(2)}\\ -\nabla_{\mathbf{x}}\cdot\left[\left(D^{(1)}\mathbf{I}+D^{(1)}\langle\nabla_{\boldsymbol{\xi}}\boldsymbol{\chi}^{(1)[1]}\rangle_{\mathcal{B}}-\mathrm{Pe}^{(s)}\langle\mathbf{u}_0\otimes\boldsymbol{\chi}^{(1)[1]}\rangle_{\mathcal{B}}\right)\cdot\nabla_{\mathbf{x}}c_0^{(1)}\right]\\ +\mathrm{Da}_{SL}^{(1,s)}\frac{|\Gamma|}{|\mathcal{B}|}\left[\mathrm{Da}_{SL}^{(1,s)}\langle\chi^{(1)[2]}\rangle_{\Gamma}+\mathrm{Da}_{SL}^{(2,s)}\langle\chi^{(2)[2]}\rangle_{\Gamma}\right]c_0^{(1)}\\ -\mathrm{Da}_{SL}^{(2,s)}\frac{|\Gamma|}{|\mathcal{B}|}\left[\mathrm{Da}_{SL}^{(1,s)}\langle\chi^{(1)[2]}\rangle_{\Gamma}+\mathrm{Da}_{SL}^{(2,s)}\langle\chi^{(2)[2]}\rangle_{\Gamma}\right]c_0^{(2)}\\ +\mathrm{Da}_{SL}^{(1,s)}\frac{|\Gamma|}{|\mathcal{B}|}\overline{c}_1^{(1)}-\mathrm{Da}_{SL}^{(2,s)}\frac{|\Gamma|}{|\mathcal{B}|}\overline{c}_1^{(2)}=0\quad\text{for }\mathbf{x}\in\Omega,\end{aligned}\tag{B12a}$$

$$
\begin{aligned}
&\frac{\partial c_0^{(2)}}{\partial t}+\frac{\partial \overline{c}_1^{(2)}}{\partial \tau_1}+\frac{\partial \langle c_2^{(2)}\rangle_{\mathcal{B}}}{\partial \tau_2}+\Big[\mathrm{Pe}^{(s)}\left(\langle \mathbf{u}_1\rangle_{\mathcal{B}}+\mathrm{Da}_{SL}^{(2,s)}\langle \mathbf{u}_0\chi^{(2)[2]}\rangle_{\mathcal{B}}\right)\\
&+\mathrm{Da}_{SL}^{(2,s)}\frac{|\Gamma|}{|\mathcal{B}|}\langle \boldsymbol{\chi}^{(2)[1]}\rangle_{\Gamma}-\mathrm{Da}_{SL}^{(2,s)}D^{(2)}\langle \nabla_{\boldsymbol{\xi}}\chi^{(2)[2]}\rangle_{\mathcal{B}}\Big]\cdot\nabla_{\mathbf{x}}c_0^{(2)}+\mathrm{Pe}^{(s)}\langle \mathbf{u}_0\rangle_{\mathcal{B}}\cdot\nabla_{\mathbf{x}}\overline{c}_1^{(2)}\\
&-\mathrm{Da}_{SL}^{(1,s)}\left[\frac{|\Gamma|}{|\mathcal{B}|}\langle \boldsymbol{\chi}^{(1)[1]}\rangle_{\Gamma}-D^{(2)}\langle \nabla_{\boldsymbol{\xi}}\chi^{(2)[2]}\rangle_{\mathcal{B}}+\mathrm{Pe}^{(s)}\langle \mathbf{u}_0\chi^{(2)[2]}\rangle_{\mathcal{B}}\right]\cdot\nabla_{\mathbf{x}}c_0^{(1)}\\
&-\nabla_{\mathbf{x}}\cdot\left[\left(D^{(2)}\mathbf{I}+D^{(2)}\langle \nabla_{\boldsymbol{\xi}}\boldsymbol{\chi}^{(2)[1]}\rangle_{\mathcal{B}}-\mathrm{Pe}^{(s)}\langle \mathbf{u}_0\otimes\boldsymbol{\chi}^{(2)[1]}\rangle_{\mathcal{B}}\right)\cdot\nabla_{\mathbf{x}}c_0^{(2)}\right]\\
&+\mathrm{Da}_{SL}^{(2,s)}\frac{|\Gamma|}{|\mathcal{B}|}\left[\mathrm{Da}_{SL}^{(2,s)}\langle \chi^{(2)[2]}\rangle_{\Gamma}+\mathrm{Da}_{SL}^{(1,s)}\langle \chi^{(1)[2]}\rangle_{\Gamma}\right]c_0^{(2)}\\
&-\mathrm{Da}_{SL}^{(1,s)}\frac{|\Gamma|}{|\mathcal{B}|}\left[\mathrm{Da}_{SL}^{(2,s)}\langle \chi^{(2)[2]}\rangle_{\Gamma}+\mathrm{Da}_{SL}^{(1,s)}\langle \chi^{(1)[2]}\rangle_{\Gamma}\right]c_0^{(1)}\\
&+\mathrm{Da}_{SL}^{(2,s)}\frac{|\Gamma|}{|\mathcal{B}|}\overline{c}_1^{(2)}-\mathrm{Da}_{SL}^{(1,s)}\frac{|\Gamma|}{|\mathcal{B}|}\overline{c}_1^{(1)}=0\quad\text{for }\mathbf{x}\in\Omega.
\end{aligned}
\tag{B12b}
$$

We now add equations (B4a), (B6a), and (B12a) together, and equations (B4b), (B6b), and (B12b) together. Upon making the substitutions $\mathrm{Pe}^{(s)}=\mathrm{Pe}\epsilon$, $\mathrm{Da}_{SL}^{(1,s)}=\mathrm{Da}_{SL}^{(1)}$, and $\mathrm{Da}_{SL}^{(2,s)}=\mathrm{Da}_{SL}^{(2)}$, we obtain

$$
\begin{aligned}
&\epsilon^{-2}\frac{\partial c_0^{(1)}}{\partial \tau_2}+\epsilon^{-1}\left(\frac{\partial c_0^{(1)}}{\partial \tau_1}+\frac{\partial \overline{c}_1^{(1)}}{\partial \tau_2}\right)+\frac{\partial c_0^{(1)}}{\partial t}+\frac{\partial \overline{c}_1^{(1)}}{\partial \tau_1}+\frac{\partial \langle c_2^{(1)}\rangle_{\mathcal{B}}}{\partial \tau_2}\\
&+\mathrm{Pe}\left[\langle \mathbf{u}_0\rangle_{\mathcal{B}}\cdot\nabla_{\mathbf{x}}c_0^{(1)}+\epsilon\left(\langle \mathbf{u}_1\rangle_{\mathcal{B}}\cdot\nabla_{\mathbf{x}}c_0^{(1)}+\langle \mathbf{u}_0\rangle_{\mathcal{B}}\cdot\nabla_{\mathbf{x}}\overline{c}_1^{(1)}\right)\right]\\
&+\mathrm{Da}_{SL}^{(1)}\left[\frac{|\Gamma|}{|\mathcal{B}|}\langle \boldsymbol{\chi}^{(1)[1]}\rangle_{\Gamma}-D^{(1)}\langle \nabla_{\boldsymbol{\xi}}\chi^{(1)[2]}\rangle_{\mathcal{B}}+\mathrm{Pe}\epsilon\langle \mathbf{u}_0\chi^{(1)[2]}\rangle_{\mathcal{B}}\right]\cdot\nabla_{\mathbf{x}}c_0^{(1)}\\
&-\mathrm{Da}_{SL}^{(2)}\left[\frac{|\Gamma|}{|\mathcal{B}|}\langle \boldsymbol{\chi}^{(2)[1]}\rangle_{\Gamma}-D^{(1)}\langle \nabla_{\boldsymbol{\xi}}\chi^{(1)[2]}\rangle_{\mathcal{B}}+\mathrm{Pe}\epsilon\langle \mathbf{u}_0\chi^{(1)[2]}\rangle_{\mathcal{B}}\right]\cdot\nabla_{\mathbf{x}}c_0^{(2)}\\
&-\nabla_{\mathbf{x}}\cdot\left[\left(D^{(1)}\mathbf{I}+D^{(1)}\langle \nabla_{\boldsymbol{\xi}}\boldsymbol{\chi}^{(1)[1]}\rangle_{\mathcal{B}}-\mathrm{Pe}\epsilon\langle \mathbf{u}_0\otimes\boldsymbol{\chi}^{(1)[1]}\rangle_{\mathcal{B}}\right)\cdot\nabla_{\mathbf{x}}c_0^{(1)}\right]\\
&+\mathrm{Da}_{SL}^{(1)}\frac{|\Gamma|}{|\mathcal{B}|}\left[\mathrm{Da}_{SL}^{(1)}\langle \chi^{(1)[2]}\rangle_{\Gamma}+\mathrm{Da}_{SL}^{(2)}\langle \chi^{(2)[2]}\rangle_{\Gamma}\right]c_0^{(1)}\\
&-\mathrm{Da}_{SL}^{(2)}\frac{|\Gamma|}{|\mathcal{B}|}\left[\mathrm{Da}_{SL}^{(1)}\langle \chi^{(1)[2]}\rangle_{\Gamma}+\mathrm{Da}_{SL}^{(2)}\langle \chi^{(2)[2]}\rangle_{\Gamma}\right]c_0^{(2)}\\
&+\epsilon^{-1}\mathrm{Da}_{SL}^{(1)}\frac{|\Gamma|}{|\mathcal{B}|}\left[c_0^{(1)}+\epsilon\overline{c}_1^{(1)}\right]-\epsilon^{-1}\mathrm{Da}_{SL}^{(2)}\frac{|\Gamma|}{|\mathcal{B}|}\left[c_0^{(2)}+\epsilon\overline{c}_1^{(2)}\right]=0\quad\text{for }\mathbf{x}\in\Omega,
\end{aligned}
\tag{B13a}
$$

$$
\begin{aligned}
&\epsilon^{-2}\frac{\partial c_0^{(2)}}{\partial \tau_2}+\epsilon^{-1}\left(\frac{\partial c_0^{(2)}}{\partial \tau_1}+\frac{\partial \overline{c}_1^{(2)}}{\partial \tau_2}\right)+\frac{\partial c_0^{(2)}}{\partial t}+\frac{\partial \overline{c}_1^{(2)}}{\partial \tau_1}+\frac{\partial \langle c_2^{(2)}\rangle_{\mathcal{B}}}{\partial \tau_2}\\
&+\mathrm{Pe}\left[\langle \mathbf{u}_0\rangle_{\mathcal{B}}\cdot\nabla_{\mathbf{x}}c_0^{(2)}+\epsilon\left(\langle \mathbf{u}_1\rangle_{\mathcal{B}}\cdot\nabla_{\mathbf{x}}c_0^{(2)}+\langle \mathbf{u}_0\rangle_{\mathcal{B}}\cdot\nabla_{\mathbf{x}}\overline{c}_1^{(2)}\right)\right]\\
&+\mathrm{Da}_{SL}^{(2)}\left[\frac{|\Gamma|}{|\mathcal{B}|}\langle \boldsymbol{\chi}^{(2)[1]}\rangle_{\Gamma}-D^{(2)}\langle \nabla_{\boldsymbol{\xi}}\chi^{(2)[2]}\rangle_{\mathcal{B}}+\mathrm{Pe}\epsilon\langle \mathbf{u}_0\chi^{(2)[2]}\rangle_{\mathcal{B}}\right]\cdot\nabla_{\mathbf{x}}c_0^{(2)}\\
&-\mathrm{Da}_{SL}^{(1)}\left[\frac{|\Gamma|}{|\mathcal{B}|}\langle \boldsymbol{\chi}^{(1)[1]}\rangle_{\Gamma}-D^{(2)}\langle \nabla_{\boldsymbol{\xi}}\chi^{(2)[2]}\rangle_{\mathcal{B}}+\mathrm{Pe}\epsilon\langle \mathbf{u}_0\chi^{(2)[2]}\rangle_{\mathcal{B}}\right]\cdot\nabla_{\mathbf{x}}c_0^{(1)}\\
&-\nabla_{\mathbf{x}}\cdot\left[\left(D^{(2)}\mathbf{I}+D^{(2)}\langle \nabla_{\boldsymbol{\xi}}\boldsymbol{\chi}^{(2)[1]}\rangle_{\mathcal{B}}-\mathrm{Pe}\epsilon\langle \mathbf{u}_0\otimes\boldsymbol{\chi}^{(2)[1]}\rangle_{\mathcal{B}}\right)\cdot\nabla_{\mathbf{x}}c_0^{(2)}\right]\\
&+\mathrm{Da}_{SL}^{(2)}\frac{|\Gamma|}{|\mathcal{B}|}\left[\mathrm{Da}_{SL}^{(2)}\langle \chi^{(2)[2]}\rangle_{\Gamma}+\mathrm{Da}_{SL}^{(1)}\langle \chi^{(1)[2]}\rangle_{\Gamma}\right]c_0^{(2)}\\
&-\mathrm{Da}_{SL}^{(1)}\frac{|\Gamma|}{|\mathcal{B}|}\left[\mathrm{Da}_{SL}^{(2)}\langle \chi^{(2)[2]}\rangle_{\Gamma}+\mathrm{Da}_{SL}^{(1)}\langle \chi^{(1)[2]}\rangle_{\Gamma}\right]c_0^{(1)}\\
&+\epsilon^{-1}\mathrm{Da}_{SL}^{(2)}\frac{|\Gamma|}{|\mathcal{B}|}\left[c_0^{(2)}+\epsilon\overline{c}_1^{(2)}\right]-\epsilon^{-1}\mathrm{Da}_{SL}^{(1)}\frac{|\Gamma|}{|\mathcal{B}|}\left[c_0^{(1)}+\epsilon\overline{c}_1^{(1)}\right]=0\quad\text{for }\mathbf{x}\in\Omega.
\end{aligned}
\tag{B13b}
$$

Considering the expansions

$$\frac{\partial\langle c^{(i)}\rangle_{\mathcal{B}}}{\partial t}=\epsilon^{-2}\frac{\partial c_0^{(i)}}{\partial\tau_2}+\epsilon^{-1}\left(\frac{\partial c_0^{(i)}}{\partial\tau_1}+\frac{\partial\overline{c}_1^{(i)}}{\partial\tau_2}\right)+\frac{\partial c_0^{(i)}}{\partial t}+\frac{\partial\overline{c}_1^{(i)}}{\partial\tau_1}+\frac{\partial\langle c_2^{(i)}\rangle_{\mathcal{B}}}{\partial\tau_2}+\mathcal{O}\left(\epsilon\right), \tag{B14a}$$

$$\mathrm{Pe}\langle\mathbf{u}\rangle_{\mathcal{B}}\cdot\nabla_{\mathbf{x}}\langle c^{(i)}\rangle_{\mathcal{B}}=\mathrm{Pe}\left[\langle\mathbf{u}_0\rangle_{\mathcal{B}}\cdot\nabla_{\mathbf{x}}c_0^{(i)}+\epsilon\left(\langle\mathbf{u}_1\rangle_{\mathcal{B}}\cdot\nabla_{\mathbf{x}}c_0^{(i)}+\langle\mathbf{u}_0\rangle_{\mathcal{B}}\cdot\nabla_{\mathbf{x}}\overline{c}_1^{(i)}\right)\right]+\mathcal{O}\left(\epsilon\right), \tag{B14b}$$

$$\langle c^{(i)}\rangle_{\mathcal{B}}=c_0^{(i)}+\epsilon\overline{c}_1^{(i)}+\mathcal{O}\left(\epsilon^2\right), \tag{B14c}$$

$$\langle\mathbf{u}\rangle_{\mathcal{B}}=\mathbf{u}_0+\mathcal{O}\left(\epsilon\right), \tag{B14d}$$

obtained using equations (10), (12), and system (13), for $i\in\{1,2\}$, we can simplify system (B13) to write the homogenized system as

$$\begin{aligned}\phi\frac{\partial\langle c^{(1)}\rangle_Y}{\partial t}+\mathbf{U}^{(1)}\cdot\nabla_{\mathbf{x}}\langle c^{(1)}\rangle_Y-\mathbf{V}^{(1)}\cdot\nabla_{\mathbf{x}}\langle c^{(2)}\rangle_Y-\nabla_{\mathbf{x}}\cdot\left(\mathbf{D}^{(1)}\cdot\nabla_{\mathbf{x}}\langle c^{(1)}\rangle_Y\right)\\=\mathscr{R}^{(2)}\langle c^{(2)}\rangle_Y-\mathscr{R}^{(1)}\langle c^{(1)}\rangle_Y+\mathcal{O}\left(\epsilon\right)\quad\text{for }\mathbf{x}\in\Omega,\end{aligned} \tag{B15a}$$

$$\begin{aligned}\phi\frac{\partial\langle c^{(2)}\rangle_Y}{\partial t}+\mathbf{U}^{(2)}\cdot\nabla_{\mathbf{x}}\langle c^{(2)}\rangle_Y-\mathbf{V}^{(2)}\cdot\nabla_{\mathbf{x}}\langle c^{(1)}\rangle_Y-\nabla_{\mathbf{x}}\cdot\left(\mathbf{D}^{(2)}\cdot\nabla_{\mathbf{x}}\langle c^{(2)}\rangle_Y\right)\\=\mathscr{R}^{(1)}\langle c^{(1)}\rangle_Y-\mathscr{R}^{(2)}\langle c^{(2)}\rangle_Y+\mathcal{O}\left(\epsilon\right)\quad\text{for }\mathbf{x}\in\Omega,\end{aligned} \tag{B15b}$$

where the effective parameters are defined as

$$\mathbf{U}^{(i)}=\mathrm{Pe}\langle\mathbf{u}\rangle_Y+\mathrm{Da}_{SL}^{(i)}\left[\phi\frac{|\Gamma|}{|\mathcal{B}|}\langle\boldsymbol{\chi}^{(i)[1]}\rangle_\Gamma-D^{(i)}\langle\nabla_{\boldsymbol{\xi}}\chi^{(i)[2]}\rangle_Y+\mathrm{Pe}\epsilon\langle\mathbf{u}\chi^{(i)[2]}\rangle_Y\right], \tag{B15c}$$

$$\mathbf{V}^{(1)}=\mathrm{Da}_{SL}^{(2)}\left[\phi\frac{|\Gamma|}{|\mathcal{B}|}\langle\boldsymbol{\chi}^{(2)[1]}\rangle_\Gamma-D^{(1)}\langle\nabla_{\boldsymbol{\xi}}\chi^{(1)[2]}\rangle_Y+\mathrm{Pe}\epsilon\langle\mathbf{u}\chi^{(1)[2]}\rangle_Y\right], \tag{B15d}$$

$$\mathbf{V}^{(2)}=\mathrm{Da}_{SL}^{(1)}\left[\phi\frac{|\Gamma|}{|\mathcal{B}|}\langle\boldsymbol{\chi}^{(1)[1]}\rangle_\Gamma-D^{(2)}\langle\nabla_{\boldsymbol{\xi}}\chi^{(2)[2]}\rangle_Y+\mathrm{Pe}\epsilon\langle\mathbf{u}\chi^{(2)[2]}\rangle_Y\right], \tag{B15e}$$

$$\mathbf{D}^{(i)}=\phi D^{(i)}\mathbf{I}+D^{(i)}\langle\nabla_{\boldsymbol{\xi}}\boldsymbol{\chi}^{(i)[1]}\rangle_Y-\mathrm{Pe}\epsilon\langle\mathbf{u}\otimes\boldsymbol{\chi}^{(i)[1]}\rangle_Y, \tag{B15f}$$

$$\mathscr{R}^{(i)}=\mathrm{Da}_{SL}^{(i)}\mathscr{R}, \tag{B15g}$$

$$\mathscr{R}=\phi\frac{|\Gamma|}{|\mathcal{B}|}\left[\epsilon^{-1}+\mathrm{Da}_{SL}^{(1)}\langle\chi^{(1)[2]}\rangle_\Gamma+\mathrm{Da}_{SL}^{(2)}\langle\chi^{(2)[2]}\rangle_\Gamma\right], \tag{B15h}$$

for $i\in\{1,2\}$. We note that $\mathrm{Da}_{SL}^{(1)}$ and $\mathrm{Da}_{SL}^{(2)}$ are left in the homogenized model, but are required to be of order $\mathcal{O}(\epsilon^0)$. As shown, we successfully homogenized the system for moderate reaction rates using the generalized closure form strategy.

Appendix C Linearly Separated Systems for $c_1^{(i)[1]}$ and $c_1^{(i)[2]}$

In this Appendix, we provide the linearly separated systems from the first order system of differential equations (system (B7)) in the second problem.

C1 Linearly Separated System for $c_1^{(1)[1]}$

$$\frac{\partial c_1^{(1)[1]}}{\partial \tau_2} - \frac{\partial \langle c_1^{(1)[1]} \rangle_{\mathcal{B}}}{\partial \tau_2} + \mathrm{Pe}^{(s)} \left(\mathbf{u}_0 - \langle \mathbf{u}_0 \rangle_{\mathcal{B}} \right) \cdot \nabla_{\mathbf{x}} c_0^{(1)} + \mathrm{Pe}^{(s)} \mathbf{u}_0 \cdot \nabla_{\mathbf{x}} c_1^{(1)[1]} \\ -\nabla_{\boldsymbol{\xi}} \cdot \left(D^{(1)} \nabla_{\mathbf{x}} c_0^{(1)} + D^{(1)} \nabla_{\boldsymbol{\xi}} c_1^{(1)[1]} \right) = 0 \quad \text{for } \mathbf{x} \in \Omega,\ \boldsymbol{\xi} \in \mathcal{B}, \tag{C1}$$

$$-\mathbf{n} \cdot D^{(1)} \left(\nabla_{\mathbf{x}} c_0^{(1)} + \nabla_{\boldsymbol{\xi}} c_1^{(1)[1]} \right) = 0 \quad \text{for } \mathbf{x} \in \Omega,\ \boldsymbol{\xi} \in \Gamma, \tag{C2}$$

C2 Linearly Separated System for $c_1^{(1)[2]}$

$$\frac{\partial c_1^{(1)[2]}}{\partial \tau_2} - \frac{\partial \langle c_1^{(1)[2]} \rangle_{\mathcal{B}}}{\partial \tau_2} - \frac{|\Gamma|}{|\mathcal{B}|} \left(\mathrm{Da}_{SL}^{(1,s)} c_0^{(1)} - \mathrm{Da}_{SL}^{(2,s)} c_0^{(2)} \right) + \mathrm{Pe}^{(s)} \mathbf{u}_0 \cdot \nabla_{\mathbf{x}} c_1^{(1)[2]} \\ -\nabla_{\boldsymbol{\xi}} \cdot \left(D^{(1)} \nabla_{\boldsymbol{\xi}} c_1^{(1)[2]} \right) = 0 \quad \text{for } \mathbf{x} \in \Omega,\ \boldsymbol{\xi} \in \mathcal{B}, \tag{C3}$$

$$-\mathbf{n} \cdot D^{(1)} \nabla_{\boldsymbol{\xi}} c_1^{(1)[2]} = \mathrm{Da}_{SL}^{(1,s)} c_0^{(1)} - \mathrm{Da}_{SL}^{(2,s)} c_0^{(2)} \quad \text{for } \mathbf{x} \in \Omega,\ \boldsymbol{\xi} \in \Gamma, \tag{C4}$$

C3 Linearly Separated System for $c_1^{(2)[1]}$

$$\frac{\partial c_1^{(2)[1]}}{\partial \tau_2} - \frac{\partial \langle c_1^{(2)[1]} \rangle_{\mathcal{B}}}{\partial \tau_2} + \mathrm{Pe}^{(s)} \left(\mathbf{u}_0 - \langle \mathbf{u}_0 \rangle_{\mathcal{B}} \right) \cdot \nabla_{\mathbf{x}} c_0^{(2)} + \mathrm{Pe}^{(s)} \mathbf{u}_0 \cdot \nabla_{\mathbf{x}} c_1^{(2)[1]} \\ -\nabla_{\boldsymbol{\xi}} \cdot \left(D^{(2)} \nabla_{\mathbf{x}} c_0^{(2)} + D^{(2)} \nabla_{\boldsymbol{\xi}} c_1^{(2)[1]} \right) = 0 \quad \text{for } \mathbf{x} \in \Omega,\ \boldsymbol{\xi} \in \mathcal{B}, \tag{C5}$$

$$-\mathbf{n} \cdot D^{(2)} \left(\nabla_{\mathbf{x}} c_0^{(2)} + \nabla_{\boldsymbol{\xi}} c_1^{(2)[1]} \right) = 0 \quad \text{for } \mathbf{x} \in \Omega,\ \boldsymbol{\xi} \in \Gamma, \tag{C6}$$

C4 Linearly Separated System for $c_1^{(2)[2]}$

$$\frac{\partial c_1^{(2)[2]}}{\partial \tau_2} - \frac{\partial \langle c_1^{(2)[2]} \rangle_{\mathcal{B}}}{\partial \tau_2} - \frac{|\Gamma|}{|\mathcal{B}|} \left(\mathrm{Da}_{SL}^{(2,s)} c_0^{(2)} - \mathrm{Da}_{SL}^{(1,s)} c_0^{(1)} \right) + \mathrm{Pe}^{(s)} \mathbf{u}_0 \cdot \nabla_{\mathbf{x}} c_1^{(2)[2]} \\ -\nabla_{\boldsymbol{\xi}} \cdot \left(D^{(2)} \nabla_{\boldsymbol{\xi}} c_1^{(2)[2]} \right) = 0 \quad \text{for } \mathbf{x} \in \Omega,\ \boldsymbol{\xi} \in \mathcal{B}, \tag{C7}$$

$$-\mathbf{n} \cdot D^{(2)} \nabla_{\boldsymbol{\xi}} c_1^{(2)[2]} = \mathrm{Da}_{SL}^{(2,s)} c_0^{(2)} - \mathrm{Da}_{SL}^{(1,s)} c_0^{(1)} \quad \text{for } \mathbf{x} \in \Omega,\ \boldsymbol{\xi} \in \Gamma. \tag{C8}$$

References

Ahmed, E. N., Bottaro, A., & Tanda, G. (2022). A homogenization approach for buoyancy-induced flows over micro-textured vertical surfaces. *J. Fluid Mech.*, *941*, A53. doi: 10.1017/jfm.2022.320

Allaire, G., Brizzi, R., Mikelić, A., & Piatnitski, A. (2010). Two-scale expansion with drift approach to the taylor dispersion for reactive transport through porous media. *Chem. Eng. Sci.*, *65*, 2292-2300.

Allaire, G., Mikelić, A., & Piatnitski, A. (2010). Homogenization approach to the dispersion theory for reactive transport through porous media. *SIAM J. Math. Anal.*, *42*, 125-144.

Allaire, G., & Raphael, A.-L. (2007). Homogenization of a convection-diffusion model with reaction in a porous medium. *C. R. Acad. Sci. Paris*, *344*, 523-528.

Alnaes, M., Blechta, J., Hake, J., Johansson, A., Kehlet, B., Logg, A., ... Wells, G. (2015). The fenics project version 1.5. *Archive of Numerical Software*, *3*.

Arunachalam, H., Onori, S., & Battiato, I. (2015). On veracity of macroscopic lithium-ion battery models. *J. Electrochem. Soc.*, *162*, A1940-A1951.

Auriault, J.-L., & Adler, P. (1995). Taylor dispersion in porous media: Analysis by multiple scale expansions. *Adv. Water Resour.*, *18*, 217-226.

Bachmat, Y., & Bear, J. (1986). Macroscopic modeling of transport phenomena in porous media. 1: The continuum approach. *Transp. Porous Media*, *1*, 213-240.

Battiato, I., Ferrero V, P. T., O'Malley, D., Miller, C. T., Takhar, P. S., Valdés-Parada, F. J., & Wood, B. D. (2019). Theory and applications of macroscale models in porous media. *Transp. Porous Media*, *130*, 5-76.

Battiato, I., & Tartakovsky, D. (2011). Applicability regimes for macroscopic models of reactive transport in porous media. *J. Contam. Hydrol.*, *120-121*, 18-26.

Battiato, I., Tartakovsky, D. M., Tartakovsky, A. M., & Scheibe, T. (2009). On breakdown of macroscopic models of mixing-controlled heterogeneous reactions in porous media. *Adv. Water Resour.*, *32*, 1664-1673.

Battiato, I., Tartakovsky, D. M., Tartakovsky, A. M., & Scheibe, T. D. (2011). Hybrid models of reactive transport in porous and fractured media. *Adv. Water Resour.*, *34*, 1140-1150.

Becker, B., Guo, B., Buntic, I., Flemisch, B., & Helmig, R. (2022). An adaptive hybrid vertical equilibrium/full-dimensional model for compositional multiphase flow. *Water Resour. Res.*, *58*(1). doi: e2021WR030990

Berkowitz, B., Cortis, A., Dentz, M., & Scher, H. (2006). Modeling non-fickian transport in geological formations as a continuous time random walk. *Rev. Geophys.*, *44*(2). doi: https://doi.org/10.1029/2005RG000178

Bloch, J.-F., & Auriault, J.-L. (2019). Upscaling of diffusion–reaction phenomena by homogenisation technique: Possible appearance of morphogenesis. *Transp. Porous Media*, *127*, 191-209.

Boso, F., & Battiato, I. (2013). Homogenizability conditions for multicomponent reactive transport. *Adv. Water Resour.*, *62*, 254-265.

Bourbatache, M. K., Le, T.-D., Millet, O., & Moyne, C. (2021). Limits of classical homogenization procedure for coupled diffusion-heterogeneous reaction processes in porous media. *Transp. Porous Media*, *140*, 437-457.

Bourbatache, M. K., Millet, O., & Moyne, C. (2020). Upscaling diffusion-reaction in porous media. *Acta Mech.*, *231*, 2011-2031.

Cushman, J. H., & Ginn, T. R. (1993). Nonlocal dispersion in media with continuously evolving scales of heterogeneity. *Transp. Porous Media*, *13*(1), 123–138.

Diffusion in random media. (1995). In J. Keller, D. McLaughlin, & G. Papanicolaou (Eds.), *Surveys in applied mathematics* (p. 205-253). Springer.

Donato, P., & Piatnitski, A. (2005). Averaging of nonstationary parabolic operators with large lower order terms. *Math. Sci. Appl.*, *24*, 153-165.

Garnier, J. (1997). Homogenization in a periodic and time-dependent potential. *SIAM J. Appl. Math.*, *57*, 95-111.

Gelhar, L. W., & Axness, C. L. (1983). Three-dimensional stochastic analysis of macrodispersion in aquifers. *Water Resour. Res.*, *19*(1), 161-180. doi: https://doi.org/10.1029/WR019i001p00161

Golfier, F., Wood, B., Orgogozo, L., Quintard, M., & Buès, M. (2009). Biofilms in porous media: Development of macroscopic transport equations via volume averaging with closure for local mass equilibrium conditions. *Adv. Water Resour.*, *32*, 463-485.

Gray, W. G., & Miller, C. T. (2014). *Introduction to the thermodynamically constrained averaging theory for porous medium systems.* Switzerland: Springer.

Haggerty, R., McKenna, S. A., & Meigs, L. C. (2000). On the late-time behavior of tracer test breakthrough curves. *Water Resour. Res.*, *36*(12), 3467-3479. doi: https://doi.org/10.1029/2000WR900214

Hornung, U. (1997). *Homogenization and porous media*. New York: Springer.

Iliev, O., Mikelić, A., Prill, T., & Sherly, A. (2020). Homogenization approach to the upscaling of a reactive flow through particulate filters with wall integrated catalyst. *Adv. Water Resour.*, *146*. doi: 103779

Le, T.-D., Moyne, C., Bourbatache, K., & Millet, O. (2022). A spectral approach for homogenization of diffusion and heterogeneous reaction in porous media. *Appl. Math Model.*, *104*, 666-681.

Lewandowska, J., Auriault, J.-L., Empereur, S., & Royer, P. (2002). Solute diffusion in fractured porous media with memory effects due to adsorption. *C. R. Mecanique*, *330*, 879-884.

Logg, A., Mardal, K.-A., & Wells, G. (2012). *Automated solution of differential equations by the finite element method*. Springer.

Lubbers, N., Agarwal, A., Chen, Y., Son, S., Mehana, M., Kang, Q., ... Viswanathan, H. S. (2020). Modeling and scale-bridging using machine learning: Nanoconfinement effects in porous media. *Sci. Rep.*, *10*. doi: 13312

Marušić-Paloka, E., & Piatnitski, A. (2005). Homogenization of a nonlinear convection-diffusion equation with rapidly oscillating coefficients and strong convection. *J. London Math. Soc.*, *2*, 391-409.

Mauri, R. (1991). Dispersion, convection, and reaction in porous media. *Phys. Fluids A*, *3*, 743-756.

Mehmani, Y., Anderson, T., Wang, Y., Aryana, S. A., Battiato, I., Tchelepi, H. A., & Kovscek, A. R. (2021). Striving to translate shale physics across ten orders of magnitude: What have we learned? *Earth Sci. Rev.*, *223*. doi: 103848

Mehmani, Y., Castelletto, N., & Tchelepi, H. A. (2021). Multiscale formulation of frictional contact mechanics at the pore scale. *J. Comput. Phys.*, *430*. doi: 110092

Mei, C. (1992). Method of homogenization applied to dispersion in porous media. *Transp. Porous Media*, *9*, 261-274.

Mikelić, A., Devigne, V., & Van Duijn, C. (2006). Rigorous upscaling of the reactive flow through a pore, under dominant peclet and damkohler numbers. *SIAM J. Math. Anal.*, *38*.

Miller, C., Valdés-Parada, F., Ostvar, S., & Wood, B. (2018). A priori parameter estimation for the thermodynamically constrained averaging theory species transport in a saturated porous medium. *Transp. Porous Media*, *122*, 611-632.

Miller, C. T., Bruning, K., Talbot, C. L., McClure, J. E., & Gray, W. G. (2019). Nonhysteretic capillary pressure in two-fluid porous medium systems: Definition, evaluation, validation, and dynamics. *Water Resour. Res.*, *55*, 6825–6849.

Molins, S., & Knabner, P. (2019). Multiscale approaches in reactive transport modeling. *Rev. Mineral. Geochem.*, *85*.

Molins, S., Trebotich, D., Arora, B., Steefel, C. I., & Deng, H. (2019). Multi-scale model of reactive transport in fractured media: Diffusion limitations on rates. *Transp. Porous Media*, *128*(2), 701–721. doi: 10.1007/s11242-019-01266-2

Morse, J. W., & Arvidson, R. S. (2002). The dissolution kinetics of major sedimentary carbonate minerals. *Earth Sci. Rev.*, *58*, 51-84.

Municchi, F., & Icardi, M. (2020). Macroscopic models for filtration and heterogeneous reactions in porous media. *Adv. Water Resour.*, *141*. doi: 103605

Neuman, S. P. (1993). Eulerian-lagrangian theory of transport in space-time nonstationary velocity fields: Exact nonlocal formalism by conditional moments and weak approximation. *Water Resour. Res.*, *29*(3), 633-645.

Pietrzyk, K., Korneev, S., Behandish, M., & Battiato, I. (2021). Upscaling and automation: Pushing the boundaries of multiscale modeling through symbolic computing. *Transp. Porous Media*, *140*, 313-349.

Rubinstein, J., & Mauri, R. (1986). Dispersion and convection in periodic porous media. *SIAM J. Appl. Math.*, *46*, 1018-1023.

Salles, J., Thovert, J.-F., Delannay, R., Prevors, L., Auriault, J.-L., & Adler, P. (1993). Taylor dispersion in porous media. determination of the dispersion tensor. *Phys. Fluids A*, *5*, 2348-2376.

Scheibe, T. D., Murphy, E. M., Chen, X., Rice, A. K., Carroll, K. C., Palmer, B. J., ... Wood, B. D. (2015). An analysis platform for multiscale hydrogeologic modeling with emphasis on hybrid multiscale methods. *Groundwater*, *53*(1), 38-56. doi: https://doi.org/10.1111/gwat.12179

Schiller, U., & Wang, F. (2018). Multiscale simulation of transport phenomena in porous media: From toy models to materials models. *MRS Commun.*, *8*, 358-371.

Tang, Y., Valocchi, A. J., & Werth, C. J. (2015). A hybrid pore-scale and continuum-scale model for solute diffusion, reaction, and biofilm development in porous media. *Water Resour. Res.*, *51*(3), 1846-1859.

Wang, Z., & Battiato, I. (2020). Patch-based multiscale algorithm for flow and reactive transport in fracture-microcrack systems in shales. *Water Resour. Res.*, *56*(2). doi: e2019WR025960

Wang, Z., & Battiato, I. (2021). Upscaling reactive transport and clogging in shale microcracks by deep learning. *Water Resour. Res.*, *57*(4). doi: e2020WR029125

Whitaker, S. (1999). *The method of volume averaging.* P.O. Box 17, 3300 AA Dordrecht, The Netherlands: Kluwer Academic Publishers.

Wood, B. (2009). The role of scaling laws in upscaling. *Adv. Water Resour.*, *32*, 723-736.

Yan, Z., Liu, C., Liu, Y., & Bailey, V. L. (2017). Multiscale investigation on biofilm distribution and its impact on macroscopic biogeochemical reaction rates. *Water Resour. Res.*, *53*(11), 8698-8714.

Yousefzadeh, M., & Battiato, I. (2017). Physics-based hybrid method for multiscale transport in porous media. *J. Comput. Phys.*, *344*, 320-338.